204
11-12

DWR-1619

MLM-1684

MLM-1684

The Compatibility of Plutonium-238 Dioxide with Platinum and Platinum-Rhodium Alloys: Interim Report

J. E. Selle, J. R. McDougal, and

D. R. Schaeffer

THIS DOCUMENT CONFIRMED AS UNCLASSIFIED
DIVISION OF CLASSIFICATION
BY JH Cahn/amh
DATE 6/17/70

AEC Research and Development Report

MOUND LABORATORY
operated by
MONSANTO RESEARCH CORPORATION
a subsidiary of Monsanto Company
for the
U. S. ATOMIC ENERGY COMMISSION

Monsanto

DISTRIBUTION OF THIS DOCUMENT IS UNLIMITED

P7441

PRINTED IN THE UNITED STATES OF AMERICA
Available from
Clearinghouse for Federal Scientific and Technical Information
National Bureau of Standards, U.S. Department of Commerce
Springfield, Virginia 22151
Price: Printed Copy $3.00; Microfiche $0.65

LEGAL NOTICE

This report was prepared as an account of Government sponsored work. Neither the United States, nor the Commission, nor any person acting on behalf of the Commission:

A. Makes any warranty or representation, expressed or implied, with respect to the accuracy, completeness, or usefulness of the information contained in this report, or that the use of any information, apparatus, method, or process disclosed in this report may not infringe privately owned rights: or
B. Assumes any liabilities with respect to the use of, or for damages resulting from the use of any information, apparatus, method, or process disclosed in this report.

As used in the above, "person acting on behalf of the Commission" includes any employee or contractor of the Commission, or employee of such contractor, to the extent that such employee or contractor of the Commission, or employee of such contractor prepares, disseminates, or provides access to, any information pursuant to his employment or contract with the Commission, or his employment with such contractor.

DISCLAIMER

This report was prepared as an account of work sponsored by an agency of the United States Government. Neither the United States Government nor any agency Thereof, nor any of their employees, makes any warranty, express or implied, or assumes any legal liability or responsibility for the accuracy, completeness, or usefulness of any information, apparatus, product, or process disclosed, or represents that its use would not infringe privately owned rights. Reference herein to any specific commercial product, process, or service by trade name, trademark, manufacturer, or otherwise does not necessarily constitute or imply its endorsement, recommendation, or favoring by the United States Government or any agency thereof. The views and opinions of authors expressed herein do not necessarily state or reflect those of the United States Government or any agency thereof.

DISCLAIMER

Portions of this document may be illegible in electronic image products. Images are produced from the best available original document.

MLM-1684
TID-4500
UC-25 Metals,
Ceramics, and Materials

The Compatibility of Plutonium-238 Dioxide with Platinum and Platinum-Rhodium Alloys: Interim Report

J. E. Selle, J. R. McDougal, and D. R. Schaeffer

Issued: January 30, 1970

LEGAL NOTICE

This report was prepared as an account of work sponsored by the United States Government. Neither the United States nor the United States Atomic Energy Commission, nor any of their employees, nor any of their contractors, subcontractors, or their employees, makes any warranty, express or implied, or assumes any legal liability or responsibility for the accuracy, completeness or usefulness of any information, apparatus, product or process disclosed, or represents that its use would not infringe privately owned rights.

MONSANTO RESEARCH CORPORATION
A Subsidiary of Monsanto Company

MOUND LABORATORY
Miamisburg, Ohio 45342

operated for

UNITED STATES ATOMIC ENERGY COMMISSION
U S Government Contract No AT-33-1-GEN-53

DISTRIBUTION OF THIS DOCUMENT IS UNLIMITED

TABLE OF CONTENTS

	Page
ABSTRACT	5
INTRODUCTION	6
PROCEDURE	7
RESULTS AND DISCUSSION	
Platinum and Pt-40 wt % Rh with Microspheres at 1200°C	9
Platinum with Powder at 1200°C	10
Platinum and Pt-40 wt % Rh in Ta-10 wt % W Inner Liner at 1200°C	11
Platinum Plus Microspheres in Hydrogen - Helium Atmospheres	12
Platinum and Pt-40 wt % Rh in TZM Inner Liner at 1200°C	13
Pt-10 wt % Rh at 1200°C	14
Pt-30 wt % Rh at 1200°C	15
Platinum and Pt-40 wt % Rh at 1200°C	16
Platinum, Pt-20 wt % Rh, and Pt-40 wt % Rh in Molybdenum Liners at 1000°C	16
Platinum, Pt-20 wt % Rh, and Pt-40 wt % Rh in Molybdenum Liners at 800°C	20
Platinum, Pt-20 wt % Rh, and Pt-40 wt % Rh in Tantalum Liners at 1000°C	22
Impurities	26
X-Ray Analysis of Fuel	27
Future Work	27
CONCLUSIONS	28
ACKNOWLEDGMENTS	28
REFERENCES	29
TABLES	31
FIGURES	41

TABLE OF CONTENTS (cont'd)

Page

APPENDICES

A. Impurity Analyses of Platinum and Platinum-Rhodium Alloys Used in Compatibility Tests 119

B. Chemical Analyses of Fuel Samples Used in Platinum and Platinum-Rhodium Compatibility Tests 120

C. Capsule Designs. 121

ABSTRACT

This report presents a summary of compatibility tests conducted to date between production grade $^{238}PuO_2$ and platinum and platinum-rhodium alloys. Test periods were as long as 360 days, and most of the work was done at 800, 1000, and 1200°C. Samples were analyzed by means of metallography, microhardness measurements, x-ray diffraction, and electron microprobe analysis. A chronology of the program to date is presented along with a discussion of the various results. The effects of impurities in the fuel, the presence of molybdenum or tantalum in the system, as well as the effects of a reducing atmosphere are presented and discussed. Attempts are made to interpret the results in terms of possible mechanisms.

INTRODUCTION

As part of a general research and development project in support of the radioisotopic heat source program, a study of the compatibility of $^{238}PuO_2$ with platinum and platinum-rhodium alloys was initiated. Production grade fuel was used in this program for several reasons. The most important of these is that it is desirable to know what reactions, if any, would take place in an actual heat source capsule in service. Secondly, production grade fuel is much more readily available than special purity fuel. In view of the large amounts of fuel needed for the entire program, this was an important consideration. Initial results showed some promise for these materials. However, subsequent work performed under slightly different conditions, indicated serious problems. As the program developed, variable test results were obtained which seemed to reflect changes in test conditions. In addition, all of the results were complicated by the presence of impurities at the reaction interface, which apparently came from the fuel. (At the time this program was initiated, production grade fuel contained up to 2.0% impurities.) In view of the various conflicts and resulting confusion, it was decided that a thorough review of the data would be in order. Upon completion of the program a final report will be written.

Much of the data discussed in this interim report have been presented in various Mound Laboratory quarterly reports. However, these reports, besides being confusing to some degree, are somewhat incomplete. In order to place the entire program in perspective, this report presents a chronology of the program and indicates the evolution of the data to date. From these results an attempt will then be made to summarize the data in terms of possible mechanisms.

It is the intent of this report to present as much of the data generated as possible. In this way the reader may analyze these data and reach his own conclusions, which may or may not agree with those presented in this report. Not all of the photomicrographs and electron microprobe data obtained are presented in this report. To do so would probably cause more confusion than it would resolve. However, a serious attempt has been made to present as much information as possible without being redundant.

PROCEDURE

Data were obtained at three different temperatures: 800, 1000, and 1200°C. For programmatic reasons the initial data were obtained at 1200°C, and most of the data have been obtained at this temperature. For these reasons the data obtained at this temperature will be discussed first. More recent data have been obtained at 800 and 1000°C.

The total matrix for the noble metal compatibility program is shown in Table 1. All of the capsules in a given series of tests and the fuel used in a given series of tests were of identical composition. The chemical analyses of the capsule materials and fuel referred to in Table 1 are given in Appendices A and B, respectively. Capsule designs used in each case are indicated in the last column and are summarized in Appendix C.

In retrospect, some of these capsule designs appear inferior. Their design was motivated primarily by a desire to obtain the maximum amount of test data in the shortest period of time for the lowest cost. This approach sometimes leads to difficulties, such as those experienced in these tests. However, the information obtained from these tests is probably more useful in the long run than data which may have shown little or no interaction.

All capsules were machined from tubing, and the end caps were punched from sheet stock and machined to size. In general, an inner liner was used to contain the fuel while an outer container was used to protect the inner liner from air oxidation at the annealing temperature. In a few cases, a secondary liner was sometimes used. Hastelloy X or Haynes alloy No. 25 were used for the outer containers, and the end caps for these capsules were machined from bar stock. All TIG welds on the inner liners were made in an argon atmosphere using high purity argon as a cover gas, and all of the closure welds on the outer containers were made in an electron beam welder. The inner liners were decontaminated prior to welding into the outer containers. In cases where discs of metal were embedded in the fuel, care was taken to avoid contact with the container wall. In most cases radiographs of the capsules were made prior to loading into the furnace in order to ensure that there was no contact with the container wall.

All capsules were annealed in muffle furnaces in an air atmosphere. Oxidation resistance was provided by the Hastelloy X or Haynes alloy No. 25 outer container.

Metallographic samples were prepared in a glovebox facility under a nitrogen atmosphere. Sectioning was done with an abrasive cutoff wheel employing a 90 grit silicon carbide wheel. The specimens were mounted in copper-filled diallyl phthalate to provide a conductive mount for electron microprobe analysis.

Coarse grinding of the metallographic mount was done with 240-320 grit silicon carbide paper, and final grinding was done with 600 grit silicon carbide paper. Carbon tetrachloride was used as a lubricant in the grinding steps as well as in the ultrasonic cleaner between the various steps in grinding and polishing. Rough polishing was done on Texmet* paper with 6 μm diamond paste with olive oil as a lubricant. An intermediate step of 3 μm diamond paste using Texmet paper was used. Final polishing was done on microcloth on a vibratory polisher with 0.3 μm alumina and water as a lubricant.

Samples were usually examined in the unetched condition. This is particularly necessary in microprobe analysis because etching can sometimes selectively leach out certain elements. Etching was done to measure the depth of impurity penetration and was done electrolytically with a solution of KCN.

All photomicrographs were taken with a Leitz MM5 metallograph. Microhardness measurements were made with a Leitz miniload hardness tester, or with a Leitz microhardness attachment for the MM5 metallograph.

Electron microprobe analysis was done on an Applied Research Laboratories instrument. Two types of analyses were made. In the first type, the electron beam scanning unit of the instrument was used to scan the specimen, and photographs were taken of various elements using the signal from the characteristic x-ray to modulate the cathode ray tube (CRT) beam. In this mode of operation the beam is scanned across an area of the sample so that a distribution of that particular element can be obtained.

The second type of analysis was done using a finely focused static beam to indicate compositional changes as the specimen was moved under the beam. Analysis was made by driving the stage translation over a selected part of the specimen and feeding the signal from the characteristic x-ray through a rate meter to a strip chart. The resulting trace gives a rough quantitative description for each of the elements sought as a function of the distance across the face of the sample. The data in this report are presented in the form of traces of these strip chart plots superimposed upon each other. The relative displacement of each curve with respect to the others should not be considered as a quantitative comparison of the amount of one element with another. This relative displacement is a function of the counting rate and hence is a variable. However, for a given element, the changes in displacement of the curve, excluding electronic noise, can be used to indicate changes in composition. The number adjacent to the identification of each curve is the counting rate used for that particular element. Different counting rates were used in an attempt to obtain maximum sensitivity and still keep the trace on scale. The higher the counting rate for a given scale of one element with respect to another, the greater is the actual relative composition of that element with respect to the other. At the same time, decreasing the counting rate necessitates an increase in amplification, resulting in an increase

*Texmet is a napless polishing paper supplied by A. B. Buehler, Ltd.

in the noise-to-signal ratio. In order to obtain a more accurate comparison of one element with respect to another, the curves must be normalized with respect to one of the elements. If element B is to be compared with element A the following relationship is used:

$$\frac{\text{Counting rate of B}}{\text{Counting rate of A}} \times \frac{\text{\% of scale of element B}}{\text{\% of scale of element A}} = \text{Relative Amount of B} \quad (1)$$

It should be emphasized that this equation will give only a relative amount of B compared to A. No quantitative comparisons are implied. In order to make the comparison quantitative, other corrections have to be made to compensate for differences in wavelength, absorption, density, etc. At the same time a standard of known composition must be used for comparison. In some cases, when standards were available, attempts were made to obtain more accurate analyses. Even in these cases, however, errors as high as several percent are present because the second and third order corrections were not made.

Several techniques were used to measure the depth of penetration of impurities into the test samples and any property changes at the reaction interface. These are electron microprobe data, etching and metallographic analysis, and microhardness measurements. The most definitive information is given by the electron microprobe. However, analysis of every sample on the microprobe places an inordinate load on this instrument and would result in a considerable delay in the overall program. Therefore, metallographic techniques and microhardness measurements were used as much as possible.

In addition to these tests, an attempt was made to determine the lattice parameters of the fuel after each test to determine whether any changes in stoichiometry or structure occurred as a result of the tests. Samples of the fuel powder were loaded into quartz capillaries with an inside diameter of 0.3 mm and a wall thickness of 0.02-0.03 mm. A standard Debye-Scherrer powder camera was used. Filtered copper k_α radiation from a high intensity GE x-ray tube, with exposure times of 2-4 hr, was used. Aluminum foil was used to cover the film in order to minimize the effects of secondary radiation.

RESULTS AND DISCUSSION

Platinum and Pt-40 wt % Rh with Microspheres at 1200°C Initially, the design shown in Figure C-1 was used for compatibility testing. Discs of Pt-40 wt % Rh were embedded in $^{238}PuO_2$ microspheres contained in a platinum cup. The wall thickness of the platinum cup was 0.025 cm (0.010 in.) and the thickness of the Pt-40 wt % Rh discs was 0.064 cm (0.025 in.). A loose fitting lid was placed on top of the platinum cup, and tungsten foil was placed between the platinum cup and the tantalum inner liner. The tantalum inner liner was TIG welded closed. A tungsten spacer was placed between the tantalum and the Hastelloy X outer container to prevent any interaction. The outer container was electron beam welded

closed. The capsule was then placed in a muffle furnace at 1200±5°C for 30 days (720 hr).

Photomicrographs of the fuel-metal interface are shown in Figures 1 and 2. Obviously, a reaction has occurred in each case although the amount and nature of the reaction in each case is different.

The most reaction is shown by platinum in Figure 1. Two pieces of platinum are shown in this photomicrograph. The left piece is part of the sidewall of the platinum cup, and the right piece is part of the bottom of the cup. These two pieces were folded so that the reaction layer was between them. This reaction product was friable, and pieces flaked off during preparation of the sample for mounting. The platinum was embrittled as indicated by the fact that one whole grain has popped out and another has separated. Also, very fine microcracks can be seen at grain boundaries. The depth of the reaction zone was calculated to be ~0.0025 cm (0.001 in.).

For Pt-40 wt % Rh considerably less reaction occurred as shown in Figure 2. The reaction layer is thin, about 0.0005 cm (0.0002 in.), uniform with no indications of intergranular attack, and hard and brittle as indicated by the scratches emanating from the reaction surface. From this test it was felt that Pt-40 wt % Rh alloy had some merit as a container material.

<u>Platinum with Powder at 1200°C</u> The regular compatibility program was then initiated using the design shown in Figure C-2. This program called for tests with platinum using $^{238}PuO_2$ production grade fines for periods of 30, 60, 90, 180, and 360 days. Production grade fines were chosen as the fuel because of the maximum number of contact points possible between the fuel and the container, the compaction properties of this type of powder, and its availability. In these tests no tungsten foil was placed between the platinum cup and the tantalum inner liner. As in the previous test the tantalum inner liner was TIG welded closed, and the Hastelloy X outer capsule was electron beam welded.

The first sample was removed after 170 hr (7.1 days). Subsequent samples were removed after 30, 69, 90, and 160 days. Metallographic analysis indicated that a reaction had occurred, even at 170 hr. At the end of 69 days the reaction layer penetrated completely through the 0.025 cm (0.010 in.) wall thickness. A photograph of platinum cups exposed for 90 days is shown in Figure 3. Included in this photograph is a standard sample which contained no fuel and a sample which contained PuO_2. Obviously the presence of PuO_2 affects the appearance of the platinum under these conditions.

Electron microprobe analysis of the 69-day sample indicates that tantalum diffused into the platinum and that plutonium reacted with tantalum to form a Ta-Pu-O compound (the oxygen is assumed). This compound is found intermittently throughout the platinum. A strip chart analysis of this sample is shown in Figure 4, and a photomicrograph of this sample is

shown in Figure 5. The dark gray particles contain both plutonium and tantalum. It was felt at the time that either the tantalum enhanced the reaction between plutonium and platinum, or it reacted with the plutonium after a PuO_2-platinum reaction had already occurred. However, in view of the fact that, thermodynamically, PuO_2 should not be reduced by platinum, it was believed that the latter alternative was least feasible. After 160 days the tests were terminated due to the extremely poor condition of the platinum cups. Metallographic analysis of these samples was completed, and the results of all the samples essentially confirm those discussed above.

Platinum and Pt-40 wt % Rh in Ta-10 wt % W Inner Liner at 1200°C In the next series of compatibility tests the capsule design shown in Figure C-3 was used. In this design discs of platinum and Pt-40 wt % Rh were embedded in the fuel, which in turn was contained in a Ta-10 wt % W inner capsule. The fuel for these tests was 50-175 μm powder rather than fines. This change was effected because the fines were found to be too fluffy and very easily got into the weld area, causing welding difficulties. Two capsules were removed after 408 hr (17 days) at 1200°C. Unfortunately, after 30 days at 1200°C a furnace malfunction caused the remaining samples to overheat to the point where the Hastelloy X outer liners melted. This resulted in the loss of the remaining samples.

An electron microprobe analysis was obtained on the Pt-40 wt % Rh sample exposed for 408 hr at 1200°C. Photomicrographs of this sample taken with the electron microprobe are shown in Figures 6-9. A photomicrograph taken with back-scattered electrons is shown in Figure 6. In this photomicrograph the fuel is shown at the bottom, the alloy at the top, and the reaction layer appears as a honeycombed layer in between. The width of the reaction layer is approximately 50-55 μm.

A photomicrograph taken with platinum L_α radiation is shown in Figure 7. From this photomicrograph it appears that the platinum is depleted in the reaction zone and is evenly distributed in the fuel. A similar photomicrograph, taken with rhodium L_α radiation, is shown in Figure 8. In this case, however, the amount of rhodium dispersed in the fuel as compared to the amount in the alloy appears to be less than in the case for platinum. Finally, a photomicrograph taken with plutonium M_α radiation (Figure 9) shows that the amount of plutonium in the reaction layer gradually decreases with distance from the fuel-metal interface.

Similar results were obtained with pure platinum. From these results it was concluded that in this particular case, the reaction with platinum and Pt-40 wt % Rh alloy is the result of solution attack of the metal by the fuel. However, this mechanism does not agree with some of the earlier results. Thermodynamic calculations indicate that neither platinum nor rhodium should reduce the fuel. Unfortunately thermodynamics cannot predict a solution-type attack.

At this point a theory was advanced which could account for all of the above observations. This theory is based on observations made at various

laboratories on platinum and platinum-rhodium thermocouples. When platinum versus platinum-rhodium thermocouples were used at elevated temperatures in contact with various ceramic materials in a hard vacuum, the thermocouples deteriorated after only a few hours. However, in air the thermocouples could be used indefinitely, suggesting that a partial pressure of oxygen is necessary to prevent a reaction. The observations made to date can be explained in terms of this theory. In the case of the tantalum or Ta-10 wt % W inner liners, the tantalum would getter the free oxygen present in the capsule. Since this free oxygen is the result of decomposition of the fuel to a substoichiometric oxide at elevated temperatures, the fuel becomes more substoichiometric with time. It is possible that the substoichiometric oxide could then take platinum and rhodium into solid solution. Other explanations, however, are also possible.

Platinum Plus Microspheres in Hydrogen-Helium Atmospheres Information on the compatibility of PuO_2 with platinum was obtained during some thermogravimetric analysis experiments on the oxidation and decomposition of PuO_{2-x} and $PuO_{2.0}$. In one experiment $^{239}PuO_2$ microspheres were heated to about 1300°C in a helium-6 vol % hydrogen atmosphere. A basket made of 0.0051 cm (0.002 in.) platinum foil was used to contain the microspheres. After a few minutes at 1300°C extensive reaction occurred, and many of the microspheres dropped through the bottom of the platinum basket. Figure 10 shows a photograph of the pan and spheres and shows that some of the microspheres became coated with platinum. Calculations revealed that at the time of loss of the microspheres, the stoichiometry of the microspheres was $^{239}PuO_{1.84}$. Metallographic analysis showed a distinct reaction between the platinum and the microspheres, as shown in Figure 11. Figure 12 shows a strip chart analysis across the interface and indicates counter diffusion of both plutonium and platinum.

Slightly different results were obtained in a similar test in which a $^{238}PuO_2$ pellet was heated in a helium-6 vol % hydrogen atmosphere. After 18 min at 1330°C the bottom of the pan disappeared. After the sample cooled and was removed from the furnace, the PuO_2 was found attached to the side of the pan. Photomicrographs of the sample are shown in Figures 13 and 14. A dendritic structure is seen surrounded by eutectic. Electron microprobe analysis indicates that the primary dendrites are primarily platinum, with about 93 wt % platinum, 4 wt % impurities, and 3 wt % plutonium, while the eutectic contains about 86 wt % platinum and 14 wt % plutonium. The impurity content of the eutectic appears to be nil.

In an attempt to determine whether a partial pressure of oxygen will inhibit the reaction between PuO_2 and platinum, the above experiment was repeated in an air atmosphere rather than a helium-hydrogen atmosphere. The microspheres were heated to 1300°C for over 1½ hr. Some of the microspheres stuck to the platinum although electron microprobe analysis could detect no counterdiffusion of either plutonium or platinum. This is indicated by the strip chart analysis shown in Figure 15.

Several references to platinum-ceramic interactions have been found in the literature. Warmkessel and Kevane[1] reported an interaction between platinum and CeO_2 in hydrogen at high temperature. The nature of the reaction is not known although the platinum was severely attacked indicating that it is not a simple catalytic action involving platinum. Bronger and Klemm[2] showed that ZrO_2 can be effectively reduced by hydrogen in the presence of platinum. Darling[3] reported that refractory metal oxide dispersants in a solid matrix are notoriously unstable which suggests a high affinity of solid platinum for the refractory metal. This affinity is confirmed by the fact that the refractory metals are soluble in solid platinum in amounts exceeding 10 at. %.

Platinum and Pt-40 wt % Rh in TZM Inner Liner at 1200°C Following the loss of the samples due to overheating of the furnace, another series of tests was initiated in which the inner liner was TZM rather than Ta-10 wt % W. This capsule design is shown in Figure C-4. The reason for this change in design was that other work[4,5] suggested that molybdenum would be compatible with PuO_2 at 1200°C. Also, it was hoped that time and money would be saved by using a container other than platinum.

Metallographic examination of samples exposed for 32 and 62 days showed a rather deep reaction zone. Figure 16 shows this reaction layer in the 62-day sample. This reaction zone is quite different from any reaction zone observed previously. The reaction layers in pure platinum and in the Pt-40 wt % Rh alloy were similar, although the reaction layer was slightly deeper in pure platinum.

Electron microprobe analysis revealed that no plutonium was present in the reaction zone. Photomicrographs of this sample taken with backscattered electrons and with platinum, rhodium, and molybdenum are shown in Figures 17 through 20. From these photomicrographs it can be seen that there is a slight decrease in platinum and rhodium near the edge of the sample and an increase in the molybdenum content. In addition to molybdenum, cobalt, chromium, and iron were found in this region. These last three elements are the major impurities in the fuel. The voids in the sample appear quite similar to Kirkendall voids. There are at least two possible causes for these voids. First, the Kirkendall mechanism in which two interdiffusing species move at different rates could be the cause. If one of these elements diffuses outward faster than the other element diffuses inward, voids will form. The second mechanism is somewhat similar to this, but is not the direct result of two interdiffusing species. If some external reaction of the atmosphere within the capsule were to remove platinum from the sample faster than coincidental diffusion of molybdenum and fuel impurities can diffuse inward, voids could also form which would look very much like Kirkendall voids. At this point the data are insufficient to determine which of these two mechanisms is responsible for the voids. However, for convenience, they will be referred to as Kirkendall voids.

Additional microprobe data for platinum on samples tested for 90, 180, and 360 days are given in Figures 21-23, respectively. The progressive

increase in the distance of void depth and impurity penetration can be seen. In the photomicrograph of Figure 23 a fine structure can be seen even in the unetched condition. Photomicrographs of this area taken with back-scattered electrons and characteristic x-rays are shown in Figures 24-30. These figures can be correlated with the x-ray strip chart analysis of Figure 23 to show the distribution of the various impurities.

Additional microprobe data for Pt-40 wt % Rh samples tested at 1200°C for 90, 180, and 360 days are shown in Figures 31-33, respectively. The same general trend of void penetration and impurity penetration shown for platinum is also shown in these figures. Photomicrographs taken of the 360-day sample are shown in Figures 34-40 and again show the distribution of various elements at the reaction interface. Of particular interest is the distribution of iron in the particle of fuel shown in Figure 40.

A summary of the depth of penetration of the void layer and the various impurity layers for all the samples tested at 1200°C is shown in Table 2. Since electron microprobe data were not obtained on all samples this table is not complete. An attempt was made to correlate microhardness data or etched microstructure with impurity penetration but this attempt was unsuccessful. There was too much scatter in the microhardness data to make this technique useful. All microhardness measurements were made using a Vickers indenter. This work will be continued as soon as a Knoop indenter is obtained.

The presence of molybdenum is probably explained by the observation of Darling[3] that refractory oxide dispersants in a platinum matrix are unstable. At elevated temperature PuO_2 decomposes to a substoichiometric oxide, PuO_{2-x}, and free oxygen. This oxygen can then form a molybdenum oxide which is volatile at this temperature. The volatile oxide can then migrate to the platinum where it can react with the platinum to yield pure molybdenum and free oxygen. The molybdenum then diffuses into the sample, and the oxygen is then free to react further with the molybdenum in the TZM liner. It should be emphasized that there was no evidence of plutonium in either the platinum or the Pt-40 wt % Rh.

The presence of impurities in these samples complicates the situation considerably. The diffusion rates and possible effects of these impurities on the materials will be discussed in a later section (page 26).

<u>Pt-10 wt % Rh at 1200°C</u> In order to test a platinum alloy with PuO_2 without the presence of any refractory metal in the system a capsule with the design shown in Figure C-5 was fabricated. This test consisted of a Pt-10 wt % Rh capsule filled about 3/4 full with microspheres and TIG welded in an argon atmosphere. This capsule was then wrapped in platinum foil and TIG welded in a Ta-10 wt % W liner which was in turn electron beam welded into the Hastelloy X outer capsule. This particular test was made at 1200°C for 2000 hr. A photomicrograph of this sample is shown in Figure 41. A small amount of intergranular penetration is indicated although microprobe analysis revealed no plutonium or other elements

in these areas. The intergranular reaction product has apparently pulled out during the polishing operations. Considerable reaction with the fuel impurities was observed. This is shown in Figure 42 which is an x-ray strip chart analysis across this interface. The iron penetration was approximately 260 μm, while the chromium penetration was approximately 75 μm. No nickel or chromium were found.

Pt-30 wt % Rh at 1200°C Further tests in which refractory metals were excluded from the interior of the capsule were conducted with the design shown in Figure C-6. In these tests, capsules were constructed of Pt-30 wt % Rh. The capsules were originally about 1½ in. (3.8 cm) long. After the capsules were loaded with fuel, the end was pinched closed in an air atmosphere, and the pinched end was then welded with a gas torch. Two different types of fuel were used: microspheres and powder. The chemical analysis of each fuel sample is given in Appendix B. Samples were heated to 1200°C for 30 and 60 days with each fuel form.

The intent of this series of tests was threefold:

1) to determine the effect of a partial pressure of oxygen;

2) to determine whether the absence of molybdenum would eliminate the Kirkendall voids; and

3) to compare the relative reactivities of $^{238}PuO_2$ microspheres and $^{238}PuO_2$ powder.

Photomicrographs of these four samples are shown in Figures 43-46. Very little direct reaction with the fuel, if any, occurred. Electron microprobe analysis revealed no plutonium penetration into the platinum alloy, although impurity reactions occurred. X-ray strip chart analyses are shown in Figures 47-50. With the exception of the 60-day powder test, these analyses are at or near the areas shown in Figures 43-46. Table 3 summarizes the depth of penetration of impurities for each case. There is a slightly deeper penetration of impurities in the powder-fueled sample, but this seems more a function of fuel purity rather than of fuel form. In Figure 43 a particle of material appears at the interface that looks like fuel with some intergranular penetration into the alloy emanating from this particle. The results of microprobe analysis of this area, shown in Figure 47, shows that the particle is high in silicon, with some plutonium.

For the 60-day powder sample, voids were observed in one area of the sample, and microprobe analysis, shown in Figure 50, shows molybdenum to be present. The presence of molybdenum is somewhat disconcerting, as it was not added intentionally. It is possible, however, that the inner capsule leaked in this area, and molybdenum transport took place as described earlier. However, this particular sample points up the fact that the Kirkendall voids seem to be associated with the presence of molybdenum.

The most important conclusion that can be drawn from these tests is that no reaction with plutonium was observed under these conditions. Basically, the results were the same as the test with the Pt-10 wt % Rh alloy, so that the effect of a deliberate addition of a partial pressure of oxygen is questionable. This may be explained by the fact that PuO_2 can dissociate to some degree at this temperature so that in a closed system an equilibrium partial pressure of oxygen can form. These tests also confirm the conclusion that molybdenum has a distinct influence on the formation of Kirkendall voids. No definite conclusions could be reached concerning the comparative reactivity of microspheres and powder.

Platinum and Pt-40 wt % Rh at 1200°C In view of the adverse effects of molybdenum on these compatibility tests it was decided to duplicate the standard tests at 1200°C with no refractory metals in the system. Accordingly a series of capsules were fabricated according to the configuration shown in Figure C-7. These tests will be extended to 360 days. At this point data are available for 30-, 60-, and 90-day tests.

Photomicrographs of the platinum coupons after each of these time periods are shown in Figures 51-53. From these figures two observations can be made: (1) the number and depth of voids increases with time; and (2) the edge becomes more serrated with time. A trace of the x-ray strip chart analysis of the 90-day sample is shown in Figure 54 and shows that iron and chromium are present at the interface as in the case of the Pt-10 wt % Rh and Pt-30 wt % Rh tests.

Photomicrographs of Pt-40 wt % Rh after each of the time periods are shown in Figures 55-57. No visible evidence of reaction is present in these samples, even though particles of fuel are observed adhering to the interface. Figure 58 is a trace of the x-ray strip chart analysis of the 90-day sample and also indicates impurity diffusion, but no diffusion of plutonium into the alloy.

Platinum, Pt-20 wt % Rh, and Pt-40 wt % Rh in Molybdenum Liners at 1000° Tests at 1000°C were conducted with the design shown in Figure C-8. In these tests platinum, Pt-20 wt % Rh, and Pt-40 wt % Rh were tested simultaneously. Discs of each of these materials were embedded in the powdered fuel contained in a molybdenum inner liner. However, in this case 0.002 in. platinum foil was placed between the molybdenum and the fuel. The platinum diffusion barrier was not continuous and some contact between the fuel and the molybdenum was possible.

Results at 1000°C were quite similar to those at 1200°C in spite of the fact that the platinum foil was present. Typical photomicrographs of the results obtained with platinum, Pt-20 wt % Rh, and Pt-40 wt % Rh after 60 and 180 days are shown in Figures 59-64. Figure 65 shows a trace of the x-ray strip chart analysis of the area given in Figure 59. No direct reaction with PuO_2 was detected. The reactions observed are basically similar in all three materials and can be described as having the following characteristics:

1. One or more surface layers are formed.

2. Particles of fuel are embedded in the surface.

3. Voids are formed parallel to the metal surface.

Detailed metallographic and electron microprobe analysis has suggested that several different mechanisms are operative, either separately or in combination with each other. These mechanisms are:

1. Contamination of the compatibility couple by molybdenum from the container.

2. Diffusion of fuel impurities into the test specimen.

3. Migration of platinum into the fuel.

No direct reaction with PuO_2 is evident. The only evidence of any reaction at the interface is the presence of voids and fuel particles that appeared to be embedded in the surface. The number of fuel particles embedded in the surface, the number of voids, and the depth of penetration of voids decreases with increasing rhodium content. This is shown in Table 4. In all cases the impurities extended below the molybdenum reaction layer.

The diffusion depths of the fuel impurities for 60 and 180 days are given in Table 5. This table shows that the depth of penetration depends on the rhodium content, and the probe traces indicate that the impurities are primarily absent in the molybdenum layer.

The presence of molybdenum at the metal-fuel interface was discussed previously and no further comment is needed here. Impurity diffusion into the interface has also been noted previously. A more detailed discussion of this complication will be made in a later section (page 26). Migration of the platinum interface has taken place to such an extent that, after 180 days some of the fuel particles appear to be completely surrounded by platinum. This was also seen after shorter time periods. The extent of this migration is shown in Figure 66. This low magnification photomicrograph shows the three metal coupons after exposure for 180 days. Originally these coupons were 762 μm thick, but their total thickness has expanded to the values shown. This expansion has served to further complicate the task of determining rate equations for these reactions.

Photomicrographs taken with polarized light of the regions shown in Figures 60, 62, and 64 are shown in Figures 67-69. These photomicrographs show appreciably more detail than the bright field photomicrographs. Corresponding traces of the electron strip chart analyses made with the electron microprobe are shown in Figures 70-72. Figure 71 is a different area from Figures 62 and 68 although it is from the same sample. The outside layer in each case is seen to have a high molybdenum content, combined with platinum or platinum-rhodium alloy. The amount of molybdenum

in this layer is constant for platinum and Pt-20 wt % Rh and increases near the surface in the case of Pt-40 wt % Rh. Microhardness measurements on this layer gave values of 650-715 VHN (15-g load) for platinum. The highest microhardness values obtained by Selman[6] for solid solution alloys of molybdenum in platinum was 500 VHN. The high hardness values obtained on these samples suggest the presence of intermetallic compounds in this layer.

In the Pt-40 wt % Rh alloy, Figure 69, two layers are seen. The electron microprobe trace of Figure 72 shows that the inner layer is higher in rhodium and lower in molybdenum than the outer layer. The microhardness of this inner layer was about 575 VHN (25-g load).

The approximate compositions of these layers for each of the three materials is shown in Table 6. These approximations were obtained by using the base alloy as a standard for platinum and rhodium and a molybdenum standard included in the same mount. No second order corrections to the data were made.

The solubility of molybdenum in platinum is about 20 at. %[7] so that the 13.5 at. % molybdenum layer in the pure platinum sample should be a solid solution. However, this is not consistent with the high microhardness values which suggest an intermetallic compound. The reason for this discrepancy is not known at this time. For the ternary system Mo-Pt-Rh a rationalization of compound formation is possible. The solubility of molybdenum in rhodium is about 11 at. %. If the solvus line between the Mo-Pt and Mo-Rh binary diagrams is assumed to be linear, the limit of solid solubility of molybdenum in the Pt-20 wt % Rh and the Pt-40 wt % Rh would be about 17.1 at. % molybdenum and 15 at. % molybdenum, respectively. According to the data in Table 6 the molybdenum content of the surface layers exceeds these values so that intermetallic compounds are possible. It can be seen in Figures 70-72 that in the region below the surface layer, a region of solid solution of molybdenum in the base metal exists. This is to be expected. Photomicrographs of these samples after etching are shown in Figures 73-76. Included in these figures are schematic diagrams, and the various regions are indicated. The region containing molybdenum in solid solution in the platinum and the Pt-20 wt % Rh coupons consists of smaller grains than the parent material. Certain artifacts within this layer suggest annealing twins which would imply that recrystallization has taken place.

A summary of the width of the Pt(Rh)Mo outer layers and the depth of bulk diffusion for the various samples tested is given in Table 7. As the rhodium content of the test sample increases the depth of diffusion of molybdenum decreases, and as seen in Table 6 the total concentration of molybdenum increases. Approximate values for the rate constants of molybdenum in platinum and Pt-40 wt % Rh are also given. The scatter in the data for Pt-20 wt % Rh was too great to permit a determination of a rate constant. These rate constants were calculated from a plot of ΔX^2 as a function of time, where ΔX is the diffusion depth.

According to the microprobe traces given in Figures 70-72, iron, chromium, and zinc, present as impurities in the fuel, also diffused into the test samples. The impurities are located primarily below the Pt(Rh)Mo outer layer indicating rapid diffusion through this layer, with little or no solid solubility. Diffusion depths for the impurities in the three materials are summarized in Table 4. The quantity and depth of impurity penetration decreases as the rhodium content increases.

In the pure platinum a 15 to 20 μm thick layer, high in impurities, was found just below the Pt-Mo solid solution layer. This layer was discontinuous in that some regions of the sample no layer was present. Figures 73 and 74 show different regions of the sample with and without this layer. Electron microprobe analysis indicates that this layer contains approximately 79 at. % platinum, 17 at. % iron, 4 at. % zinc, and a trace of chromium, suggesting a compound of the order of $Pt_3(Fe, Zn)$.

As in the 1200°C tests, void formation appears to be present at the edge of the molybdenum layer. Attempts were made to detect impurity elements in these voids in order to determine whether these voids are actually voids and not pulled out inclusions. All attempts to identify impurity elements with the microprobe or inclusions by microscopic examinations were unsuccessful.

The migration of the platinum interface into the fuel is somewhat disconcerting since it makes it virtually impossible to determine the original interface. Several different mechanisms for this phenomenon are possible:

1. Dissolution of platinum into a slightly substoichiometric fuel, PuO_{2-x}, where $x \ll 1$.

2. Volatilization of platinum.

3. Formation of a volatile platinum oxide and subsequent deposition onto the fuel particles.

4. Deposition of molybdenum on the surface and subsequent diffusion of platinum into this layer.

Experiments conducted to date are not adequate to determine which of the above mechanisms, if any, are responsible for the platinum movement. The volatilization of platinum seems to be the least plausible of those mentioned. When no molybdenum is present in the system, platinum migration is not observed. It has also been observed that the amount of molybdenum migration is greater at 1000°C than it is at either 800 or 1200°C. At 1200°C some platinum was observed on the surface of the TZM liner.

Trace amounts of platinum (<1 at. %) were found in the embedded fuel particles, and the amount of platinum in the fuel at the surface of the coupons was less than that in the particles embedded within the Pt(Rh)Mo layer. No dissolution of rhodium was detected.

Platinum, Pt-20 wt % Rh, and Pt-40 wt % Rh in Molybdenum Liners at 800°C

Tests at 800°C were also conducted with the design shown in Figure C-8. In earlier work in which platinum was tested for 30 and 66 days, voids were found 3 μm and 10 μm, respectively, below the fuel-metal interface. Photomicrographs of these samples are shown in Figures 77 and 78. Examination of these photomicrographs indicates that although the voids after 66 days are larger and deeper, they are fewer. Regions with voids and without voids were examined with the electron microprobe, and it was found that the fuel impurities (iron, zinc, and chromium) had diffused into the platinum sample. Microprobe analysis revealed no difference in the depth of diffusion in the two areas although the concentration of zinc and iron was higher in the void region.

The results of tests run for longer periods are shown in Figures 79-83. Figures 79-81 show extreme void formation, and the surface layer appears only partially attached to the parent material. In addition it should be noted that the grain size of this layer is much finer than that of the parent material. In a few isolated areas another row of voids was found about 30 μm below the surface. This row is shown in Figure 82. A summary of the depths at which these voids were found is given in Table 8. In no instance was plutonium found to interact with the platinum even though plutonium was found at the surface of the platinum. This is shown in Figure 83, which is an x-ray strip chart analysis of the sample shown in Figure 82. This trace shows a depletion of platinum to a point 45 μm from the surface. The relationship between the voids and the impurities is also shown in this figure. Iron, chromium, and zinc were found near the surface to a depth of about 50 μm. No molybdenum was found in the sample. The slight indication of plutonium near the reaction interface is due to the fact that the electron beam is not infinitely small, but has a finite beam width of about 2 μm. Therefore the width of this region would be about 4 μm.

In 30- and 66-day tests with Pt-20 wt % Rh there was no visible evidence of any attack due to reaction with PuO_2, although interaction with the fuel impurities was found. Photomicrographs of samples tested for 90 and 180 days are shown in Figures 84-88. Figure 84 is a representative portion of the edge of the 90-day sample. The only apparent effect is a layer of small grains at the surface. A 1 to 2 μm layer was found on the 90-day sample that had separated from the parent material. This layer, shown in Figures 85 and 86, was found on one end of the coupon and was not a typical occurrence in the rest of the coupon. This layer has a small grain size, as shown in Figure 86, and appears to be enriched in fuel impurities. An x-ray strip chart analysis across this region is shown in Figure 89. The parent material below this layer is enriched in fuel impurities and contains a trace of molybdenum. No molybdenum could be detected in the layer. The typical reaction interface after 180 days is shown in Figures 88 and 89 which were taken in the unetched and etched condition, respectively. No other effect is seen other than a surface layer of fine grains. The grain at the edge of the sample near the center of the field of view contains artifacts which appear to be annealing twins. These annealing twins are not uncommon in these

samples, and the region of fine grains along the edge of the samples usually contain these twins. Annealing twins imply recrystallization but the reason recrystallization occurs is not known. Fuel impurities were found in this region. Figure 90 shows a trace of an x-ray strip chart analysis of this sample. The concentration of iron and chromium was high in the region roughly corresponding to the layer of recrystallized grains. A small peak of iron was found about 50 μm below the surface suggesting either an iron rich inclusion or preferential grain boundary diffusion. No molybdenum was found in this sample.

In the 90-day sample some voids were found 2-3 μm from the surface, although no voids were found in the 180-day sample.

In earlier studies on Pt-40 wt % Rh there was no visible evidence of any attack due to reaction with PuO_2 although interaction with fuel impurities was found. These samples had been tested for 30 and 66 days. More recently, data have been obtained on samples treated for 90 and 180 days. Photomicrographs of these samples are shown in Figures 91-97. In the 90-day sample, shown in Figure 91, there are voids 1 to 4 μm below the fuel-metal interface. The etched structure shown in Figure 92 reveals the presence of extremely small grains at the interface. It can also be seen in this figure that the row of voids seems to correspond with the edge of the layer of small grains. Figure 93 shows a photomicrograph taken with the electron microprobe using the characteristic x-rays for iron of the same area shown in Figure 92. From this figure it is obvious that preferential grain boundary diffusion of iron is taking place. This suggests that the small iron peak found in Figure 90 probably was due to grain boundary diffusion of iron. The high iron surface layer indicated in Figure 93 also contains some molybdenum.

Typical photomicrographs obtained from the 180-day samples at 800°C are shown in Figures 94 and 95. As with the 90-day sample a surface layer of small grains was found. The width of this layer is 5-7 μm. A segment of the small grain layer, 5 to 7 μm thick, which appears to be partially spalled off, was found on this coupon, and this is shown in Figure 96. A trace of the x-ray strip chart analysis is shown in Figure 97. An iron-rich inclusion within this layer is indicated by the high iron peak $2\frac{1}{2}$-3 μm from the surface in Figure 97. Photomicrographs taken with backscattered electrons and characteristic x-rays, Figures 98-104, show the distribution of each element over the region scanned. Concentrations of iron at various points are indicated which correspond to the small inclusions shown in Figures 96 and 97. A small amount of molybdenum is indicated in Figure 97. While this photomicrograph represents an exception rather than the rule, it indicates that spalling is possible. It is not known whether this spalling occurs during heat treatment, cooling, or sectioning for metallographic examination.

A summary of the depth of penetration of iron, chromium, nickel, and zinc in each of the three materials tested at 800°C is given in Table 9. The difference between the 66- and 180-day values of iron diffusion into Pt-20 wt % Rh is quite small. In view of the fact that spalling of the

surface occurred it is possible that this is responsible for this discrepancy. The absence of the original interface would certainly lead to confusion in interpretation. It should be noted that all evidence of spalling was found at the end of the coupons, which are in closer proximity to the molybdenum than the center. Whether this is a valid observation or not is open to conjecture.

At 800°C, the formation of voids does not appear to be distinctly associated with the presence of molybdenum as it is at higher temperatures. Instead, it appears that the diffusion of impurities, possible formation of Pt-Rh impurity intermetallics, and preferential grain boundary diffusion of iron could very well cause scaling without the presence of molybdenum.

Platinum, Pt-20 wt % Rh, and Pt-40 wt % Rh in Tantalum Liners at 1000°C

A series of tests was conducted with platinum, Pt-20 wt % Rh, and Pt-40 wt % Rh at 1000°C with the capsule design shown in Figure C-9. In these tests the coupons were embedded in the fuel as in the previous tests at 1000°C, but in this case the inner liner was tantalum rather than molybdenum, and there was no platinum between the fuel and the liner.

This series of tests was run to verify the concept that platinum and platinum-rhodium alloys react with a reduced form of $^{238}PuO_2$. At elevated temperatures PuO_2 decomposes to $PuO_{2-x} + (x/2)\ O_2$. The presence of a strong oxygen getter such as tantalum would remove the free oxygen and cause further reduction of the fuel. In effect, this capsule design is similar to the second series of tests described earlier, except that in the earlier tests the platinum and tantalum were in direct contact. This experiment was designed to determine whether tantalum was interfering directly with the Pt/PuO_{2-x} reaction by diffusion into the platinum, or whether it was enhancing the reaction by producing a reduced fuel. The capsules in this case were radiographed to ensure that the coupons were not touching the side of the tantalum liner.

The platinum-PuO_{2-x} interaction after 30 days at 1000°C is shown in Figures 105 and 106. In Figure 105 the reaction appears as a thick two-phase reaction product about 225-275 μm thick. Figure 106 shows that this reaction product consists of a mixture of fuel particles and a platinum-plutonium phase. Particles of a second phase are seen in the platinum-plutonium phase and these secondary particles seem to be emanating from the fuel particle. Electron microprobe analysis could not resolve this second phase because of the extremely small size of the particles. Only plutonium and platinum were found in this region, but no conclusions could be reached as to whether or not the small particles contained platinum. Below the reaction product on the exterior edge of the coupon, an 80 μm layer enriched with zinc, with trace quantities of iron and chromium, was found. No platinum coupon was found upon opening the 90-day capsule. Either the coupon was lost or it was totally consumed during the test.

A typical reaction between PuO_{2-x} and Pt-20 wt % Rh after 60 days at 1000°C is shown in Figures 107 and 108. Some differences in the appearance of

this reaction compared to the reaction in pure platinum can be seen. The most obvious is the porous layer at the edge of the Pt-20 wt % Rh coupon. This layer is shown at higher magnification in Figure 108. The large two-phase particles (20-100 μm) contain platinum, rhodium, and plutonium, and are basically the same as the large reaction product in the platinum sample. As in the platinum sample, the small dark gray particles were too small to be resolved with the electron microprobe.

Between the massive reaction product and the porous edge of the coupon (Figure 108) smaller two-phase particles are seen. These particles consist of a light-gray continuous phase and a white discontinuous phase. The light-gray phase contains plutonium, platinum, and rhodium, and the white phase contains rhodium, iron, and chromium.

The porous edge of the coupon is 30 μm wide and is basically parent material, depleted in platinum and enriched in rhodium. The platinum is depleted to about 80 μm from the interface, and the rhodium enrichment also extends to about 80 μm. A very slight enrichment of iron and chromium is also seen to a depth of 10-15 μm in the porous layer. Some dark particles are present in the parent material of the porous layer, and these particles were found to contain plutonium, platinum, and possibly rhodium.

Photomicrographs of the reaction interface after 90 days at 1000°C are shown in Figures 109 and 110. These two photomicrographs show two contrasting areas of the same coupon. In Figure 109 a porous edge is seen along one side of the sample in agreement with Figure 107. However, the opposite edge shows the extremes of no apparent attack and deep pits 50 to 125 μm deep. Some reaction product is seen in some of the pits. This is shown more clearly in Figure 111. Presumably the unattacked area was not in intimate contact with the fuel. A trace of the x-ray strip chart analysis across one of the embedded fuel particles seen in Figure 111 is shown in Figure 112. The morphology of the reaction interface seen in the photomicrograph is quite similar to that of the 69-day test shown in Figure 108. The massive white phase contains approximately 76 at. % platinum, 17 at. % rnodium, and 7 at. % plutonium plus trace amounts of iron and zinc. The large dark particle is primarily plutonium, while the small dark particles embedded in the white phase are too small to be resolved but are probably PuO_{2-x}.

High impurity concentrations were found near the edge of the parent material. Photomicrographs taken with back-scattered electrons and characteristic x-rays of the region shown in Figure 112 are shown in Figures 113-119. The distribution of plutonium in the massive white phase can be seen in Figure 114.

A slightly different appearing phase is shown in Figure 111 at the left side of the photomicrograph, slightly displaced from the interface. A higher magnification photomicrograph of this particle is shown in Figure 120. A photomicrograph of this same particle taken with polarized light is shown in Figure 121. This particle is shown to be made up of two major phases, with the lightest colored phase being optically active.

This phase is also polycrystalline. A trace of an x-ray strip analysis across the interface between these two phases is shown in Figure 122. From this figure it is seen that the optically active phase contains more platinum and less plutonium than the darker phase. The approximate composition of each phase is given in Table 10. Microhardness measurements indicate that the gray phase (A) has a Vicker's hardness of about 594 (25-g load) and the light-colored phase has a hardness of about 550 (25-g load).

A typical area of the porous edge found on most of the coupon is shown in Figure 123. Gray particles are seen in the base metal. Some of these appear rodlike while others appear globular. This suggests a disc-shaped particle. The composition of these particles could not be determined although they appear to be enriched in platinum and plutonium, and depleted in rhodium. Two-phase particles similar to those described in Figure 108 are also shown in Figure 124. These photomicrographs suggest that the darker phase in Figure 108 is the same as the darker particles embedded in the parent material in Figures 123 and 124.

Photomicrographs of reactions with Pt-40 wt % Rh are shown in Figures 125-128. The reaction between Pt-40 wt % Rh and $^{238}PuO_{2-x}$ was identical to that between Pt-20 wt % Rh and $^{238}PuO_{2-x}$ as seen by the similarities in Figures 107 and 125. The basic difference is that in the case of the Pt-40 wt % Rh alloy, more rhodium is found in the reaction product. In view of the similarity between platinum and rhodium, this is not unexpected. Figure 126 is an enlarged view of the reaction zone after 60 days. As in the case of the platinum and the Pt-20 wt % Rh tests, the fine second phase of the massive particles could not be resolved, although the large conglomerate in this massive phase contained about 80 wt % plutonium (theoretical: 88.3 wt % of plutonium in PuO_2). Also seen in this photomicrograph are smaller two-phase particles similar to two-phase particles between the massive reaction product and the porous layer. These particles are similar to those obtained in the Pt-20 wt % Rh coupon. Dark precipitates are present in the parent material of the porous layer and contain plutonium, platinum, and possibly rhodium.

Photomicrographs of the reaction after 90 days at 1000°C are shown in Figures 127 and 128. In general these results are similar to the 90-day tests with Pt-20 wt % Rh. A trace of the x-ray strip chart analysis is shown in Figure 129. By comparing this figure with Figure 112 it can be seen that there is greater enrichment of rhodium and plutonium at the reaction interface in Figure 129, as well as less impurity penetration. The concentration of rhodium is about 68 wt % at the edge and only about 6 wt % in the reaction product. A summary of the depth of penetration of the various impurities in the 90-day samples is given in Table 11. This table shows that the impurity penetration into Pt-40 wt % Rh alloys is appreciably less than the penetration into Pt-20 wt % Rh alloy.

A photomicrograph of a typical portion of the reaction edge is shown in Figure 130. In this figure, all of the phases found in the Pt-20 wt % Rh coupon are seen.

A trace of the x-ray strip chart analysis of the porous interface is shown in Figure 131. A small two-phase reaction product is seen. The dark phase was found to be about 47 at. % platinum, 34 at. % rhodium, and 19 at. % plutonium. The white phase contains rhodium, platinum, fuel impurities, and possibly a trace of plutonium; its approximate composition is given in Table 12. The rhodium-enriched porous layer, which is seen in the trace, appears identical to the white phase just mentioned, with the exception of a lower fuel impurity concentration.

A summary of the approximate composition of the various phases found in these analyses is found in Table 12. In no case was any tantalum found in the reaction products.

With the exception of the phase which is plutonium rich (Figure 112) all of the reaction products exhibit a metallic appearance under the microscope. This suggests a solution of the plutonium by the platinum. This could be explained if substoichiometric PuO_2 is unstable in the presence of platinum and is reduced to plutonium metal. This metal could then combine with the platinum to form intermetallic compounds, leaving behind rhodium-rich phases. Binary phase diagrams between plutonium and platinum and between plutonium and rhodium[8] indicate the existence of several intermetallic compounds: $PuPt_5$, $PuPt_3$, $PuPt_2$, PuPt, and Pu_5Pt_3; and $PuRh_3$, $PuRh_2$, Pu_3Rh_4, PuRh, $PuRh_4$, $PuRh_3$, and Pu_2Rh. No studies of the ternary system platinum-plutonium-rhodium appear to have been made.

Differences in attack between the Pt-20 wt % Rh and Pt-40 wt % Rh include less depletion of platinum (and subsequent enrichment of rhodium) for the latter alloy. This composition change extends to about 50 μm in Pt-40 wt % Rh compared to about 80 μm in Pt-20 wt % Rh. The width of the porous layer was about 30 μm in Pt-40 wt % Rh, which is about the same as in Pt-20 wt % Rh.

Three basic reactions were observed between platinum and platinum-rhodium alloys and $^{238}PuO_2$. (1) In pure platinum, the reaction appeared more continuous compared to the platinum-rhodium alloys. (2) In platinum-rhodium alloys, small two-phase particles were found. One of these phases, best seen in Figure 128, contains plutonium, platinum, and rhodium, while the other phase contains rhodium, iron, and chromium. (3) Finally, impurity diffusion into the substrate was found which decreased with increasing rhodium content. In no case was tantalum found in any of the reaction products. Although it is not possible at this point to establish a mechanism for the reaction, the data suggest that intermetallic compounds between plutonium, platinum, and rhodium are formed. The presence of oxygen in these compounds is questionable. It has been suggested in this report that the production of a substoichiometric PuO_2 may contribute to the incompatibility observed in these samples. However, it should be emphasized that the requirement for a substoichiometric fuel has not been definitely established. Tests are planned to check this possibility.

Impurities In previous descriptions of the interactions of PuO_2 with platinum and platinum-rhodium alloys considerable mention has been made of the presence of fuel impurities at the fuel-metal interface. The presence of these impurities complicates the interpretation of the results. At this point very little information is available as to the effects of these impurities on the surface of platinum or platinum-rhodium alloys. Thus, it is not possible to determine whether these impurities produce a beneficial or a deleterious effect on the surface. Certainly the presence of Kirkendall voids cannot be considered beneficial. However, as noted previously, these voids appear to be associated with the presence of molybdenum in the system. At 1200°C, when molybdenum is absent, no voids are observed. Spalling of the reaction layer implies either a weakened interface or a brittle layer which, of course, cannot be considered beneficial.

According to the fuel analyses given in Appendix B, the most common impurities are aluminum, calcium, chromium, iron, magnesium, manganese, nickel, lead, and zinc. A survey of the binary phase diagrams of these elements with platinum and rhodium is summarized in Table 13.[9,10] From this table it appears that the transition metals (iron, chromium, cobalt, and nickel) form solid solutions with platinum and rhodium, and the rest of the impurities form intermetallic compounds. Some of the latter group of elements, namely manganese and zinc, exhibit some solid solubility in addition to forming compounds. The elements iron, chromium, nickel, cobalt, manganese, and zinc usually appear in a relatively broad reaction zone at the fuel-metal interface which is a manifestation of the solid solubility of these elements in platinum and rhodium. The concentration of these elements is usually highest at the surface, decreasing to zero at some distance from the interface. In Figure 74, a $Pt_3(Fe,Zn)$ compound was found along with a solid solution layer. In general the compound-forming elements have not been observed. Either they do not form the intermetallic compounds predicted by the phase diagrams, or they form small particles that may be pulling out during the polishing operation, or these particles may have been missed by the electron beam microprobe and hence not detected.

The effects of the solid solution layer have not been determined. The presence of these elements could be serious if the solid solution hardening effects of these impurities is great enough or if the density of the reaction layer is low enough so that spalling of the surface could occur. Hardening effects could be appreciable since the differences in the closest approach of atoms for iron, chromium, cobalt, and nickel are 10-11% while for zinc this difference is about 4%.

Microhardness traverses were made across the reaction interface, and typical results are shown in Figures 132 and 133. These curves show an increase in hardness at the interface as expected. From the increase in hardness, it is expected that the strength would increase also. It is conceivable that these impurities could be beneficial to the system by increasing the strength of the metal without enhancing the attack of the

metal by PuO_2. Definite conclusions on the true effect of the impurities must await further testing.

An attempt was made to correlate microhardness changes with microprobe results in order to substitute microhardness data for microprobe data on impurity penetration. If the impurity solid solution hardening was chiefly responsible for the surface hardness increase, then a correlation should be possible. In the curve in Figure 132 a correlation seems feasible. The point of maximum impurity penetration determined with the microprobe is indicated on the curves. Unfortunately, however, this correlation is not universal as shown in Figure 133, and therefore, does not appear useful except perhaps for platinum. The hardness measurements were made with the Vickers indenter, and this may be a large source of error. Another attempt will be made at establishing a correlation using a Knoop indenter.

In view of this inability to establish an acceptable correlation between microprobe data and some other technique, the total number of samples for which penetration data are available is somewhat limited. Impurity penetration data are summarized in Tables 2, 3, 5, 7, and 9. This limited amount of data makes it rather difficult to calculate meaningful rate equations and activation energies. An attempt was made to make these calculations, but scatter in the data produced severe discrepancies in the results. Consequently, further calculation will have to await more data.

X-Ray Analysis of Fuel Attempts to correlate x-ray data in these samples with amount of interaction has met with little success. A summary of x-ray analysis data obtained to date is given in Table 14. While there are some variations in the lattice parameter, these variations are all within the experimental error of the measurements. Therefore, it is not possible to say conclusively that PuO_2 in tantalum containers becomes substoichiometric. In a few cases a lattice expansion is indicated, but unfortunately the trend is not consistent. One explanation of this might be that the samples were stored several months in an argon atmosphere prior to analysis. Whether this had any effect on the results is unknown at this time.

Future Work In view of the difficulties experienced with the molybdenum and the fuel impurities, some of the tests in Table 1 are being duplicated using high purity fuel. These tests are summarized in Table 15. The analyses of the fuel to be used are summarized in Appendix A under the designation PPX-6 and PP-5-69. This material was received at Mound Laboratory as Savannah River Product (SRP). It was given no chemical treatment, although it was sintered at 1200°C for 4 hr and sieved to size. The material was then loaded into capsules as shown in Figures C-7 and C-10. At the present time, SRP material represents the highest purity fuel available in production quantities. Higher purity fuel is possible, but requires special treatment and is therefore not available in the quantities required for a reasonably complete compatibility program. All future tests at Mound Laboratory will be conducted with SRP material. In

addition, studies are under way which are aimed at improving the production processes so that impurities will not be added to the SRP fuel during the reprocessing steps.

In addition it is planned to test substoichiometric fuel, PuO_{2-x}, with these materials in an attempt to determine whether substoichiometry contributes to the incompatibility. The starting material will be $PuO_{1.80-1.85}$ produced from SRP fuel by heating to high temperature in a helium-6 vol % hydrogen atmosphere.

CONCLUSIONS

From the results presented in this report, the following conclusions can be drawn:

1. In the absence of refractory metals no penetration of plutonium into platinum or platinum-rhodium alloys was found, although reactions with fuel impurities occurred.

2. Impurities which form solid solutions with platinum penetrated into the metal surface.

3. In a reducing atmosphere, considerable reaction between PuO_2 and platinum occurred.

4. In the presence of tantalum extensive reaction between PuO_2 and platinum and platinum-rhodium alloys occurred.

5. When molybdenum is present in the system, a molybdenum transport phenomenon occurred, along with the formation of voids parallel to the interface.

6. In the presence of molybdenum a migration of platinum into the fuel was observed.

7. The microhardness of the reaction layer was greater than that of the parent metal.

8. Some spalling of the impurity-platinum reaction layer was observed.

ACKNOWLEDGMENTS

Several members of the Compatibility Group at Mound Laboratory have contributed to this report. Mr. K. L. Breakall and Mr. R. L. Fitzharris were responsible for the metallography, Mr. D. L. Roesch performed all of the electron microprobe analyses, and Mr. L. A. Greene assisted in the welding of the capsules. The authors would also like to thank Dr. B. R. Kokenge for the use of data from the TGA experiments and Dr. R. J. DeSando for the x-ray diffraction data.

REFERENCES

1. B. M. Warmkessel and C. J. Kevane, J. A. Ceram. Soc., 51:11, 663 (1968).

2. W. Bronger and W. Klemm, Z. Anorg. Allgem. Chem., 319, 58 (1962).

3. A. S. Darling, Platinum Metals Review, 11:4, 138 (1967).

4. S. J. Paprocki, K. L. Keller, and W. M. Pardue, The Chemical Reaction of PuO_2 with Reactor Materials, BMI-1580, Battelle Memorial Institute, Columbus, Ohio (May 1962), p. 12.

5. W. C. Pritchard, K. A. Johnson, J. A. Leary, and W. J. Maraman, Compaction and Sintering of PuO_2-Mo Powder Mixtures, LA-2621, Los Alamos Scientific Laboratory, Los Alamos, New Mexico (November 1961), p. 45.

6. G. L. Selman, Platinum Metals Review, 11:4, 132 (1967).

7. H. Ocken and J. H. N. Van Vucht, J. Less Common Metals, 15, 193 (1968).

8. F. H. Ellinger, W. N. Miner, D. R. O'Boyle and F. W. Schonfeld, Constitution of Plutonium Alloys, LA-3870, Los Alamos Scientific Laboratory, Los Alamos, New Mexico (December 1968).

9. M. Hansen and K. Anderko, Constitution of Binary Alloys, 2nd Edition, McGraw-Hill Book Company, Inc., New York, N. Y. (1958).

10. R. P. Elliott, Constitution of Binary Alloys: First Supplement, McGraw-Hill Book Company, Inc., New York, N. Y. (1965).

This page

intentionally

left blank

Table 1

TOTAL TEST MATRIX FOR THE $^{238}PuO_2$-PLATINUM AND PLATINUM-RHODIUM COMPATIBILITY PROGRAM

	Test Series	Material	Time Period (days)	Fuel Batch No.	Sample Analysis	Capsule Design
1200°C	A	Pt, Pt-40 wt % Rh	30	Not Available	569,568	C-1
	B	Pt	7.1, 30, 69, 90, 160	MS-45	569	C-2
	C	Pt, Pt-40 wt % RH	17, __,[a] __,[a] __,[a] ___[a]	P-377 & 378	569, 567	C-3
	D	Pt, Pt-40 wt % Rh	32, 62, 90, 180, 360	P-377 & 378	569, 567	C-4
	E	Pt-10 wt % Rh	83 1/3	69-S-9	Not Available	C-5
	F	Pt-30 wt % Rh	30, 60	PP-6 (micro-spheres)	730	C-6
	G	Pt-30 wt % Rh	30, 60	PPX-25-IV (Powder)	730	C-6
	H	Pt, Pt-40 wt % Rh	30, 60, 90,(180),(360)	PPX-25-IV	569, 360, 361	C-7
1000°C	J	Pt, Pt-20 wt % Rh, Pt-40 wt % Rh	30, 60, 90, 180, 360[a], 720[a]	PPX-18-1	542, 543, 673	C-8
	K	Pt, Pt-20 wt % Rh, Pt-40 wt % Rh	30, 60, 90, 180[a], 360[a], 720[a]	PPX-18-1	542, 543, 673	C-9
800°C	L	Pt, Pt-20 wt % Rh, Pt-40 wt % Rh	30, 66, 90, 180, (360) (720)	PPX-18-1	542, 543, 673	C-8
	M	Pt, Pt-20 wt % Rh, Pt-40 wt % Rh		69-S-52		

[a] = Sample destroyed due to furnace overheat
() = Samples still in furnace

Table 2

SUMMARY OF VOID LAYER AND IMPURITY PENETRATION AT 1200°C

Material	Length of Test (days)	Depth of Void Layer (μm)	Depth of Impurity Penetration (μm)					
			Fe	Cr	Co	Ni	Mo	Mn
Pt-40 wt % Rh, in Ta-10 wt % W	17	52						
Pt-40 wt % Rh in TZM	32	110						
	62	134	190[a]	136[a]	190[a]		105[a]	
	90	189						
	180	200	225	225	225	200	125	
	360	268	300	288	325			
Pt in TZM	32	107						
	62	260						
	90	175	200	187	?	100	50	
			56	125	112	around void	50	81
	180	205	Trace run on corner					
	360	410	475+	400	475+		75	
Pt-10 wt % Rh capsule	83.5	None	260	75				
Pt-30 wt % Rh capsule	30 (powder)	None	175	125				
Pt-30 wt % Rh capsule	30 (micro-spheres)	13 (few)	82	62	82			
Pt-30 wt % Rh capsule	60 (micro-spheres)	None	130	40	175			
Pt-30 wt % Rh capsule	60 (powder)	69 (few)	375				75	
Pt-40 wt % Rh capsule	30	None	75	30				
Pt disc	30	None						
Pt-40 wt % Rh capsule	60	None						
Pt disc	60	None						
Pt-40 wt % Rh capsule	90	None						
Pt-40 wt % Rh disc	90	None	125	25				
Pt disc	90	12	400	170				

[a] Probe trace run in from corner of sample. Impurity penetration not accurate.

Table 3

DEPTH OF PENETRATION OF IMPURITIES AT 1200°C INTO PLATINUM-30 wt % RHODIUM ALLOY SEALED IN AN AIR ATMOSPHERE

	Depth of Penetration (μm) After 30 days		Depth of Penetration (μm) After 60 days	
Powder (Batch No. PPX-25-IV)	Fe	175	Fe	375
	Cr	125	Mo	75
Particles at interface:	Ti, Fe, Si, Pu			
Microspheres (Batch No. PP-6)	Fe	82	Co	175
	Co	82	Fe	130
	Cr	62	Cr	40

Table 4

SUMMARY OF VOID PENETRATION AT 1000°C

Material	Void Penetration (μm) After 30 days	Void Penetration (μm) After 60 days
Platinum	General: 56-150 Line: 113-188	Line: 100 and 150
Pt-20 wt % Rh	General: 66	General: 75
Pt-40 wt % Rh	General: 43	General: 45

	Void Penetration (μm) After 90 days	Void Penetration (μm) After 180 days
Platinum	General: 150 Line: 179 and 216	General: 94 Line: 150 and 207
Pt-20 wt % Rh	General: 94	General: 66 Line: 94
Pt-40 wt % Rh	General: 75	General: 94

Table 5

1000°C IMPURITY DIFFUSION DEPTHS

Material	Diffusion Depth[a] (μm) of Fe After 60 Days	Fe After 180 Days	Zn After 60 Days	Zn After 180 Days	Cr After 60 Days	Cr After 180 Days	Ni After 60 Days	Ni After 180 Days
Pt	220	428	315	439	165	267	0	0
Pt-20 wt % Rh	110	199	110	204	105	140	0	0
Pt-40 wt % Rh	70 85[b]	169	60	166	75	126	0	0

[a] These depths are measured from the sample edge though most of the impurities lie below the molybdenum diffusion.

[b] Concentration found below the bulk diffusion, assumed to be in a grain boundary.

Table 6

APPROXIMATE COMPOSITIONS OF SURFACE LAYERS
IN 180 DAY - 1000°C TEST SAMPLES

Test Material	Molybdenum Concentration Across Intermetallic	Composition (at.%) Pt	Rh	Mo	Pt/Rh Std	Pt/Rh Layer	Pt+Rh / Mo
Pt	level	86.6	-	13.4	∞	∞	6.46
Pt-20 wt % Rh	level	57.5	22.5	20.0	2.067	2.56	4.00
Pt-40 wt % Rh	Two Intermetallics						
	(1) Gradient						
	(a) Exterior	31.9	41.6	26.5	0.795	0.767	2.77
	(b) Interior	40.5	37.5	22.0	0.795	1.080	3.55
	(2) Gradient						
	(a) Exterior	31.2	49.8	19.1	0.795	0.627	4.24
	(b) Interior	31.6	50.6	17.8	0.795	0.625	4.62

Table 7

MOLYBDENUM DIFFUSION DATA[a] AT 1000°C

Test Material	Length of Thermal Exposure (days)	Thickness of Intermetallic (μm)	Bulk Diffusion Depth (μm)	Rate Constant (cm^2/sec) (Bulk)
Pt	30		60	
	60	53	85	1.4×10^{-11}
	90	95	135	
	180	107	150	
Pt-20 wt % Rh	30		66	
	60	38	80	
	90	62	87	
	180	72	94	
Pt-40 wt % Rh	30		30	
	60	27	48	4.76×10^{-12}
	90	56	66	
	180	66	85	

[a] These values are typical of the middle of the coupon. Depths and thicknesses varied along surface, being larger at the ends. (see Figure 66)

Table 8

SUMMARY OF VOID PENETRATION AT 800°C

Material	Depth of Penetration (μm) after 30 Days	66 Days	90 Days	180 Days
Pt	3	7-21	10-35	15-36
Pt-20 wt % Rh	None	None	2-3	None
Pt-40 wt % Rh	None	None	1-4	5-7

Table 9

IMPURITY DIFFUSION DEPTHS AT 800°C

Test Material	Depth of Diffusion (μm) of Fe after 66 Days	Fe after 180 Days	Zn after 66 Days	Zn after 180 Days	Cr after 66 Days	Cr after 180 Days	Ni after 66 Days	Ni after 180 Days
Pt	20	63	30	63	10-15	53	0	0
Pt-20 wt % Rh	25-30 55[a]	35 55[a]	10	20	25	31	0	0
Pt-40 wt % Rh	5-10 35[a]	40	0	0	5	28	5-10	0

[a] Concentrations of iron were found below the bulk diffusion, apparently the result of preferential grain boundary diffusion.

Table 10

APPROXIMATE COMPOSITIONS OF PHASES IN PARTICLE OF REACTION PRODUCT IN Pt-20 wt % Rh SAMPLE AFTER 90 DAYS AT 1000°C IN TANTALUM CONTAINER

	Composition of Phase A (gray phase) (at. %)	Composition of Phase B (light colored - optically active) (at. %)
Platinum	78	84.5
Rhodium	2.4	2.9
Plutonium	19.6	12.6

Table 11

DIFFUSION OF FUEL IMPURITIES IN Pt-40 wt % Rh AFTER 90 DAYS AT 1000°C IN TANTALUM CONTAINER

Fuel Impurity	Diffusion Depth (μm) in Pt-20 wt % Rh	Diffusion Depth (μm) in Pt-40 wt % Rh	Impurity conc in Pt-40 wt % Rh / Impurity conc in Pt-20 wt % Rh
Fe	43	28	0.32
Zn	58	48	0.41
Cr	33	15	0.17

Table 12

SUMMARY OF APPROXIMATE COMPOSITIONS OF PHASES IN SAMPLES TESTED IN TANTALUM CONTAINER AT 1000°C

Material	Test Period (days)	Phase	Composition Pt (wt %)	Pt (at.%)	Rh (wt %)	Rh (at.%)	Pu (wt %)	Pu (at.%)
Pt	60	Massive phase (B in Fig. 106)	75	?	-	-	?	?
Pt-20 wt % Rh	60	Massive phase (C in Fig. 108)	45	?	10	?	?	?
	90	Massive phase (Reaction product in Fig. 112)	74	76	9	17	10	8
	90	Massive						
		Recrystallized (B in Fig. 120)	75	84	3	6	11	10
		Unrecrystallized (A in Fig. 120)	68	79	2	5	17	16
Pt-20 wt % Rh	60	Small Two-phase						
		Dark Phase (A in Fig. 108)	56	?	14	?	?	?
		White Phase	44	?	50	?	Minor	
Pt-40 wt % Rh	60	Massive (C in Fig. 126)	38	41	15	30	33	29
	90	Massive (C in Fig. 130)	61	?	6	?	?	?
Pt-40 wt % Rh	60	Small Two-phase						
		Dark Phase (A in Fig. 126)	44	41	23	41	23	18
		White Phase[a]	20	?	42	?	Possible Trace	
	90	Small Two-phase						
		Dark Phase (A in Fig. 130)	48	47	18	34	24	19
		White Phase[a] (B in Fig. 130)	22	?	86	?	Trace	

[a] Impurity concentration (Fe & Cr) of the white phase in the 60-day sample was about 4 times that of the 90-day sample.

Table 13

SUMMARY OF THE BINARY PHASE DIAGRAMS OF IMPURITY ELEMENTS WITH PLATINUM AND RHODIUM

Impurity Element	Impurity Element-Platinum System	Impurity Element-Rhodium System
Al	Intermetallic compounds	Intermetallic compounds
Ca	At least one intermetallic compound	At least one intermetallic compound
Co	Complete solid solubility, with some ordering	Complete solid solubility, with some ordering
Cr	Extensive solid solubility with intermetallic compound possible	Solid solution with intermetallic compounds
Fe	Complete solid solubility, with some ordering	Extensive solid solubility with ordering
Mg	Intermetallic compounds	Intermetallic compounds
Mn	Complete solid solubility with some ordering (compounds possible)	Solid solubility with ordering with intermetallic compounds
Ni	Complete solid solubility with some ordering	No information available
Pb	Intermetallic compounds	Intermetallic compounds
Zn	Solid solubility with intermetallic compounds	Intermetallic compounds

Table 14

SUMMARY OF X-RAY ANALYSES PERFORMED

Test Series[a]	Temperature (°C)	Time (days)	Lattice Parameter (Å)	Phases Present
B	1200	7.1	5.4126(6)	$PuO_{1.96}$-$PuO_{2.00}$ + α Al_2O_3[b]
	1200	30	5.4152(3)	$PuO_{1.96}$-$PuO_{2.00}$
	1200	69	5.4147(5)	$PuO_{1.96}$-$PuO_{2.00}$
	1200	90	5.4155(4)	$PuO_{1.96}$-$PuO_{2.00}$
C	1200	17	5.4089(10)	$PuO_{1.96}$-$PuO_{2.00}$
D	1200	32	5.4164(13)	$PuO_{1.96}$-$PuO_{2.00}$
	1200	32	5.4098(6)	$PuO_{1.96}$-$PuO_{2.00}$
	1200	62	5.4081(17)	$PuO_{1.96}$-$PuO_{2.00}$ + αAl_2O_3[b]
	1200	62	5.4134(19)	$PuO_{1.96}$-$PuO_{2.00}$
	1200	90	5.4143(3)	$PuO_{1.96}$-$PuO_{2.00}$
	1200	90	5.4134(4)	$PuO_{2.00}$
	1200	180	5.4147(4)	$PuO_{2.00}$
	1200	180	5.4138(4)	$PuO_{1.96}$-$PuO_{2.00}$ + αAl_2O_3[b] Possible α CuTi (?)
E	1200	$83\frac{1}{3}$	5.4141(2)	$PuO_{1.96}$-$PuO_{2.00}$
F	1200	30	5.4145(24)	$PuO_{1.96}$-$PuO_{2.00}$
	1200	60	5.4151(4)	$PuO_{2.00}$
G	1200	30	5.4140(5)	$PuO_{1.96}$-$PuO_{2.00}$
	1200	60	5.4133(4)	$PuO_{1.96}$-$PuO_{2.00}$
J	1000	30	5.4150(4)	$PuO_{1.96}$-$PuO_{2.00}$
	1000	60	5.4130(6)	$PuO_{1.96}$-$PuO_{2.00}$
K	1000	30	5.4175(9)	$PuO_{1.96}$-$PuO_{2.00}$
	1000	60	5.4128(11)	$PuO_{1.96}$-$PuO_{2.00}$
L	800	30	5.4147(5)	$PuO_{1.96}$-$PuO_{2.00}$ + αAl_2O_3[b]
	800	60	5.4135(3)	$PuO_{1.96}$-$PuO_{2.00}$

[a] See Table 1.
[b] The αAl_2O_3 probably came from the abrasive cutoff wheel.

Table 15

SUMMARY OF WORK PLANNED IN THE NEAR FUTURE

Temperature (°C)	Material	Time Period (days)	Capsule Design
1200	Pt,Pt-40 wt % Rh	30, 60, (90), (180), (360)	C-7
1000	Pt,Pt-20 wt % Rh Pt-40 wt % Rh	(30), (60), (90), (180), (360), (720)	C-10
800	Pt,Pt-20 wt % Rh Pt-40 wt % Rh	(30), (60), (90), (180), (360), (720)	C-10
1000[a]	Pt,Pt-20 wt % Rh Pt-40 wt % Rh	30, 60, 120, 360	C-10 (Substoichiometric fuel)
1000[a]	Pt,Pt-20 wt % Rh Pt-40 wt % Rh	30, 60, 90, 180, 360, 720	C-9

[a] = Sample not loaded as yet (9/15/69)
( ) = Sample still in furnace

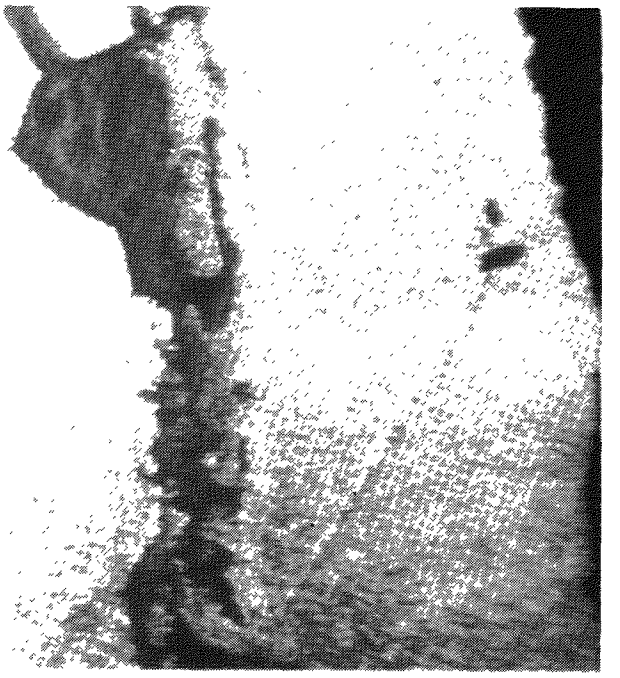

FIGURE 1 - Photomicrograph of reaction between platinum and 238-plutonium dioxide microspheres after 30 days at 1200°C. 240X

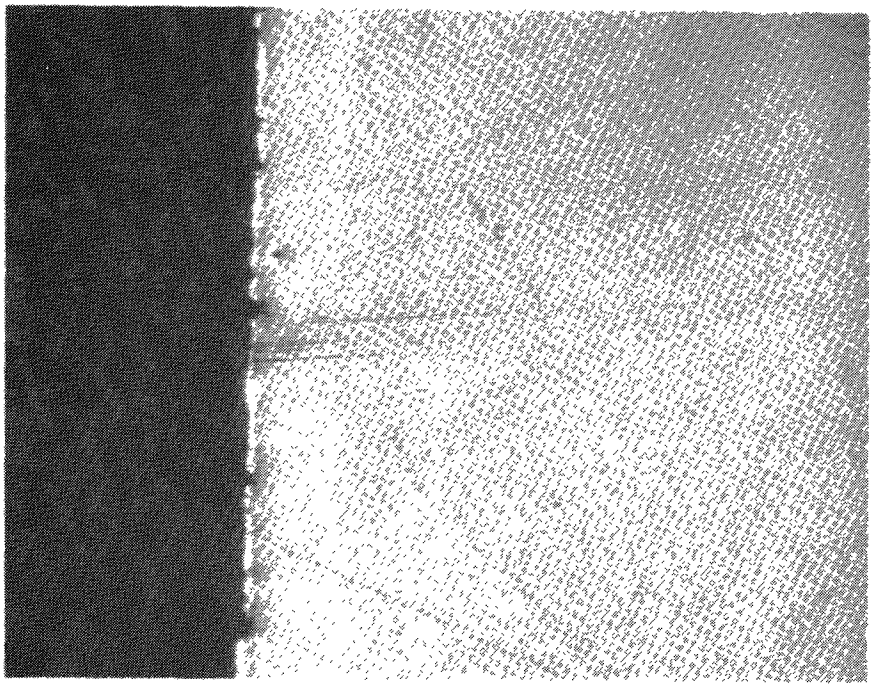

FIGURE 2 - Photomicrograph of reaction between platinum-40 wt % rhodium alloy and 238-plutonium dioxide microspheres after 30 days at 1200°C. 240X

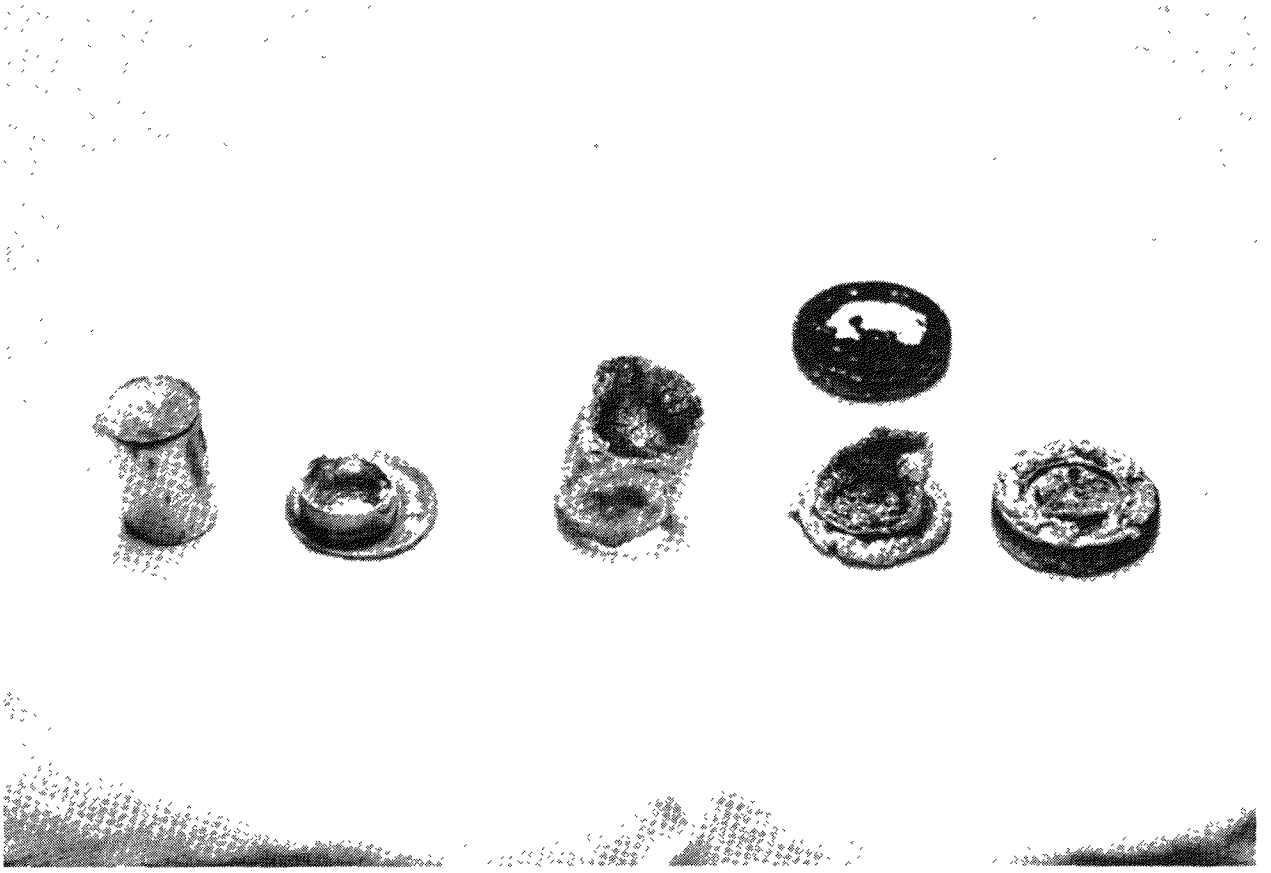

FIGURE 3 - Platinum sample after 90 days at 1200°C. Capsule on the left was a standard with no fuel. Capsule on the right contained fuel.

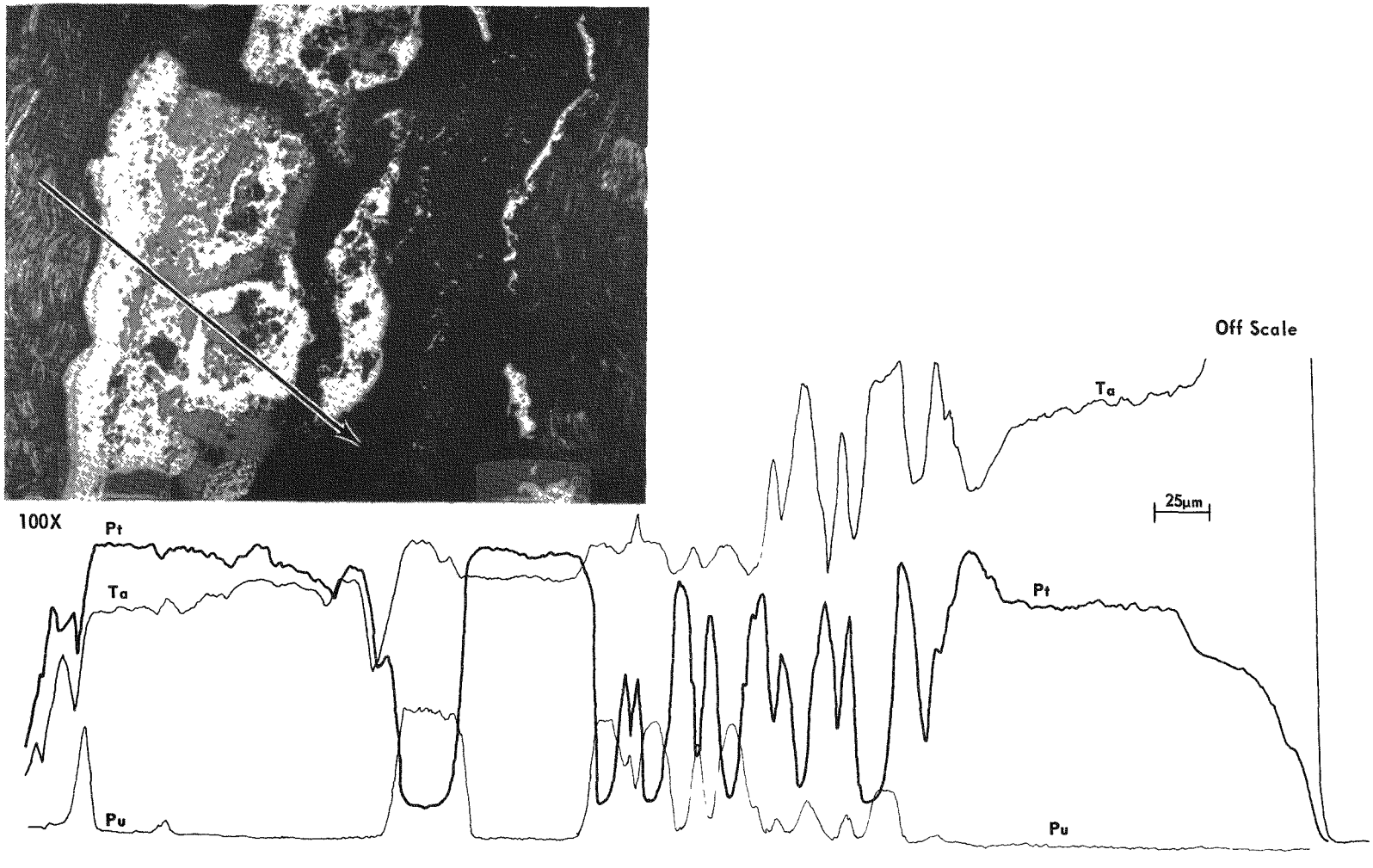

FIGURE 4 - X-ray strip chart analysis of interface between platinum/tantalum and $^{238}PuO_2$ after 69 days at 1200°C.

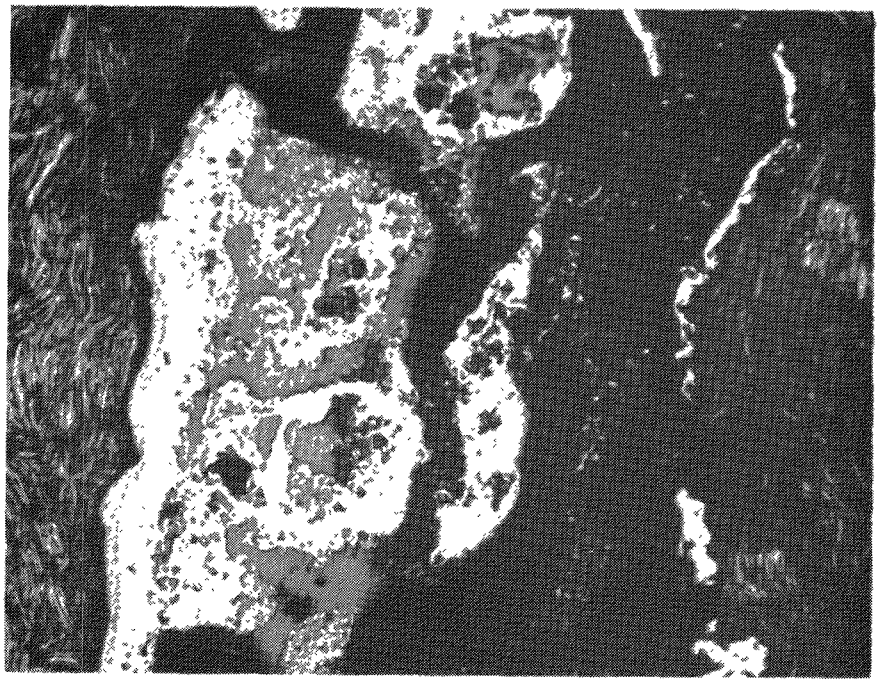

FIGURE 5 - Photomicrograph of reaction in platinum cup, in contact with tantalum, after 69 days at 1200°C. Unetched 100X

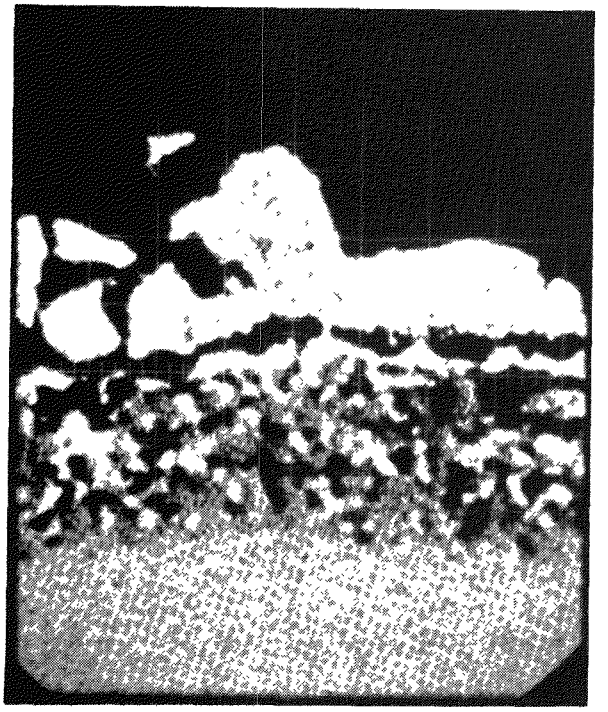

FIGURE 6 - Photomicrograph of platinum-40 wt % rhodium sample taken with back-scattered electrons: 408 hr at 1200°C. 440X

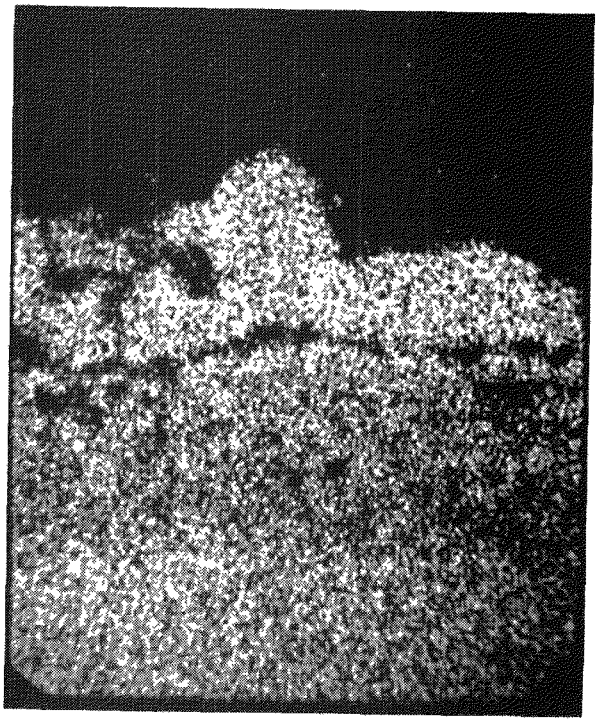

FIGURE 7 - Photomicrograph of platinum-40 wt % rhodium sample taken with platinum Lα radiation: 408 hr at 1200°C. 440X

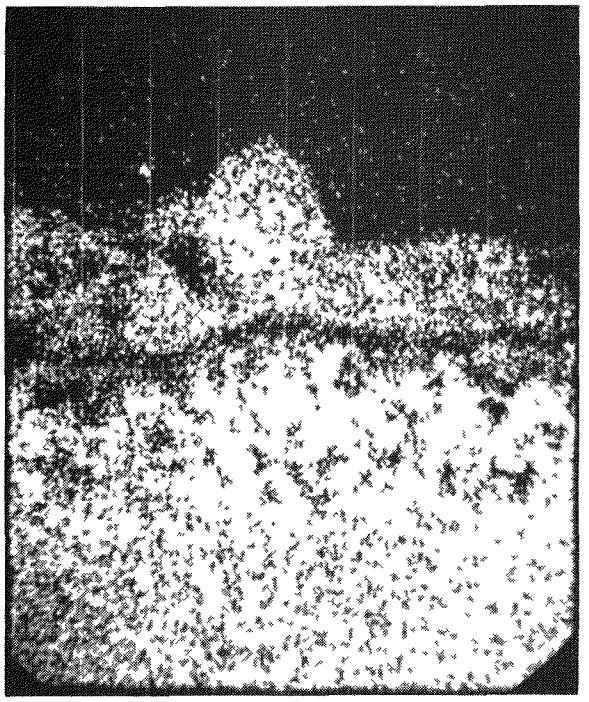

FIGURE 8 - Photomicrograph of platinum-40 wt % rhodium sample taken with rhodium Lα radiation: 408 hr at 1200°C. 440X

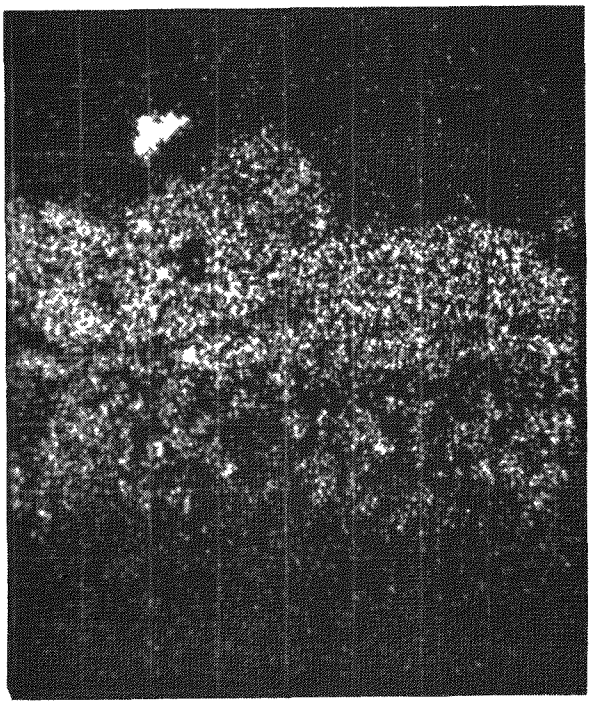

FIGURE 9 - Photomicrograph of platinum-40 wt % rhodium sample taken with plutonium Mα radiation: 408 hr at 1200°C. 440X

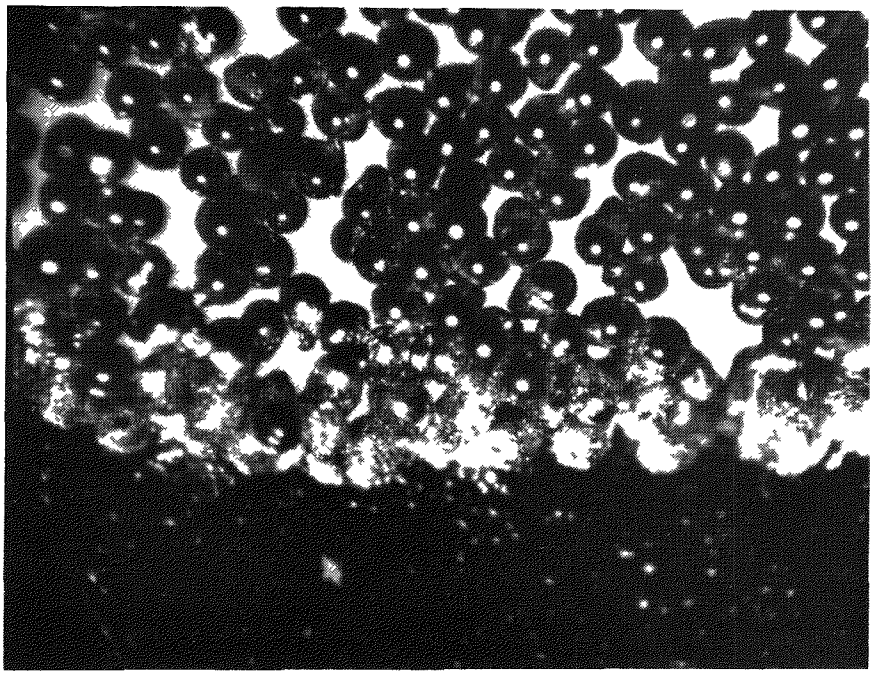

FIGURE 10 - Photograph of the edge of the platinum pan showing platinum coating on the microspheres. 30X

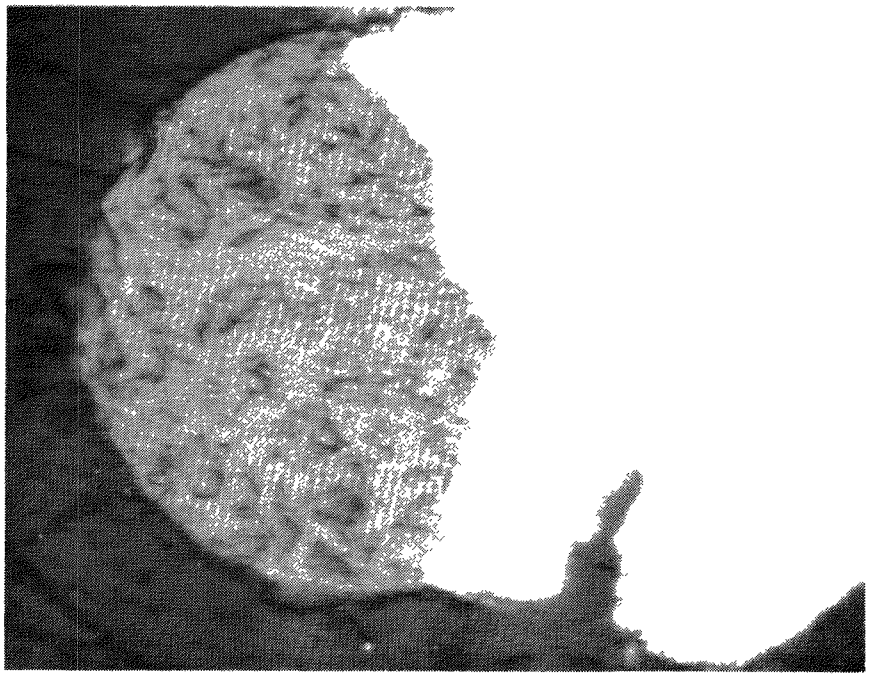

FIGURE 11 - Photomicrograph of the interface between 239-plutonium dioxide microsphere and platinum heated in helium-6 wt % hydrogen atmosphere. unetched 100X

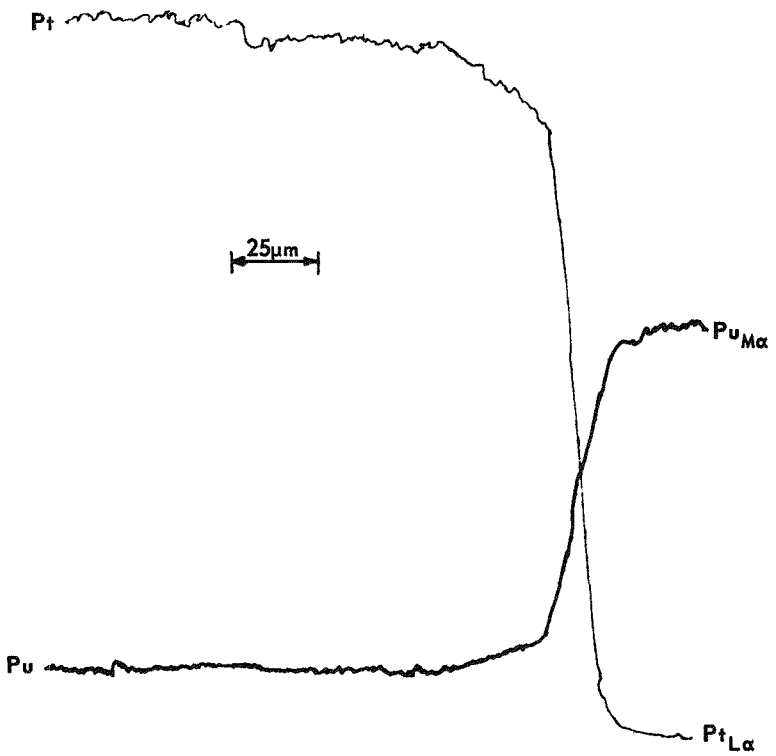

FIGURE 12 - X-ray strip chart analysis across the microsphere-platinum interface after heating in helium-6 wt % hydrogen atmosphere.

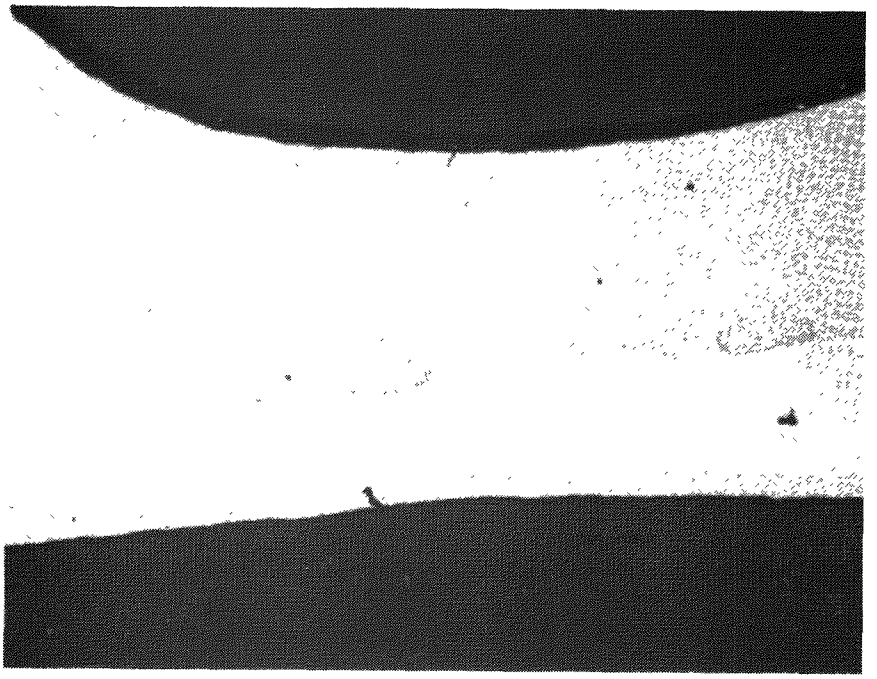

FIGURE 13 - Photomicrograph of reaction interface between 238-plutonium dioxide pellet and platinum after heating to 1330°C in a helium-6 wt % hydrogen atmosphere. unetched 25X

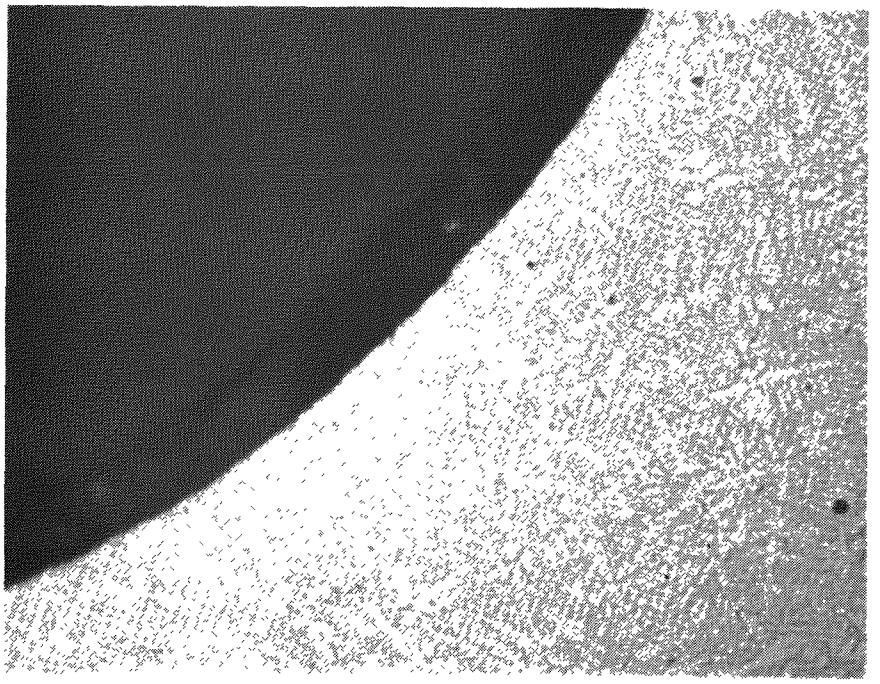

FIGURE 14 - Photomicrograph of reaction product between 238-plutonium dioxide pellet and platinum after heating to 1330°C in a helium-6 wt % hydrogen atmosphere. unetched 250X

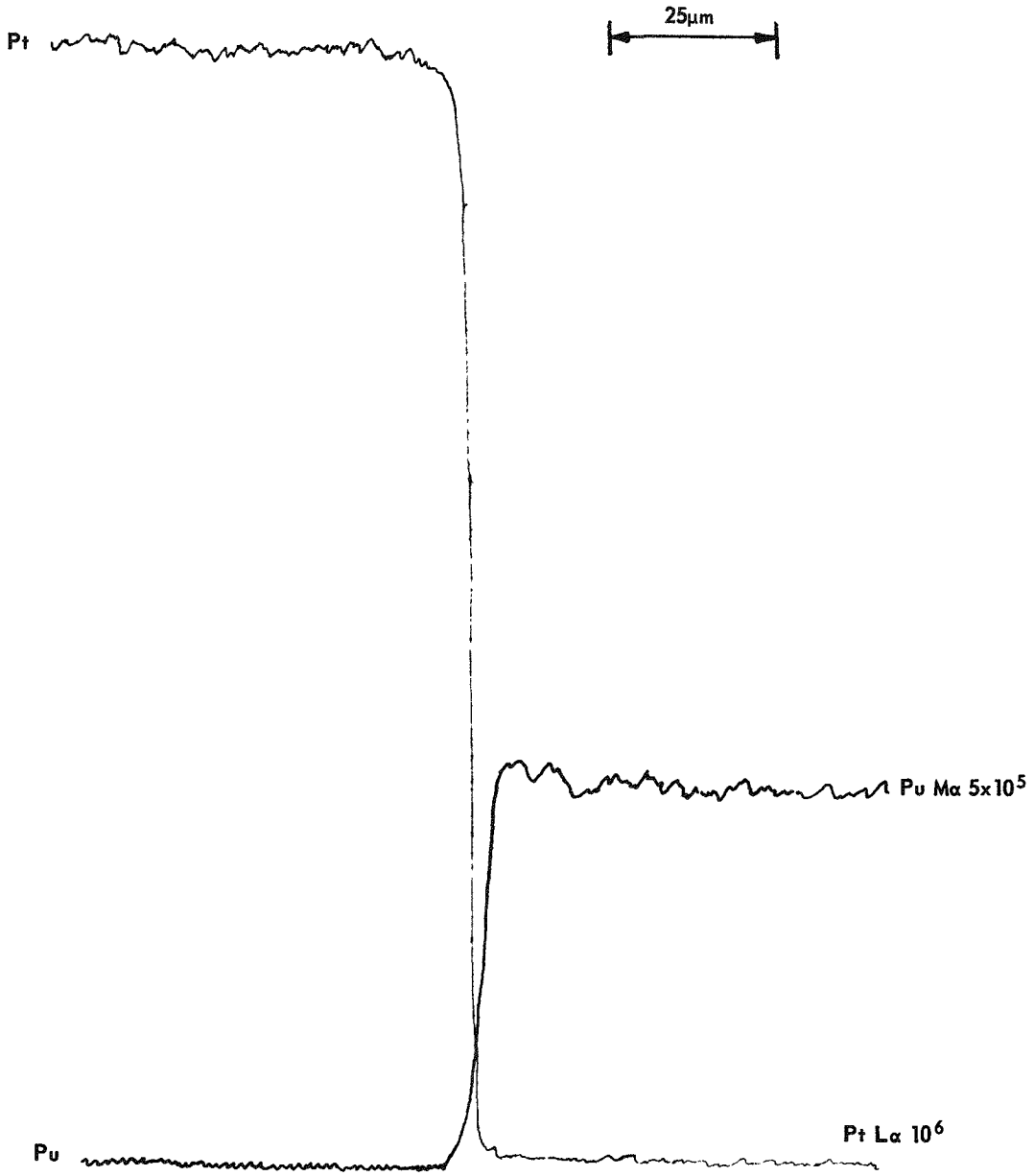

FIGURE 15 - X-ray strip chart analysis of microsphere-platinum interface after heating in air.

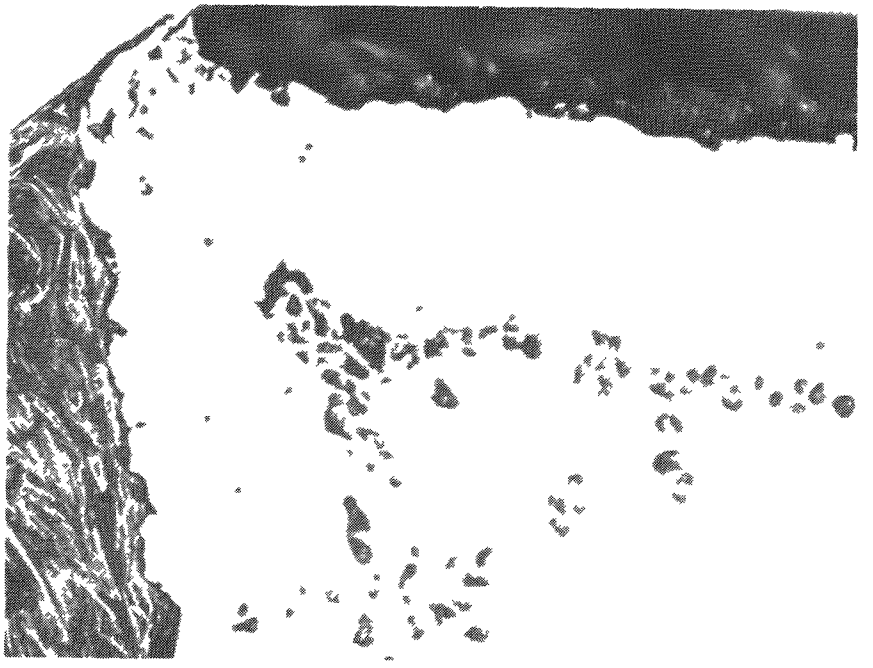

FIGURE 16 - Reaction zone of a platinum-40 wt % rhodium sample in contact with 238-plutonium dioxide in a TZM liner; 62 days at 1200°C. unetched 260X

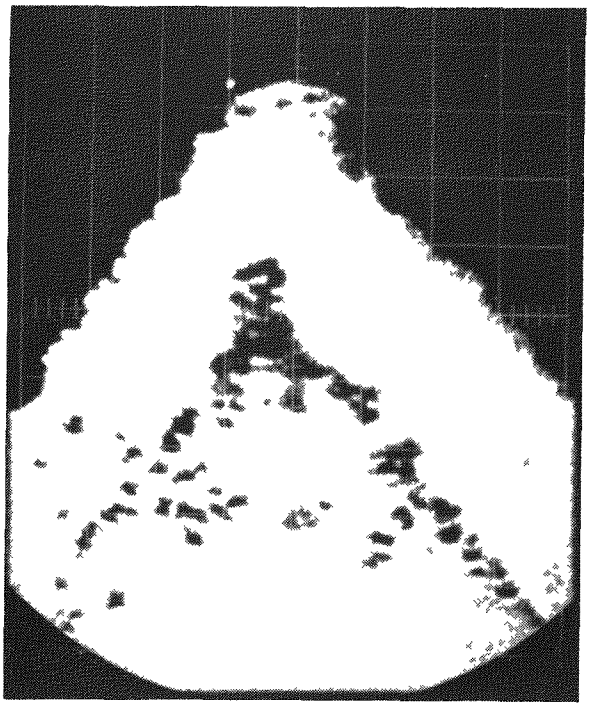

FIGURE 17 - Photomicrograph of reaction zone in platinum-40 wt % rhodium sample taken with backscattered electrons: 62 days at 1200°C. 220X

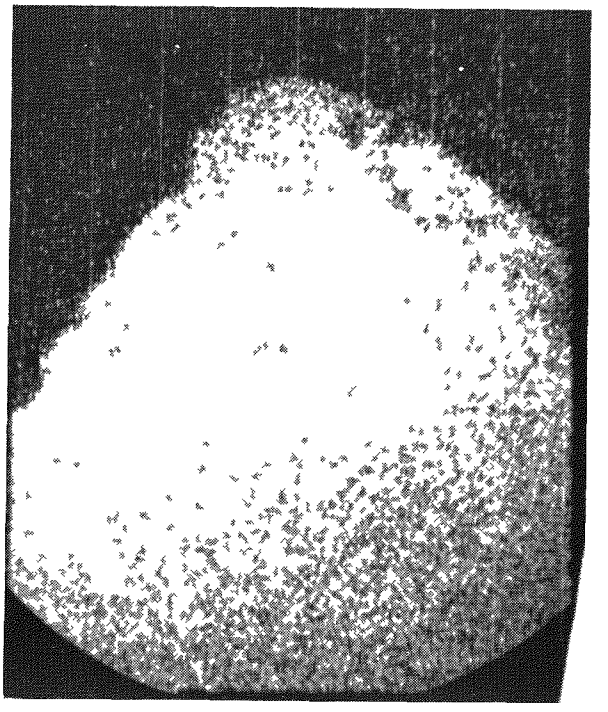

FIGURE 18 - Photomicrograph of reaction zone in platinum-40 wt % rhodium sample taken with platinum Lα radiation: 62 days at 1200°C. 220X

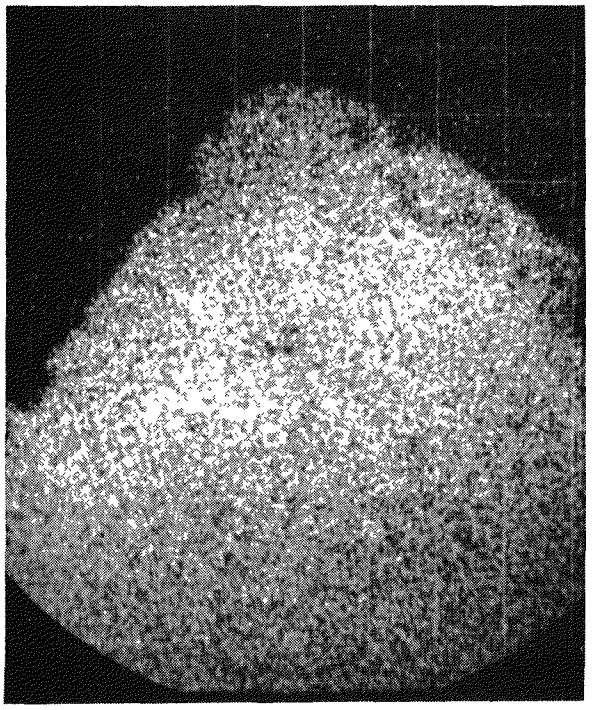

FIGURE 19 - Photomicrograph of reaction zone in platinum-40 wt % rhodium sample taken with rhodium Lα radiation: 62 days at 1200°C. 220X

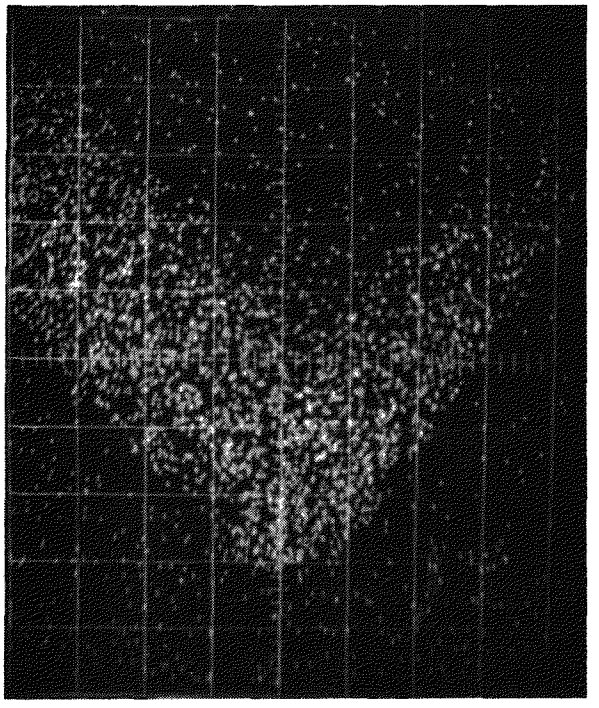

FIGURE 20 - Photomicrograph of reaction zone in platinum-40 wt % rhodium sample taken with molybdenum Lα radiation: 62 days at 1200°C. 220X

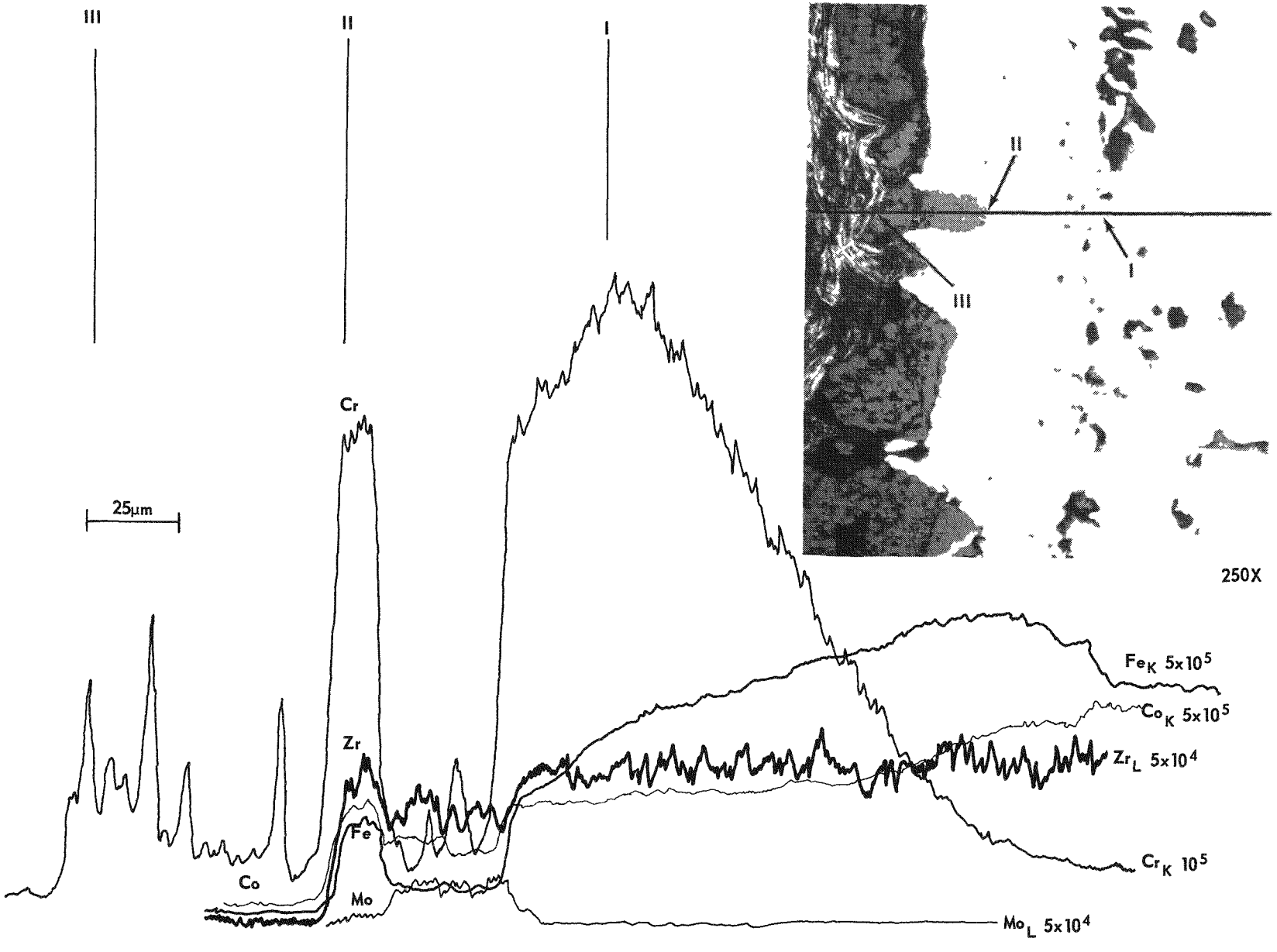

FIGURE 21a - X-ray strip chart analysis of platinum sample tested for 90 days at 1200°C.

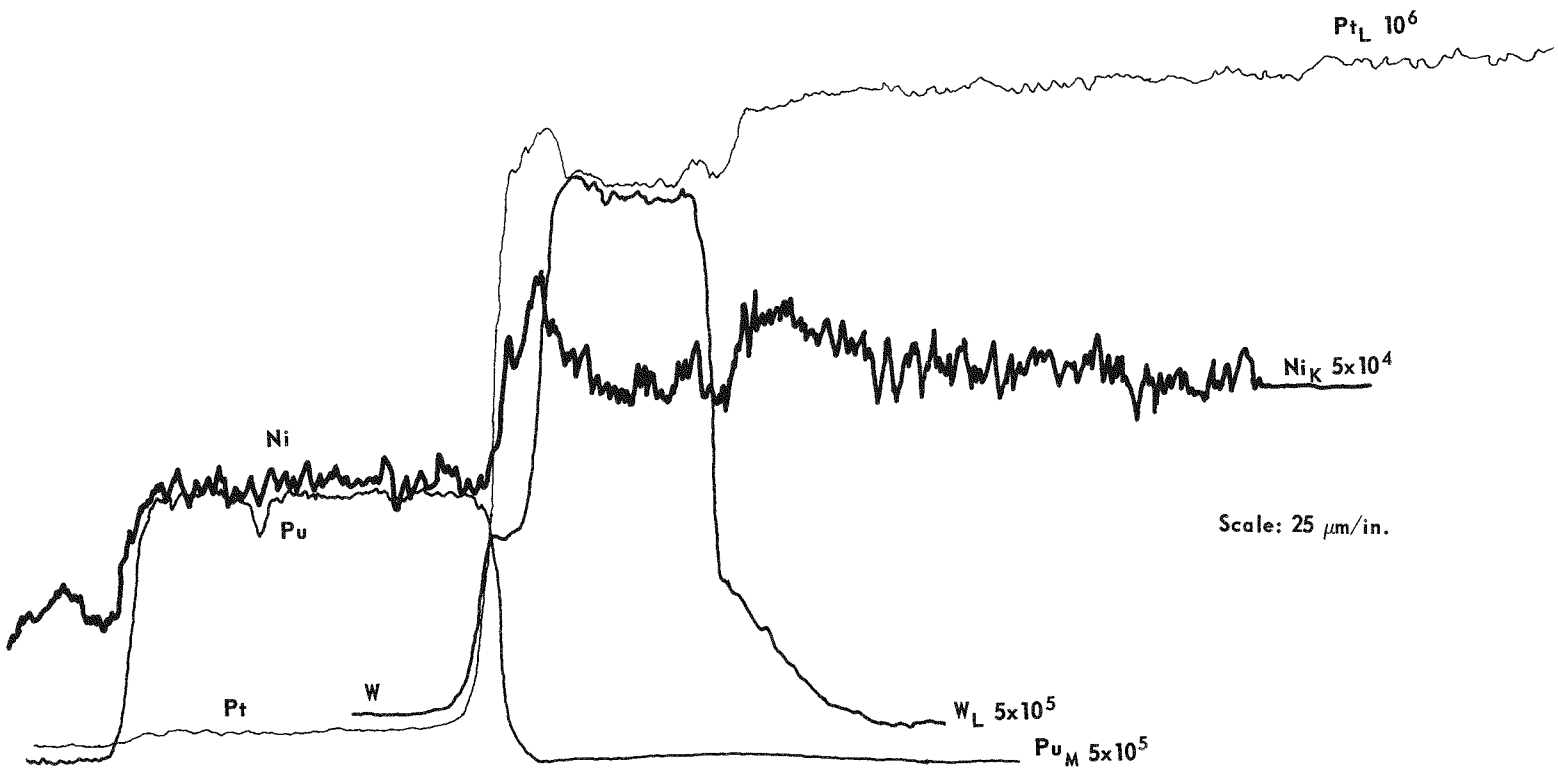

FIGURE 21b - X-ray strip chart analysis of platinum sample tested for 90 days at 1200°C.

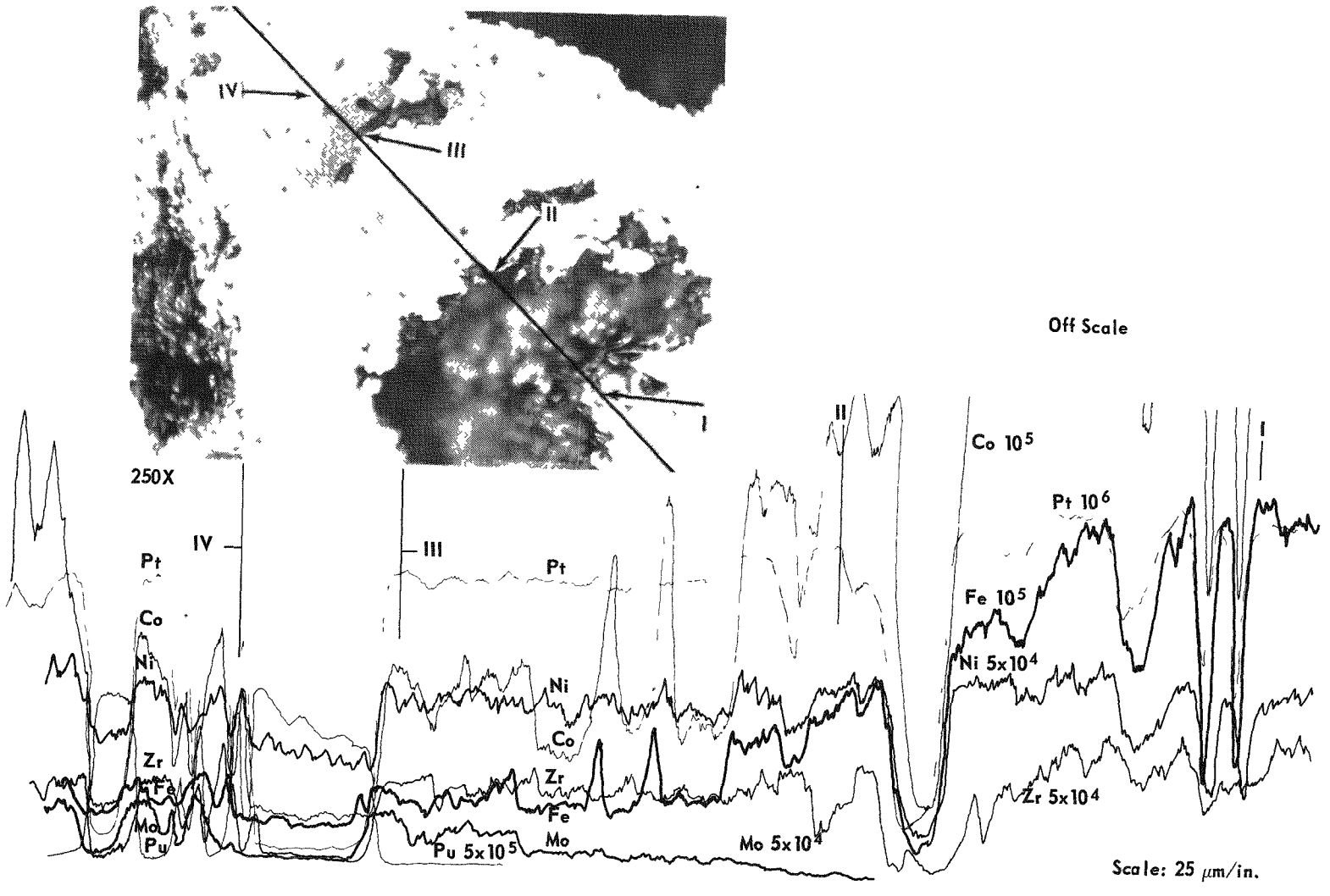

FIGURE 22 - X-ray strip chart analysis of platinum sample tested for 180 days at 1200°C.

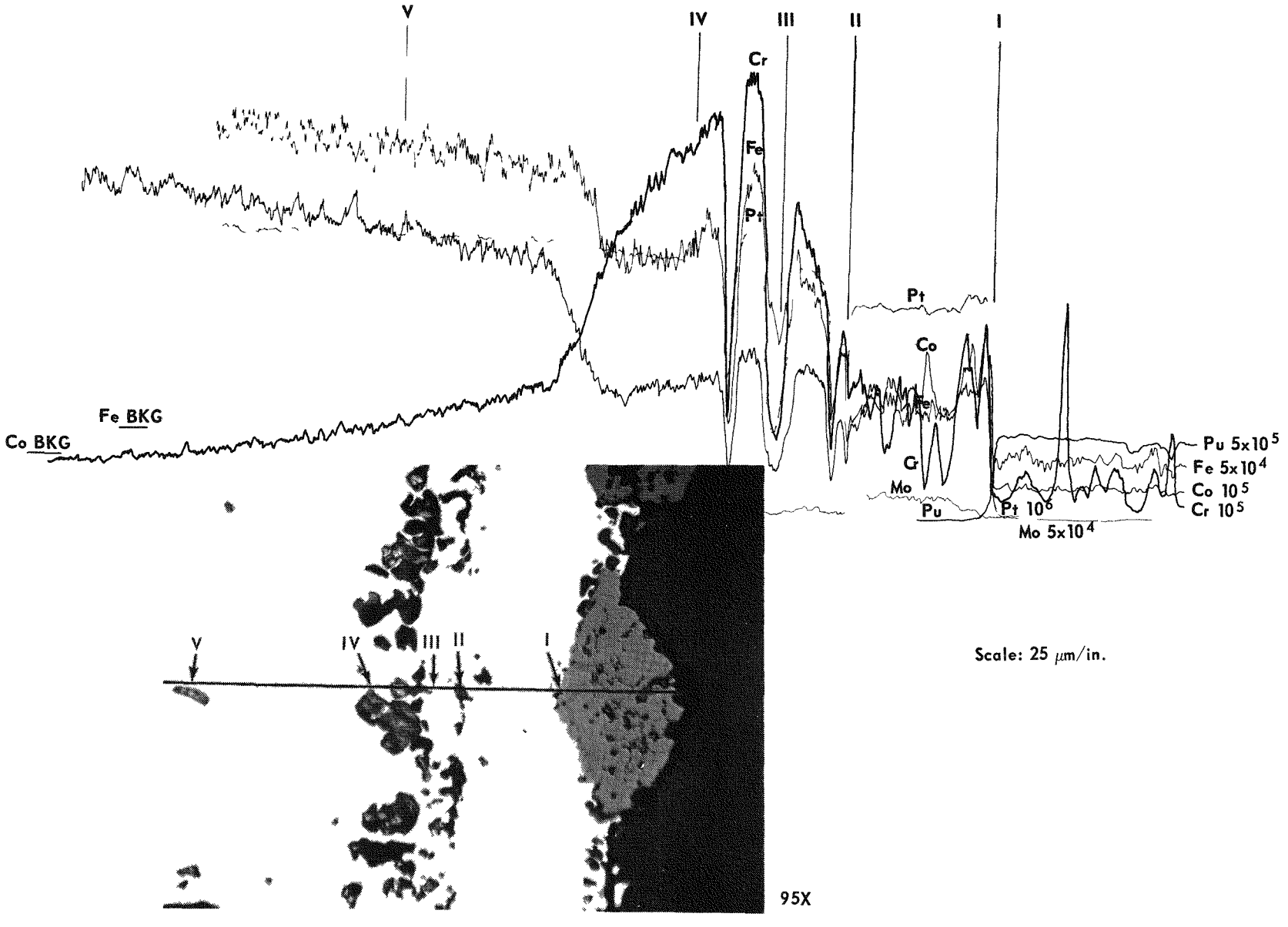

FIGURE 23 - X-ray strip chart analysis of platinum sample tested for 360 days at 1200°C.

FIGURE 24 - Photomicrograph of reaction zone in platinum sample taken with back-scattered electrons: 360 days at 1200°C. 220X

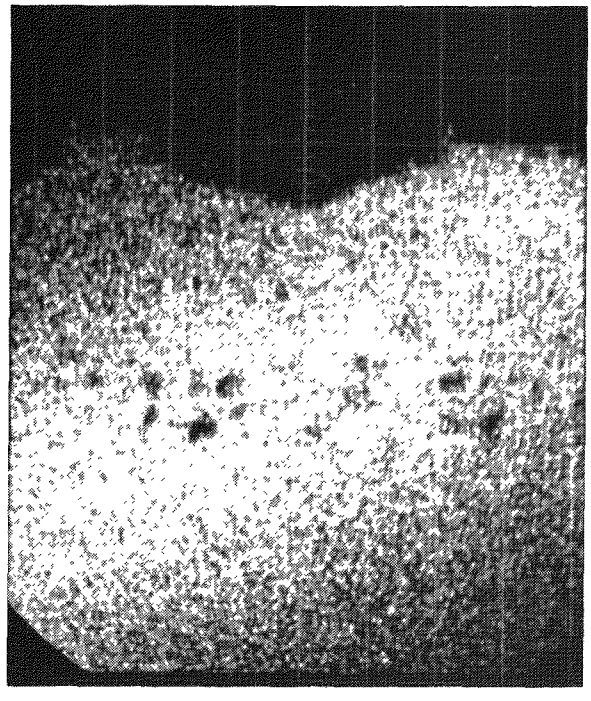

FIGURE 25 - Photomicrograph of reaction zone in platinum sample taken with platinum Lα radiation: 360 days at 1200°C. 220X

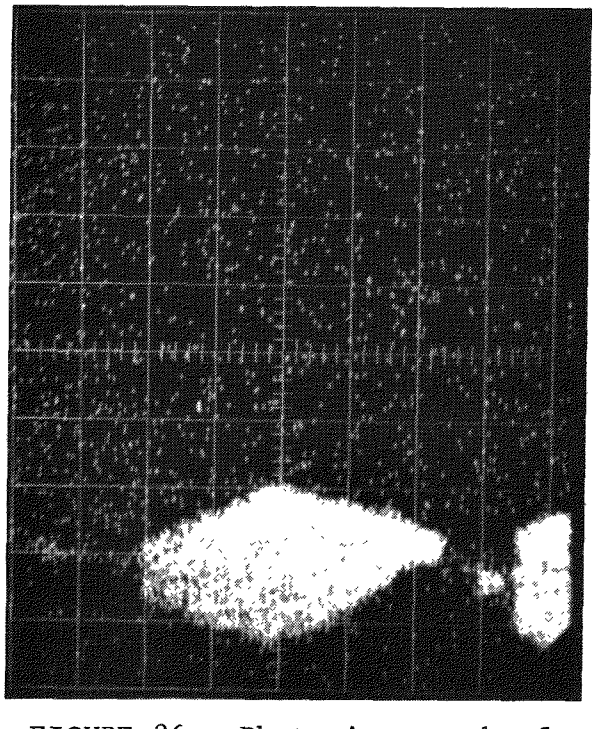

FIGURE 26 - Photomicrograph of reaction zone in platinum sample taken with plutonium Mα radiation: 360 days at 1200°C. 220X

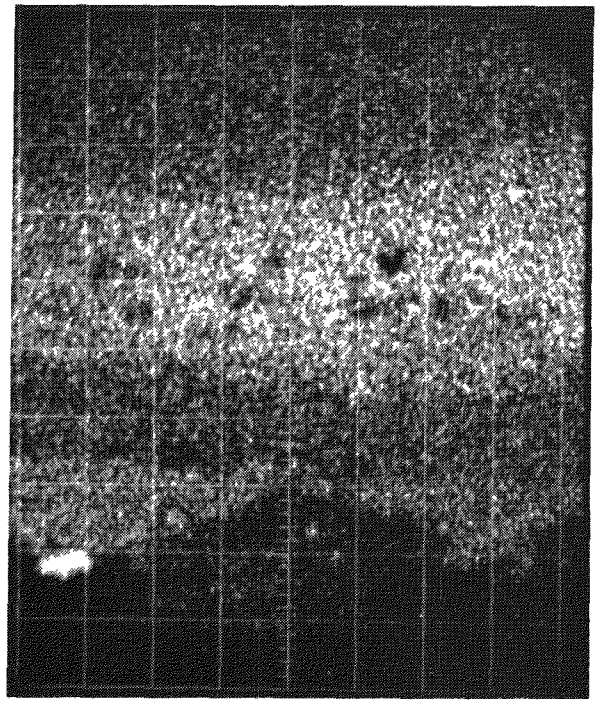

FIGURE 27 - Photomicrograph of reaction zone in platinum sample taken with chromium Kα radiation: 360 days at 1200°C. 220X

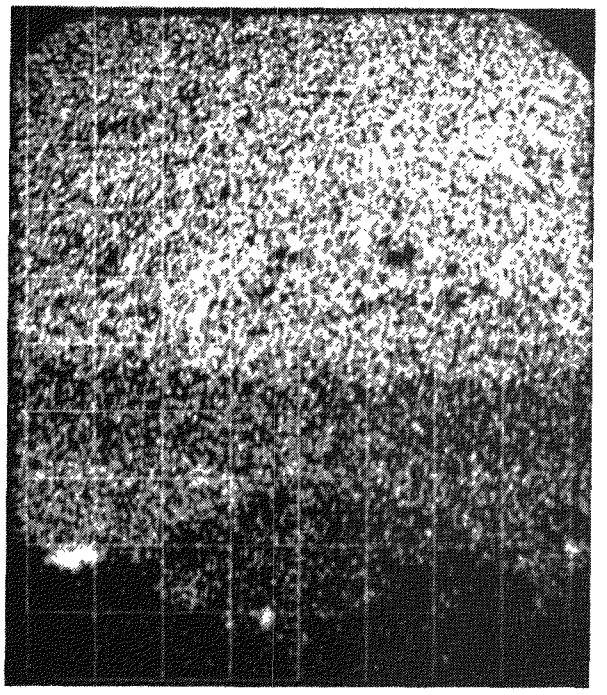

FIGURE 28 - Photomicrograph of reaction zone in platinum sample taken with iron Kα radiation: 360 days at 1200°C. 220X

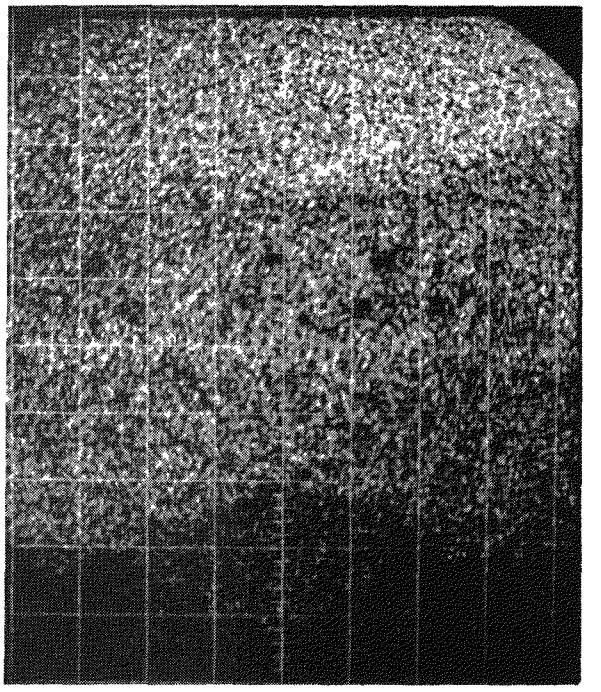

FIGURE 29 - Photomicrograph of reaction zone in platinum sample taken with cobalt Kα radiation: 360 days at 1200°C. 220X

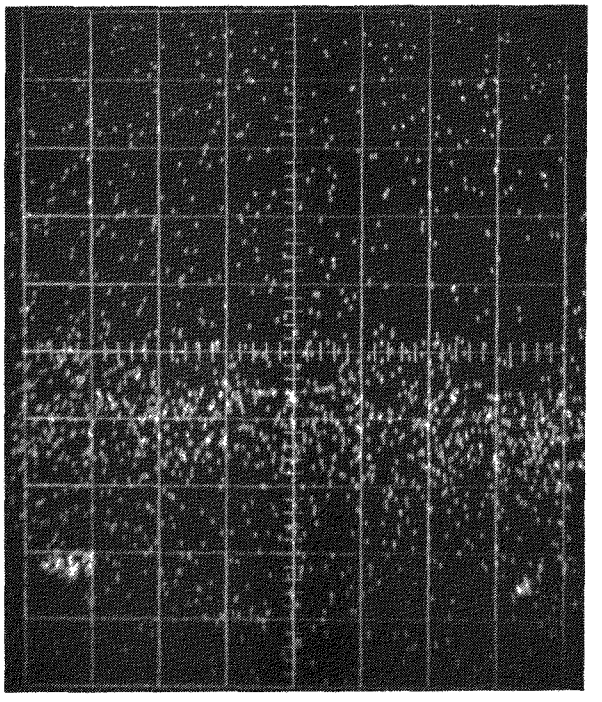

FIGURE 30 - Photomicrograph of reaction zone in platinum sample taken with molybdenum Lα radiation: 360 days at 1200°C. 220X

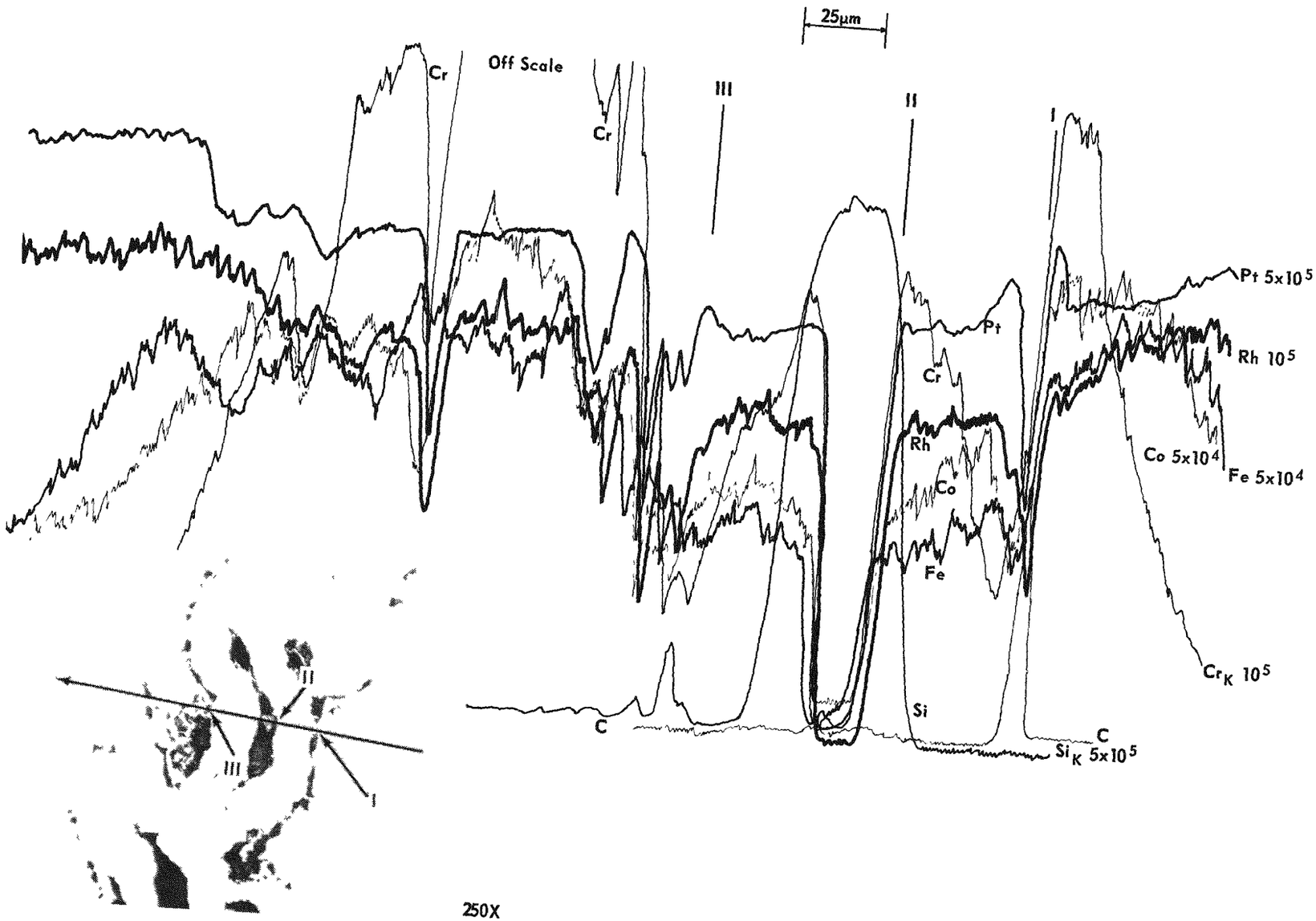

FIGURE 31 - X-ray strip chart analysis of platinum-40 wt % rhodium sample tested for 90 days at 1200°C.

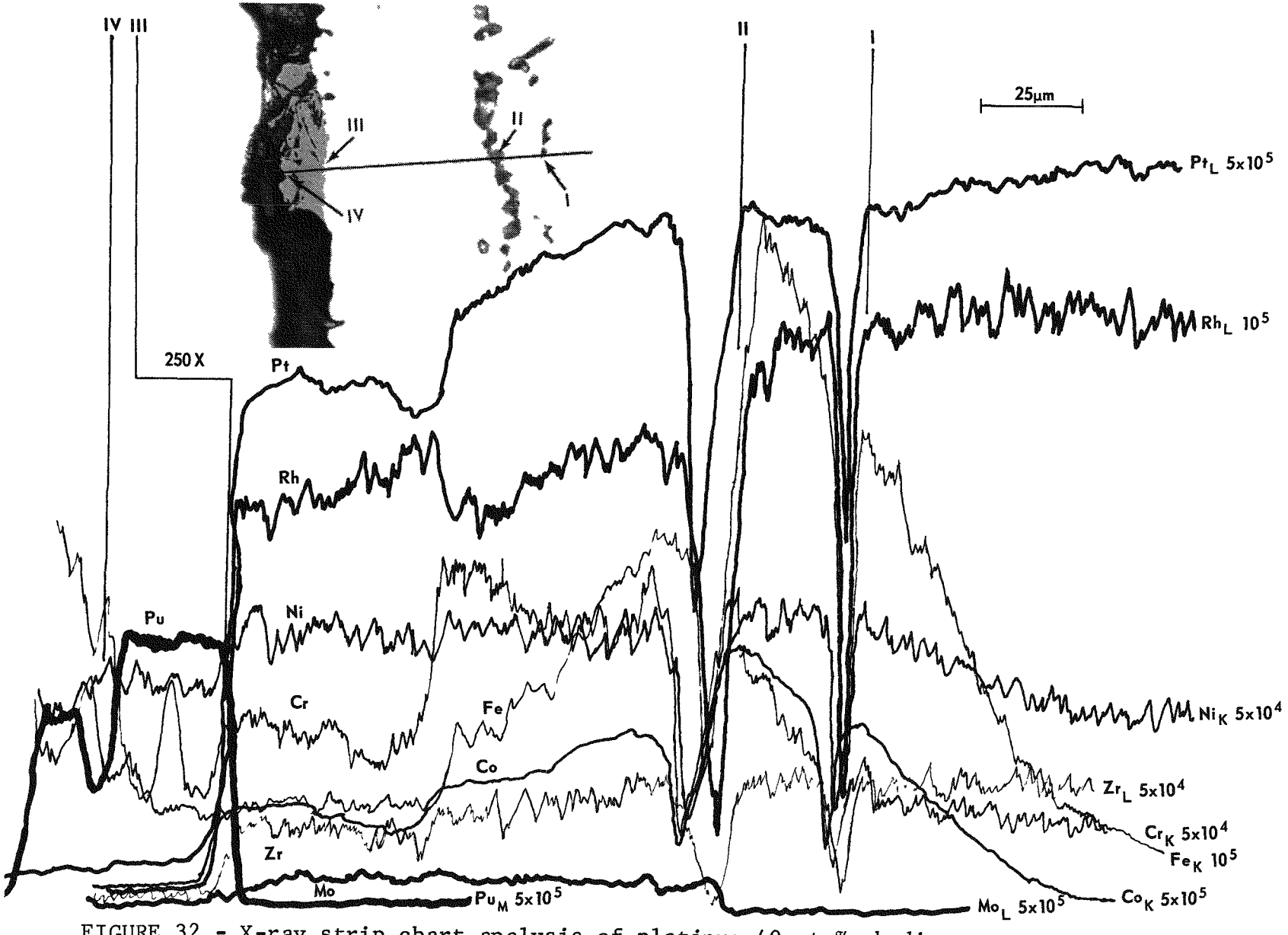

FIGURE 32 - X-ray strip chart analysis of platinum-40 wt % rhodium sample tested for 180 days at 1200°C.

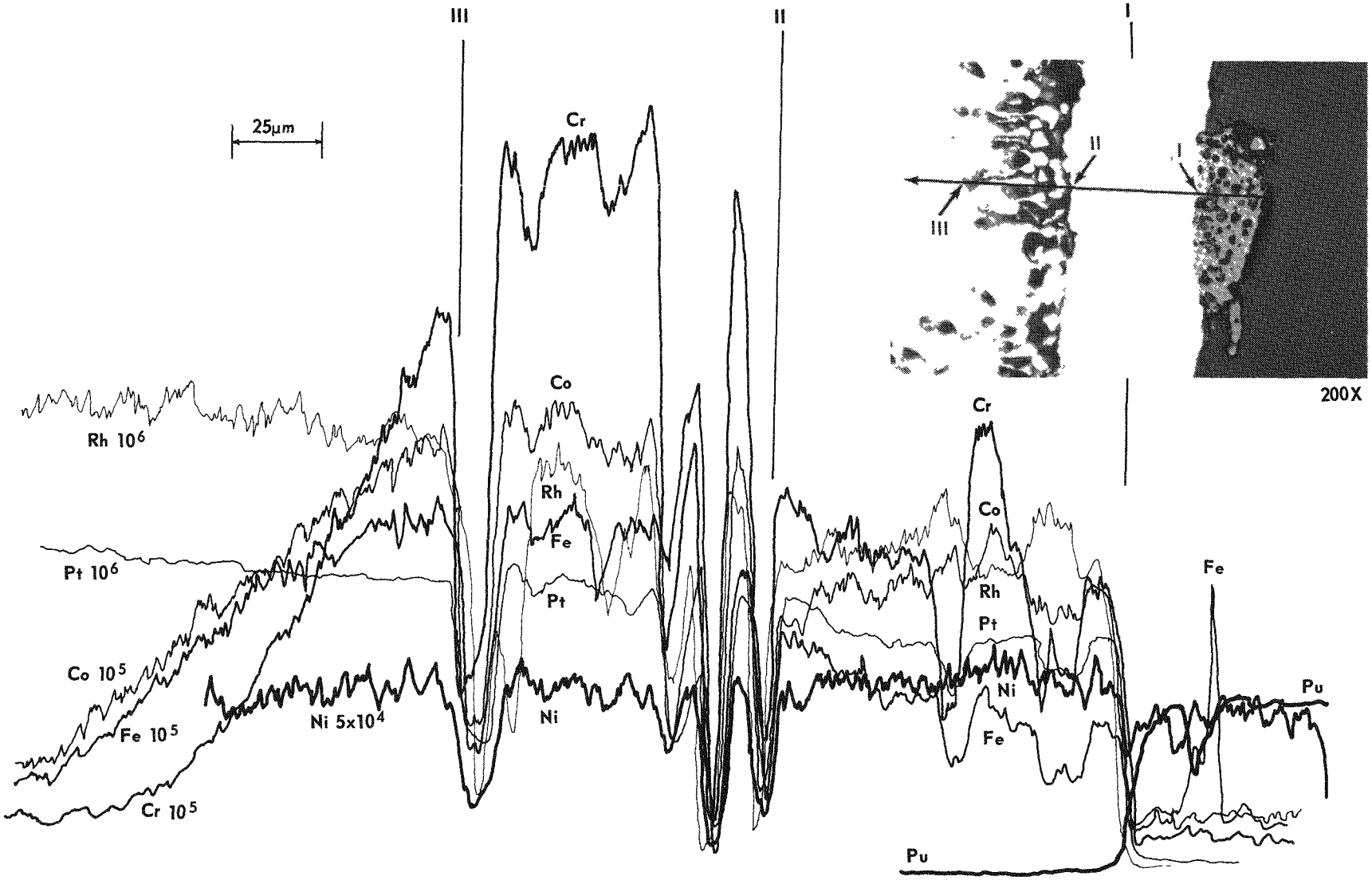

FIGURE 33 - X-ray strip chart analysis of platinum-40 wt % rhodium sample tested for 360 days at 1200°C.

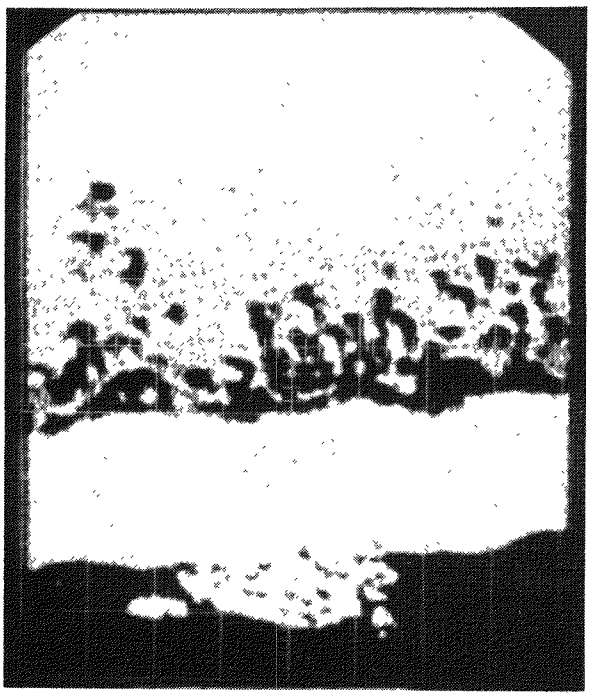

FIGURE 34 - Photomicrograph of reaction zone in platinum-40 wt % rhodium sample taken with back scattered electrons: 360 days at 1200°C. 220X

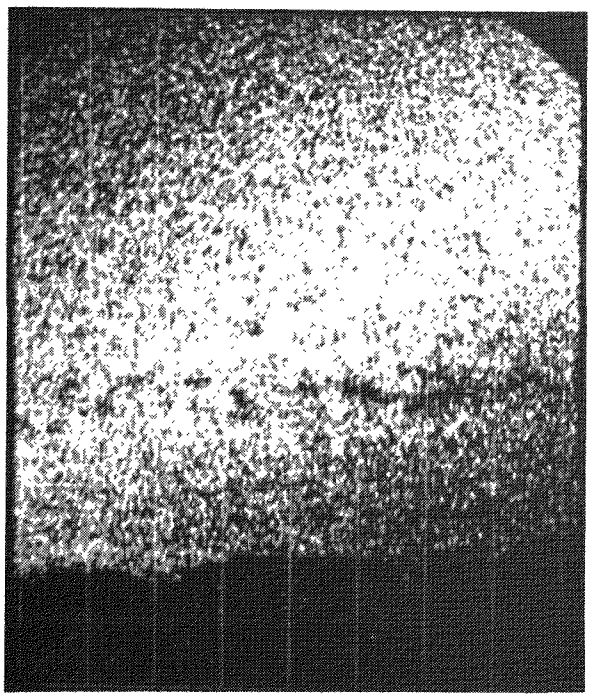

FIGURE 35 - Photomicrograph of reaction zone in platinum-40 wt % rhodium sample taken with platinum Lα radiation: 360 days at 1200°C. 220X

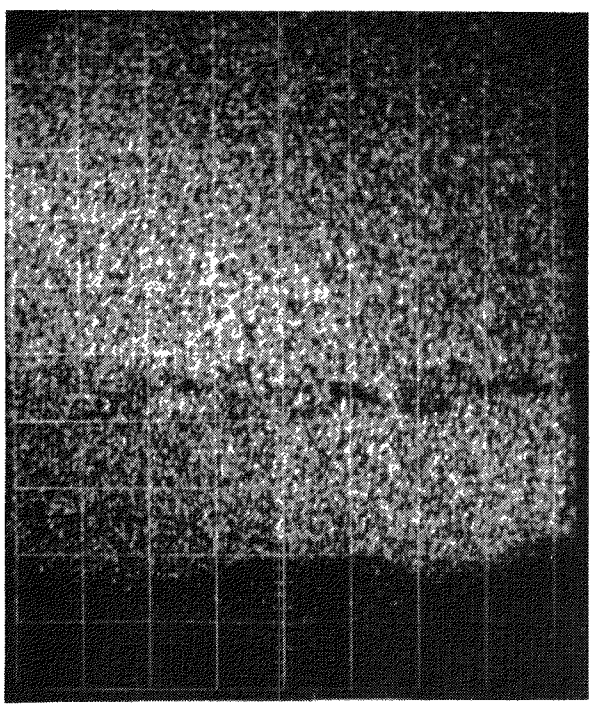

FIGURE 36 - Photomicrograph of reaction zone in platinum-40 wt % rhodium sample taken with rhodium Lα radiation: 360 days at 1200°C. 220X

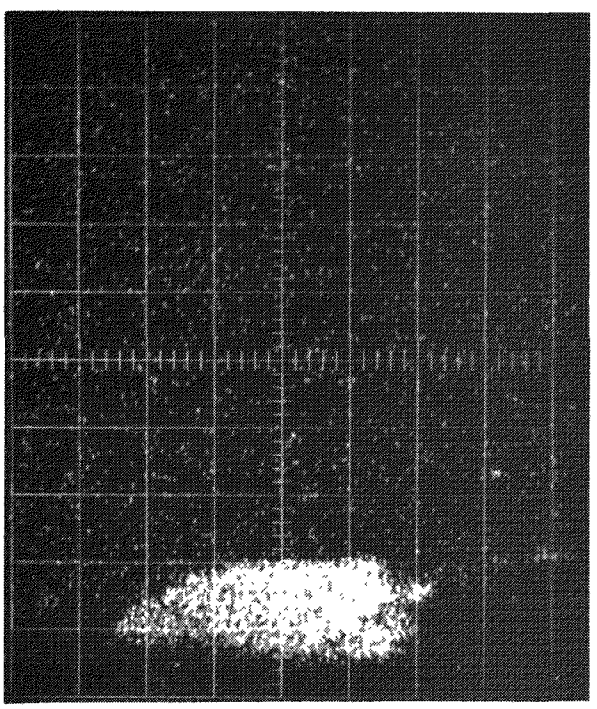

FIGURE 37 - Photomicrograph of reaction zone in platinum-40 wt % rhodium sample taken with plutonium Mα radiation: 360 days at 1200°C. 220X

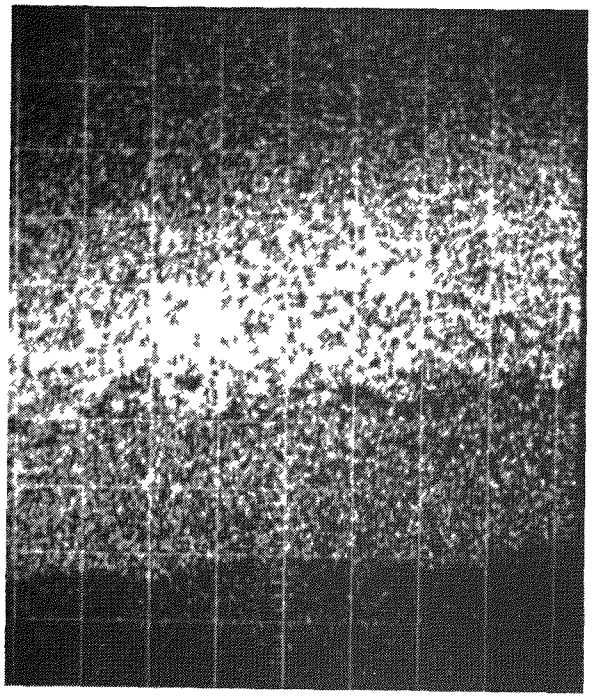

FIGURE 38 - Photomicrograph of reaction zone in platinum-40 wt % rhodium sample taken with cobalt Kα radiation: 360 days at 1200°C. 220X

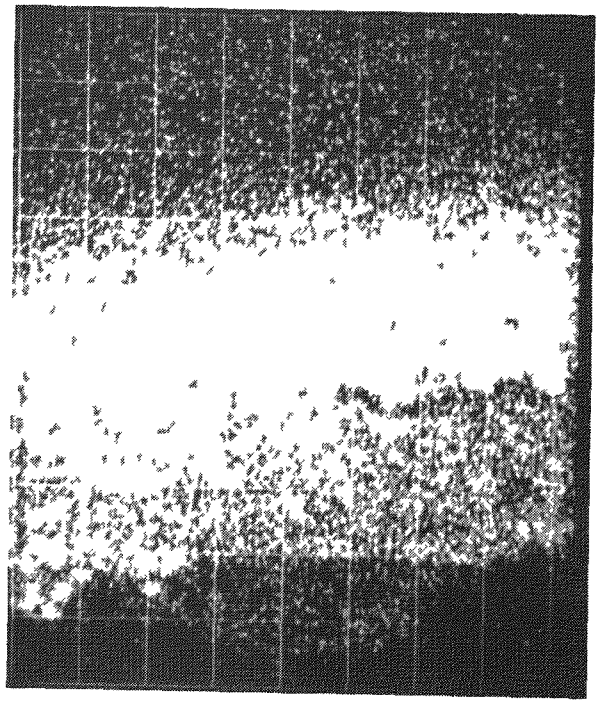

FIGURE 39 - Photomicrograph of reaction zone in platinum-40 wt % rhodium sample taken with chromium Kα radiation: 360 days at 1200°C. 220X

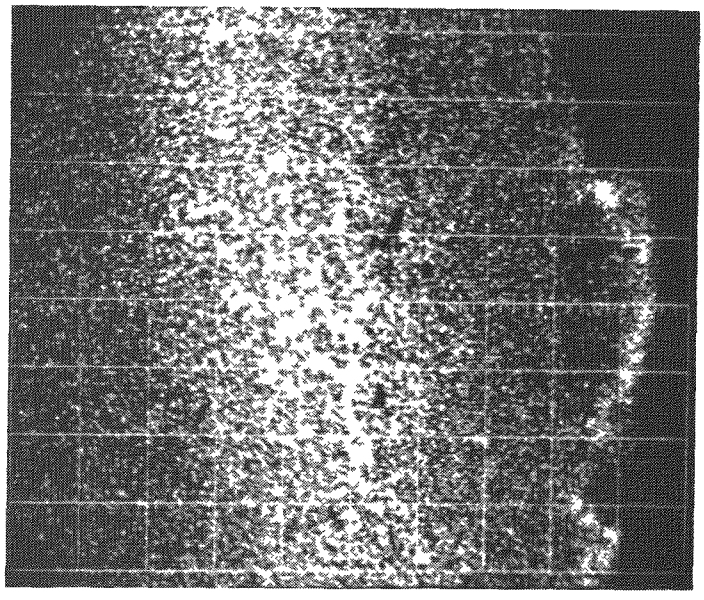

FIGURE 40 - Photomicrograph of reaction zone in platinum-40 wt % rhodium sample taken with iron Kα radiation: 360 days at 1200°C. 220X

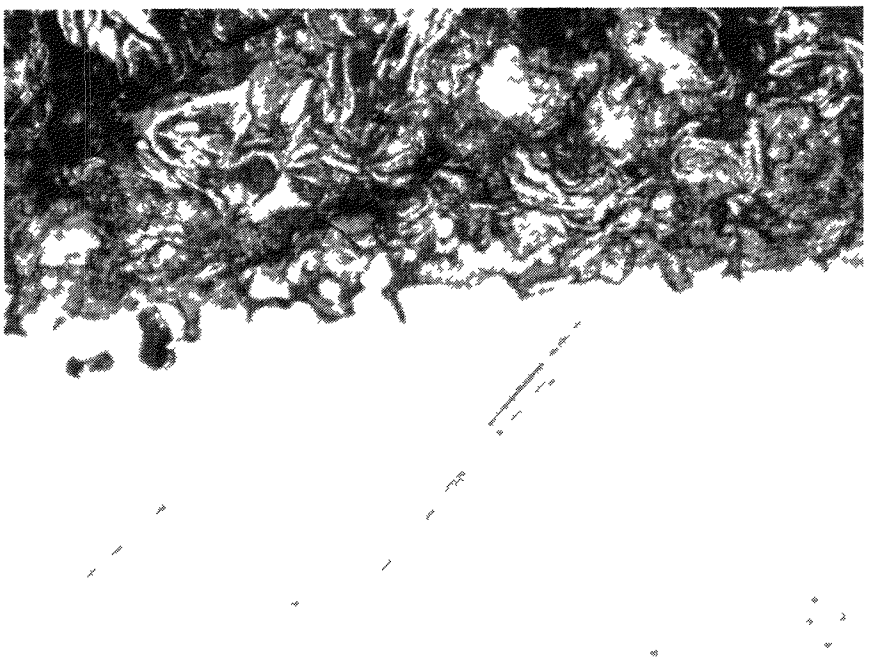

FIGURE 41 - Photomicrograph of the interface between $^{238}PuO_2$ and platinum-10 wt % rhodium alloy after 2000 hours at 1200°C, with no refractory metals in the system. Unetched 250X

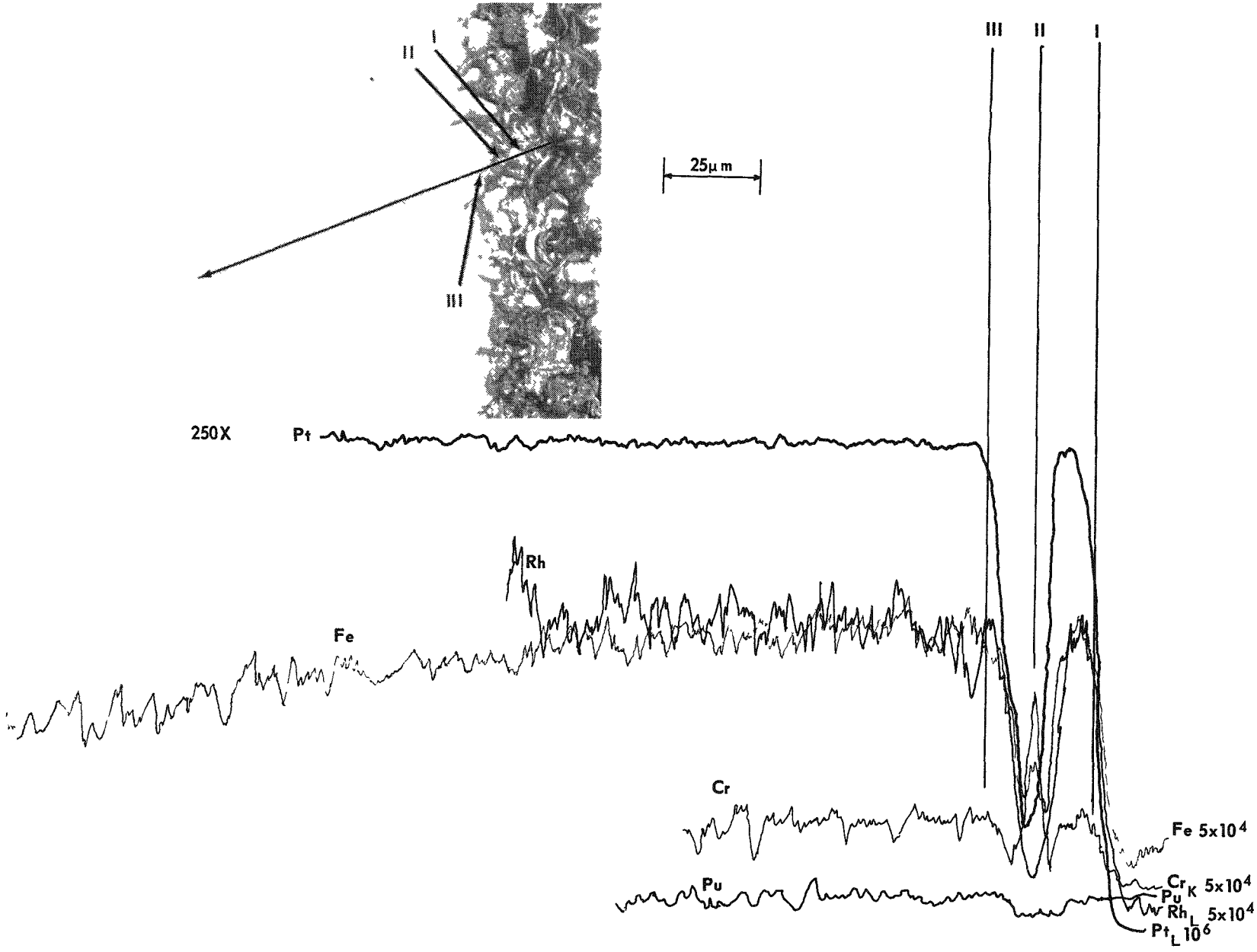

FIGURE 42 - X-ray strip chart analysis of the interface between $^{238}PuO_2$ and platinum-10 wt % rhodium alloy after 2000 hours at 1200°C, with no refractory metals in the system.

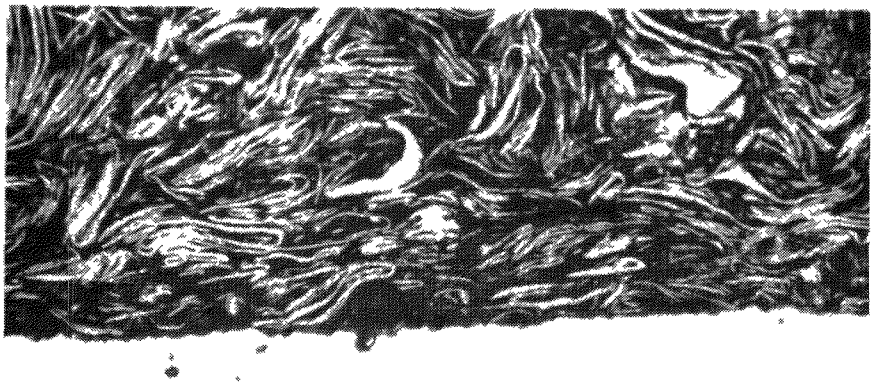

FIGURE 43 - Photomicrograph of the interface between $^{238}PuO_2$ microspheres and platinum-30 wt % rhodium alloy after 30 days at 1200°C. The fuel was sealed in an air atmosphere. Unetched 250X

FIGURE 44 - Photomicrograph of the interface between $^{238}PuO_2$ powder and platinum-30 wt % rhodium alloy after 30 days at 1200°C. The fuel was sealed in an air atmosphere. Unetched 250X

FIGURE 45 - Photomicrograph of the interface between $^{238}PuO_2$ microspheres and platinum-30 wt % rhodium alloy after 60 days at 1200°C. The fuel was sealed in an air atmosphere. Unetched 250X

FIGURE 46 - Photomicrograph of the interface between $^{238}PuO_2$ powder and platinum-30 wt % rhodium alloy after 60 days at 1200°C. The fuel was sealed in an air atmosphere. Unetched 250X

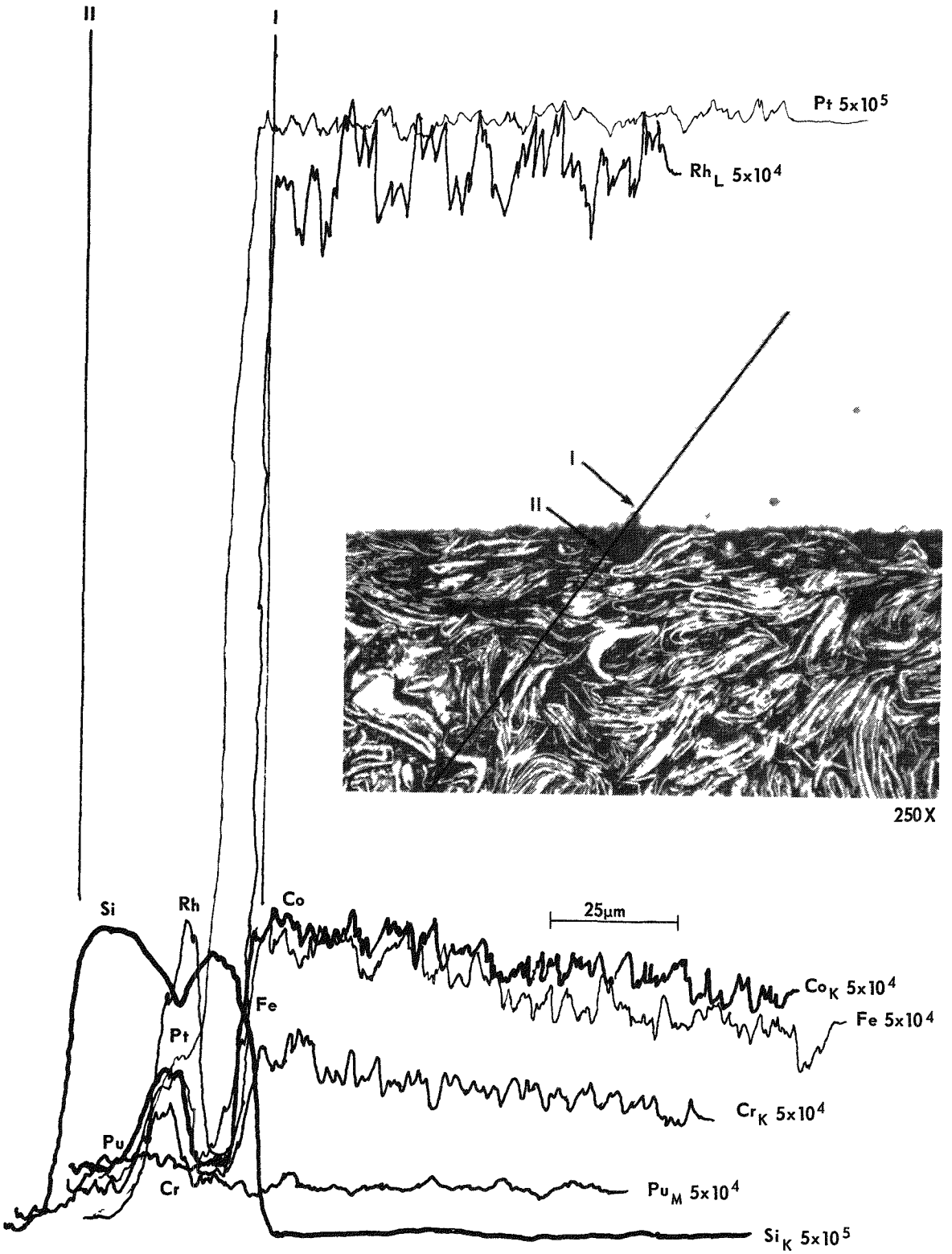

FIGURE 47 - X-ray strip chart analysis of the interface between $^{238}PuO_2$ microspheres and platinum-30 wt % rhodium alloy after 30 days at 1200°C.

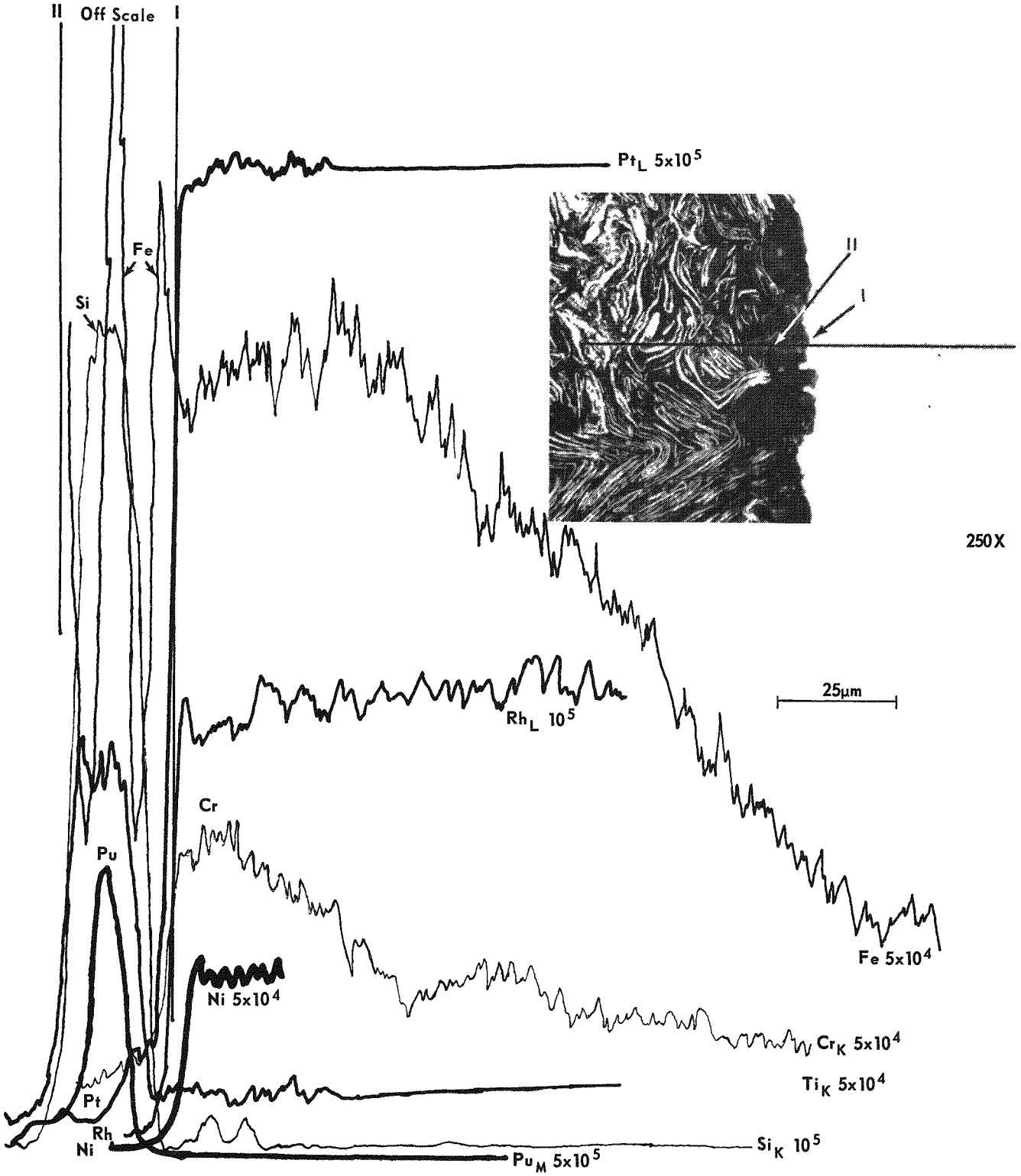

FIGURE 48 - X-ray strip chart analysis of the interface between $^{238}PuO_2$ powder and platinum-30 wt % rhodium alloy after 30 days at 1200°C.

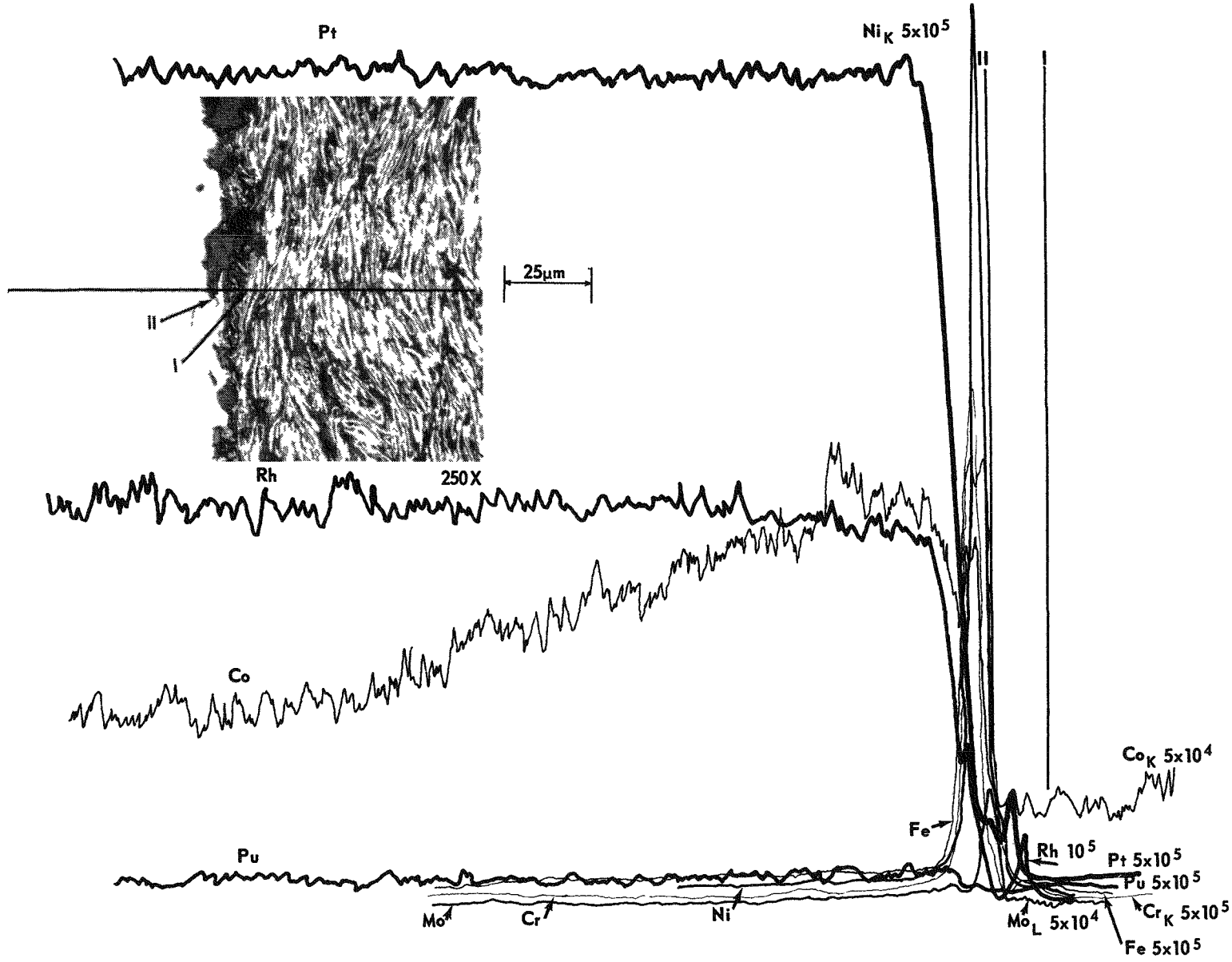

FIGURE 49 - X-ray strip chart analysis of the interface between $^{238}PuO_2$ microspheres and platinum-30 wt % rhodium alloy after 60 days at 1200°C.

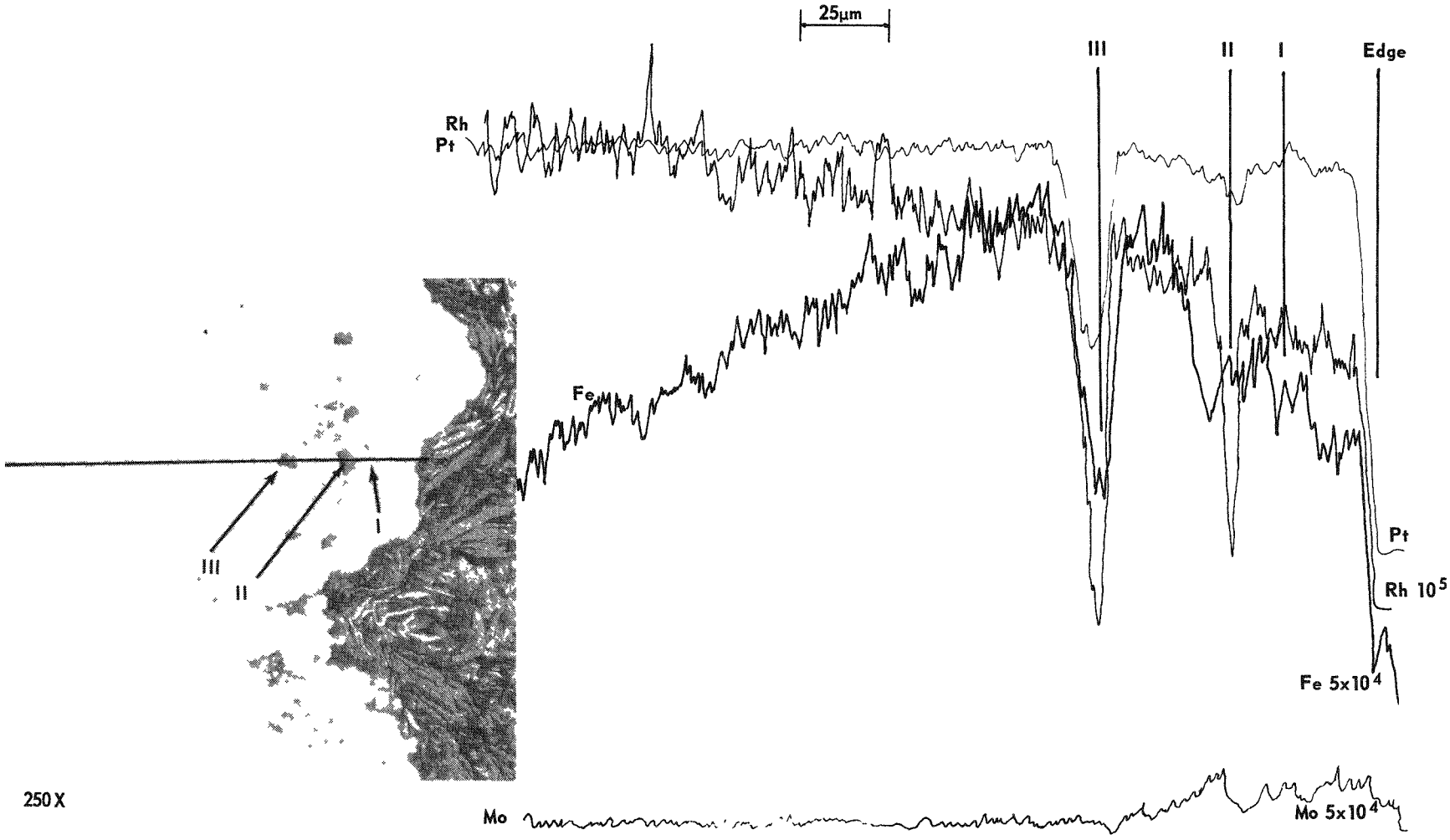

FIGURE 50 - X-ray strip chart analysis of the interface between $^{238}PuO_2$ powder and platinum-30 wt % rhodium after 60 days at 1200°C - taken at region containing voids.

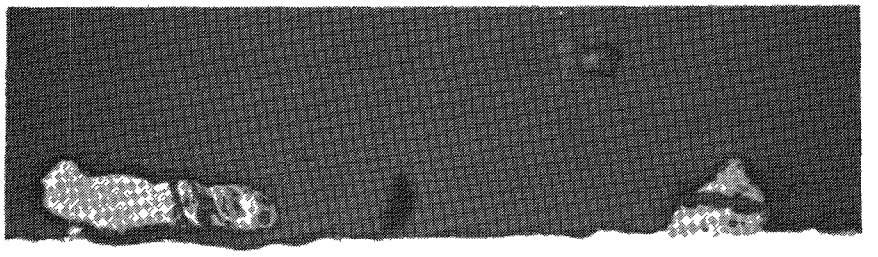

FIGURE 51 - Photomicrograph of the interface between $^{238}PuO_2$ and platinum after 30 days at 1200°C, with no refractory metals in the system. Unetched 195X

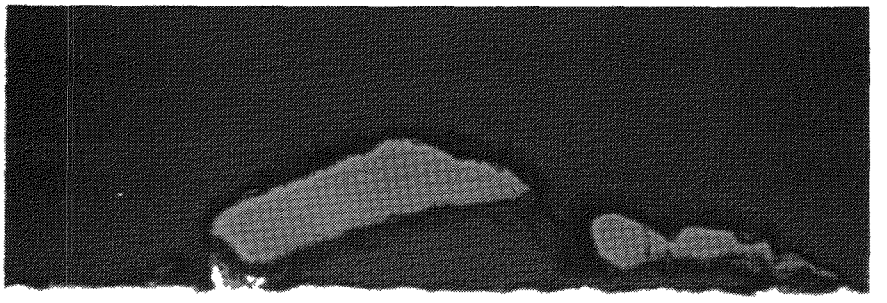

FIGURE 52 - Photomicrograph of the interface between $^{238}PuO_2$ and platinum after 60 days at 1200°C, with no refractory metals in the system. Unetched 250X

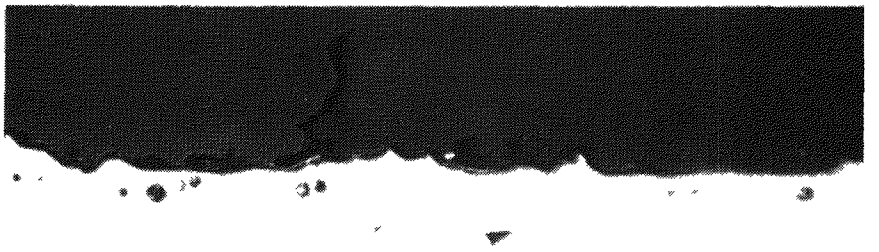

FIGURE 53 - Photomicrograph of the interface between $^{238}PuO_2$ and platinum after 90 days at 1200°C, with no refractory metals in the system. Unetched 250X

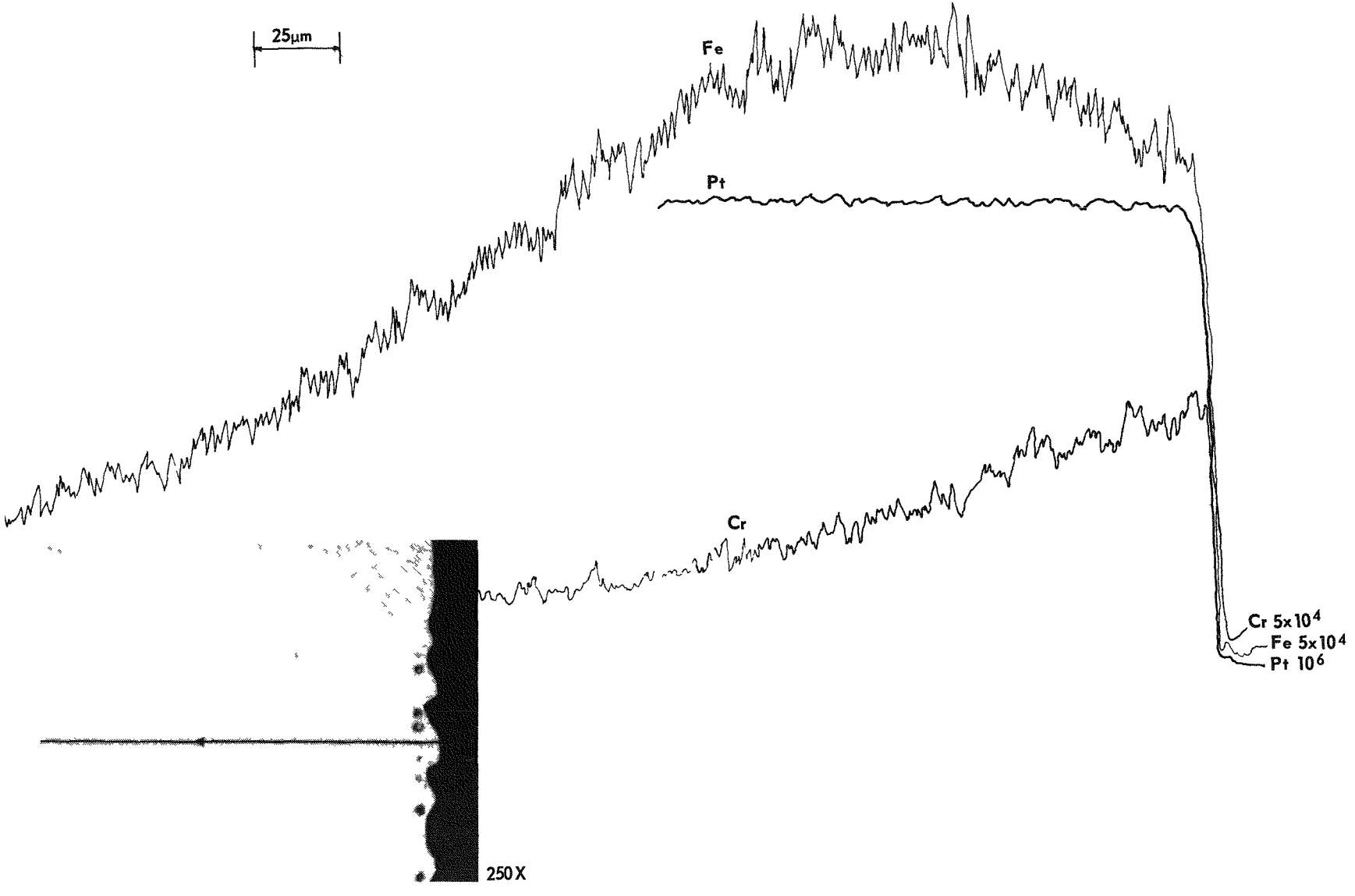

FIGURE 54 - X-ray strip chart analysis of the interface between $^{238}PuO_2$ and platinum after 90 days at 1200°C, with no refractory metals in the system

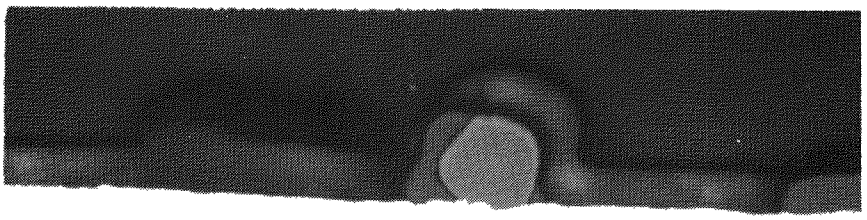

FIGURE 55 - Photomicrograph of the interface between $^{238}PuO_2$ and platinum-40 wt % rhodium after 30 days at 1200°C, with no refractory metals in the system. Unetched 250X

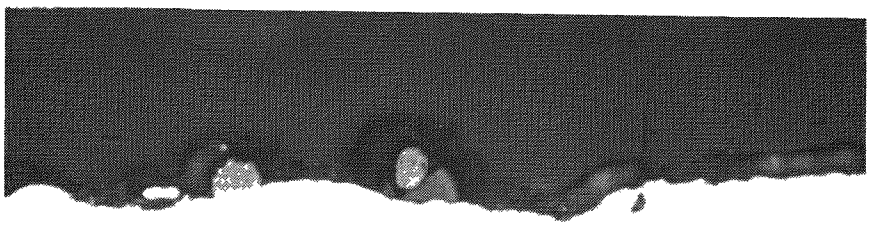

FIGURE 56 - Photomicrograph of the interface between $^{238}PuO_2$ and platinum-40 wt % rhodium after 60 days at 1200°C, with no refractory metals in the system. Unetched 250X

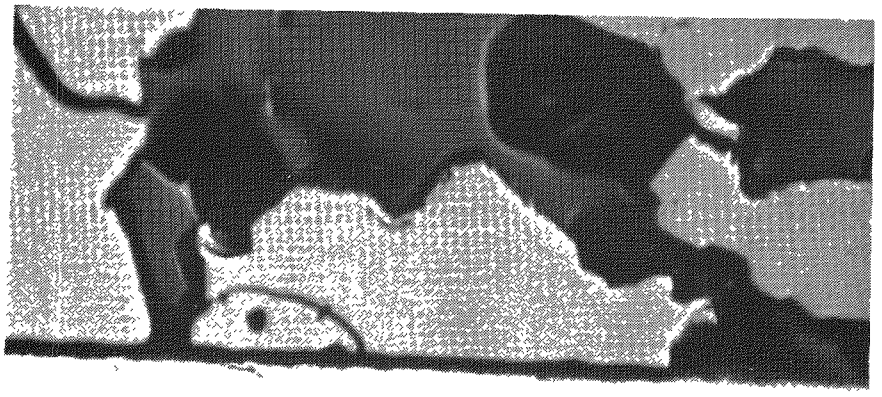

FIGURE 57 - Photomicrograph of the interface between $^{238}PuO_2$ and platinum-40 wt % rhodium after 90 days at 1200°C, with no refractory metals in the system. Unetched 250X

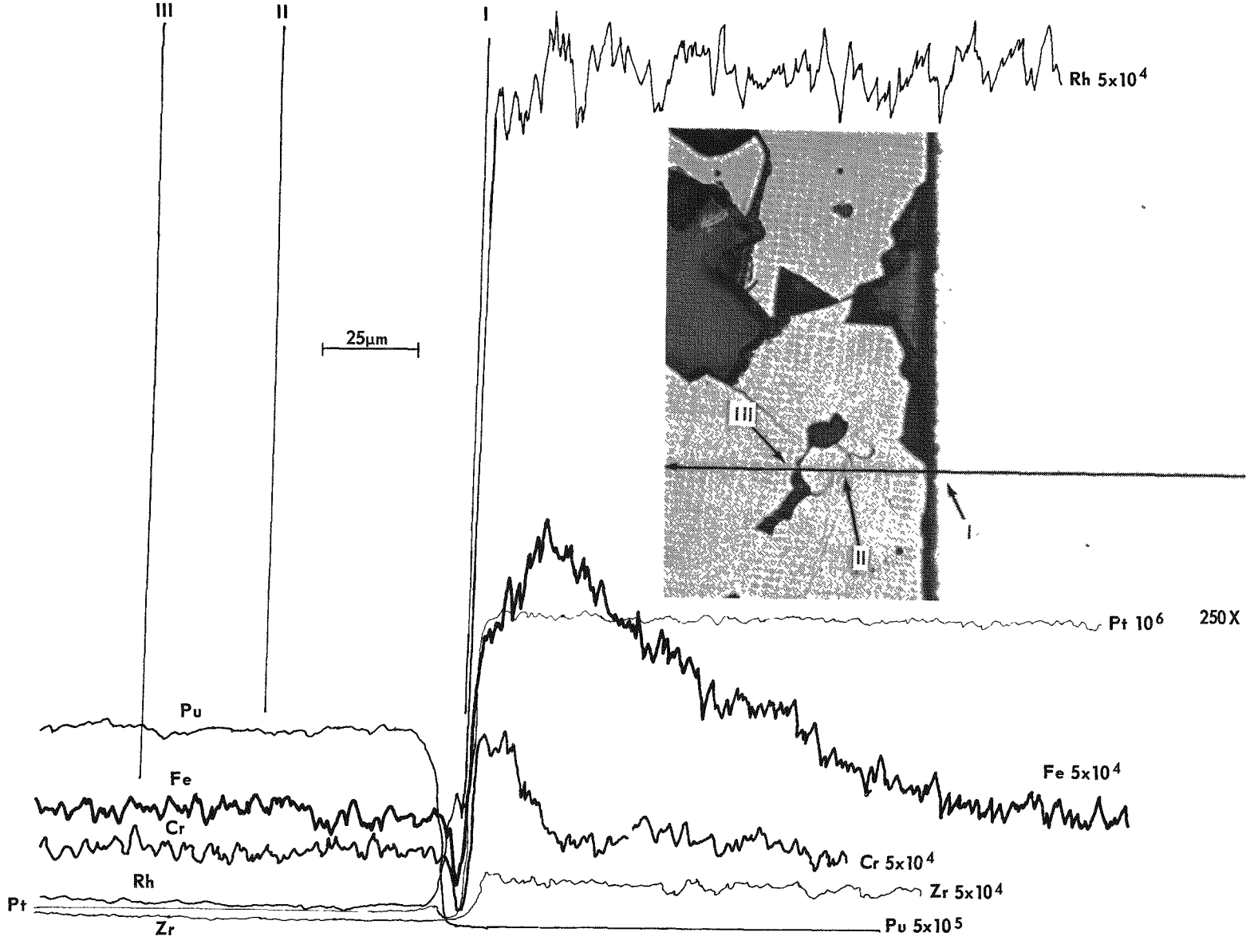

FIGURE 58 - X-ray strip chart analysis of the interface between $^{238}PuO_2$ and platinum-40 wt % rhodium after 90 days at 1200°C, with no refractory metals in the system.

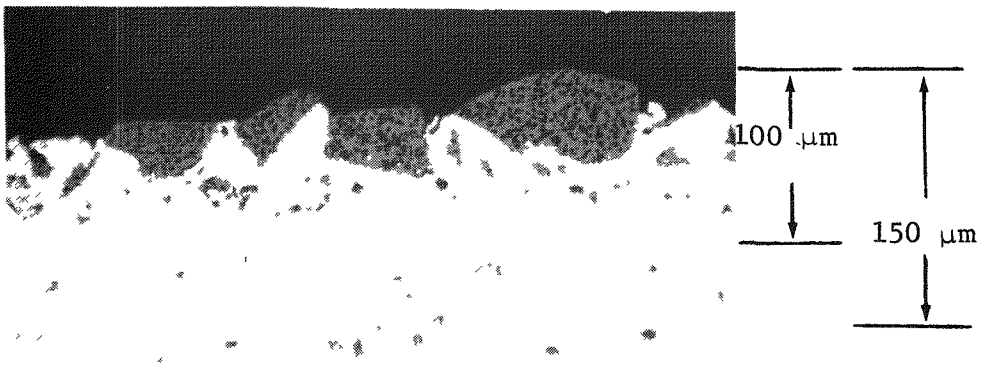

FIGURE 59 - Photomicrograph of reaction in platinum in contact with $^{238}PuO_2$ for 60 days at 1000°C in a molybdenum container. Note line formation of voids 100 and 150 μm below the surface. Unetched 235X

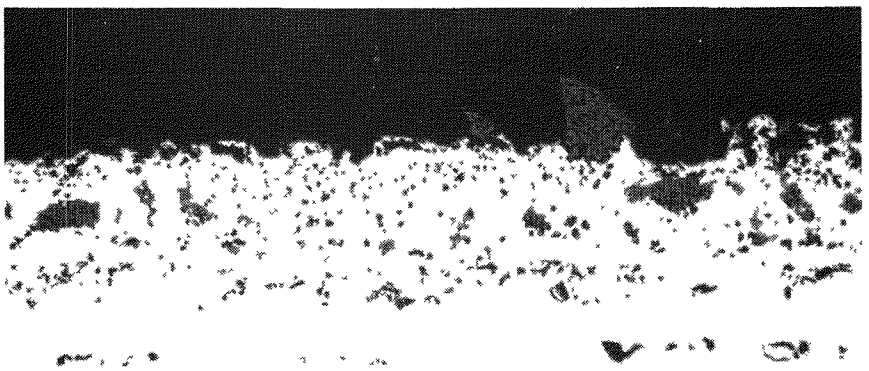

FIGURE 60 - Photomicrograph of reaction in platinum in contact with $^{238}PuO_2$ for 180 days at 1000°C in a molybdenum container. Unetched 135X

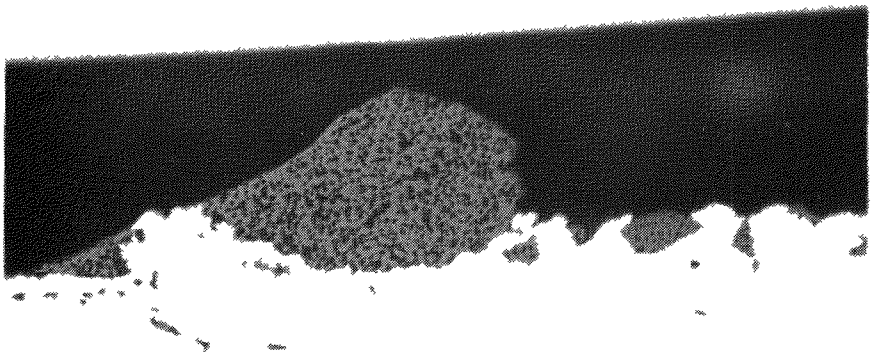

FIGURE 61 - Photomicrograph of reaction in platinum-20 wt % rhodium in contact with $^{238}PuO_2$ for 60 days at 1000°C in a molybdenum container. Unetched 250X

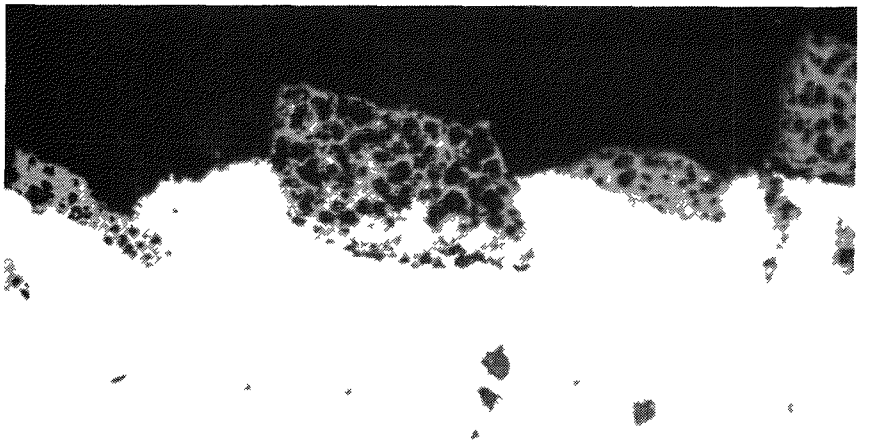

FIGURE 62 - Photomicrograph of reaction in platinum-20 wt % rhodium in contact with $^{238}PuO_2$ for 180 days at 1000°C in a molybdenum container. Unetched 250X

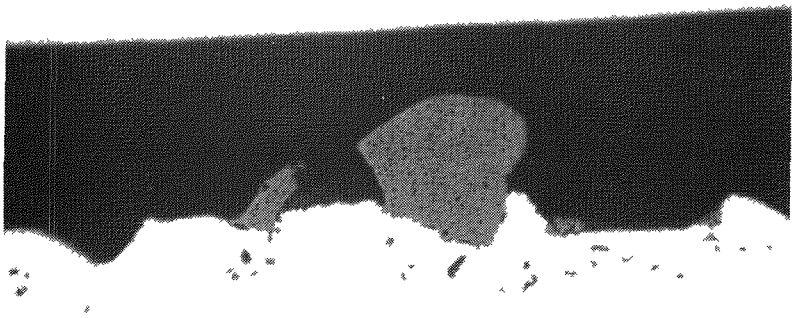

Edge
Retainer

FIGURE 63 - Photomicrograph of reaction in platinum-40 wt % rhodium in contact with $^{238}PuO_2$ for 60 days at 1000°C in a molybdenum container. Unetched 235X

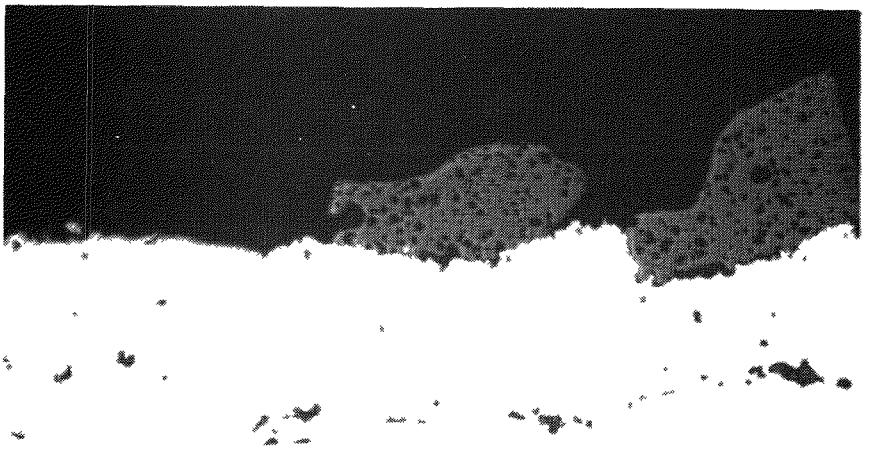

FIGURE 64 - Photomicrograph of reaction in platinum-40 wt % rhodium in contact with $^{238}PuO_2$ for 180 days at 1000°C in a molybdenum container. Unetched 250X

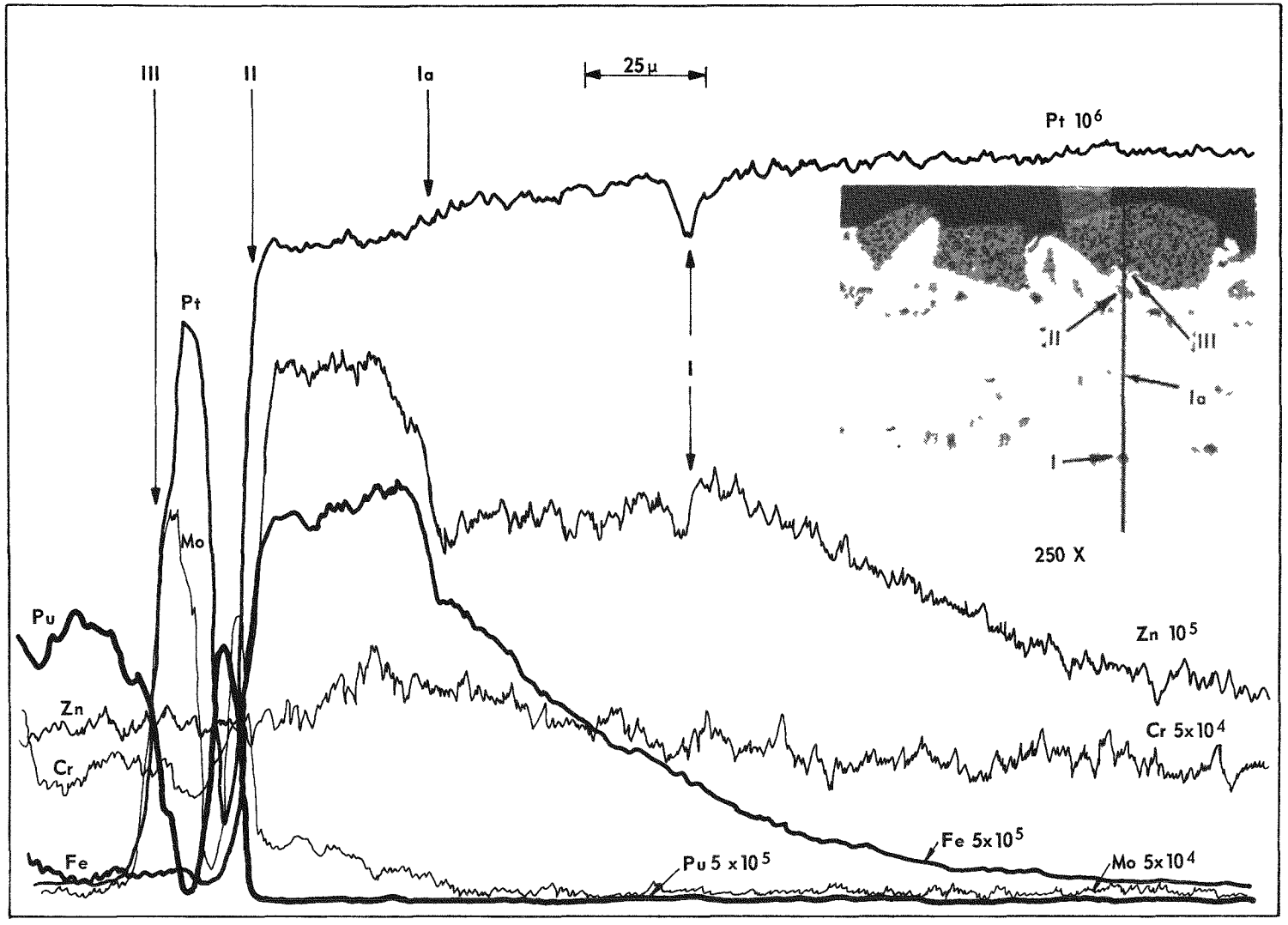

FIGURE 65 - X-ray strip chart analysis of platinum sample in contact with $^{238}PuO_2$ after 60 days at 1000°C in a molybdenum container.

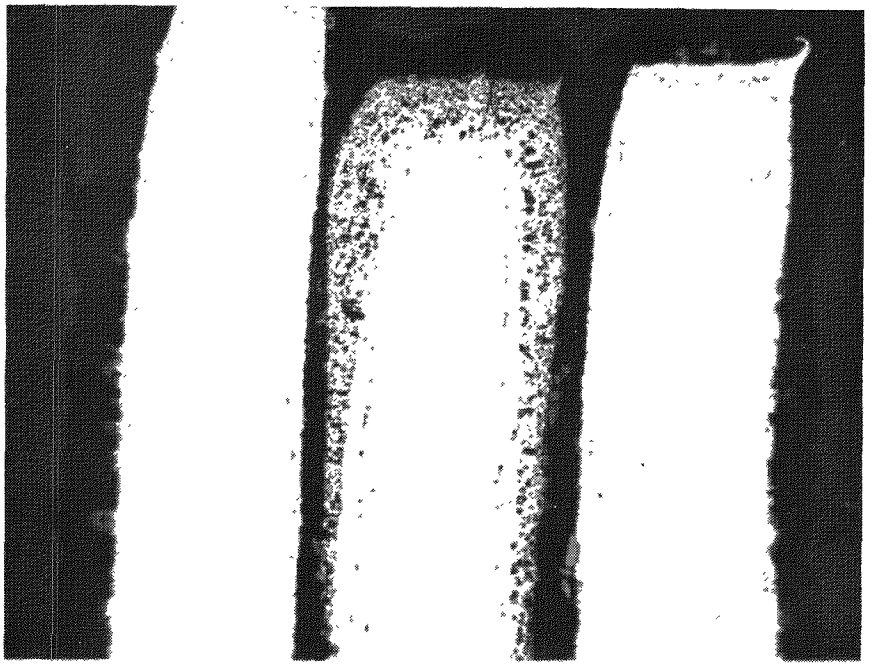

Pt-40 Rh 32-33 mils | Pt 37-41 mils | Pt-20 Rh 34-35 mils

FIGURE 66 - Photomicrograph of platinum, platinum-20 wt % rhodium and platinum-40 wt % rhodium coupons after 180 days at 1000°C in a molybdenum container. Original thickness of coupons was 760 μm. Unetched 29.6X

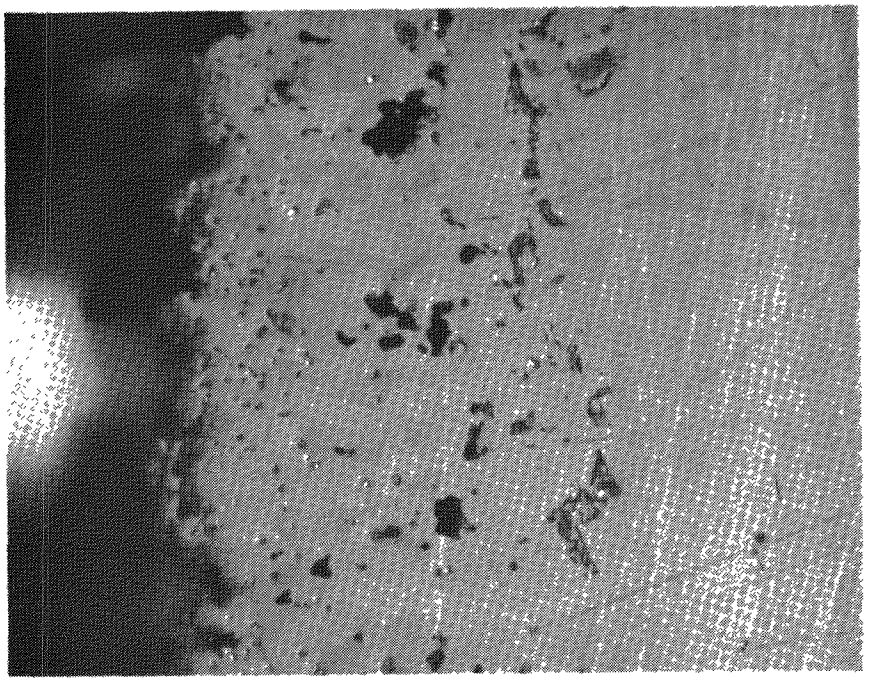

FIGURE 67 - Photomicrograph of platinum in contact with $^{238}PuO_2$ for 180 days at 1000°C in a molybdenum container. Unetched, polarized light 330X

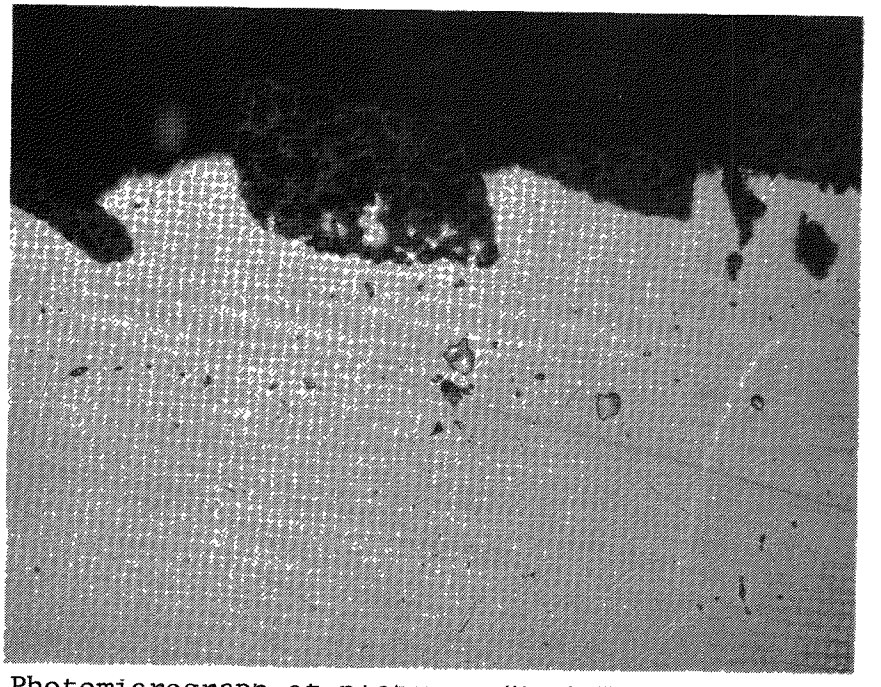

FIGURE 68 - Photomicrograph of platinum-20 wt % rhodium in contact with $^{238}PuO_2$ for 180 days at 1000°C in a molybdenum container.
Unetched, polarized light 250X

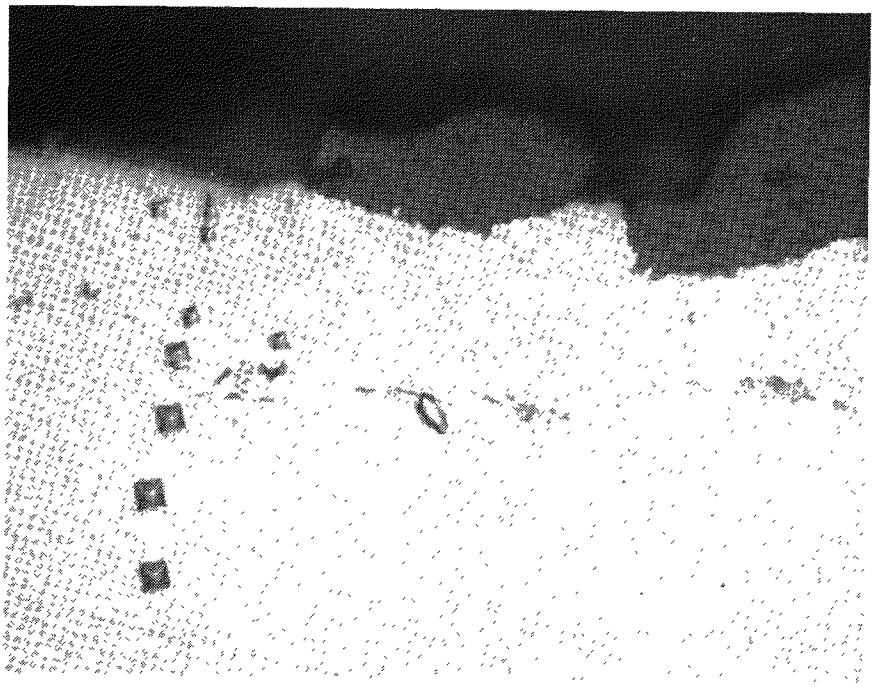

FIGURE 69 - Photomicrograph of platinum-40 wt % rhodium in contact with $^{238}PuO_2$ for 180 days at 1000°C in a molybdenum container.
Unetched, polarized light 250X

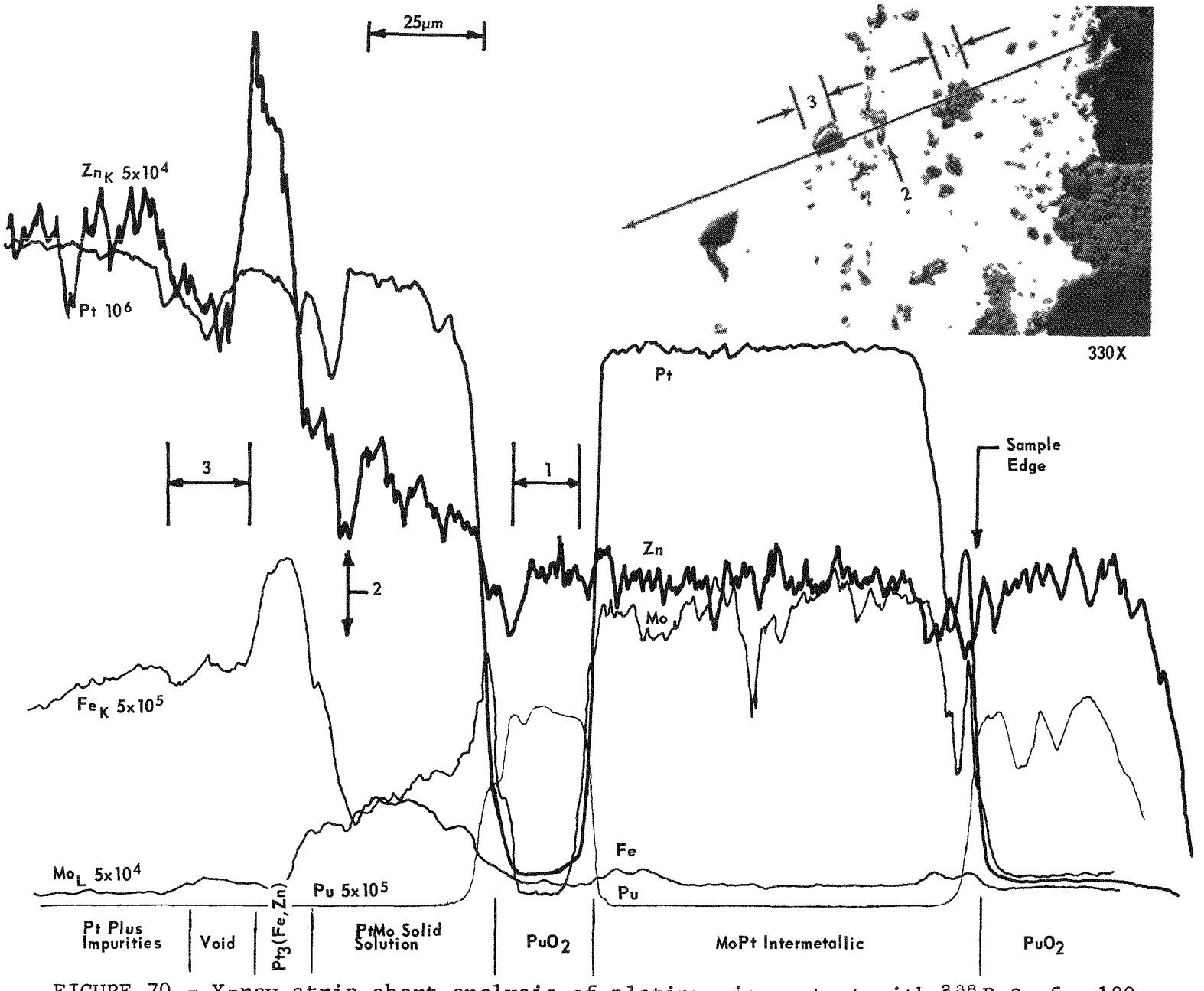

FIGURE 70 - X-ray strip chart analysis of platinum in contact with $^{238}PuO_2$ for 180 days at 1000°C in a molybdenum container.

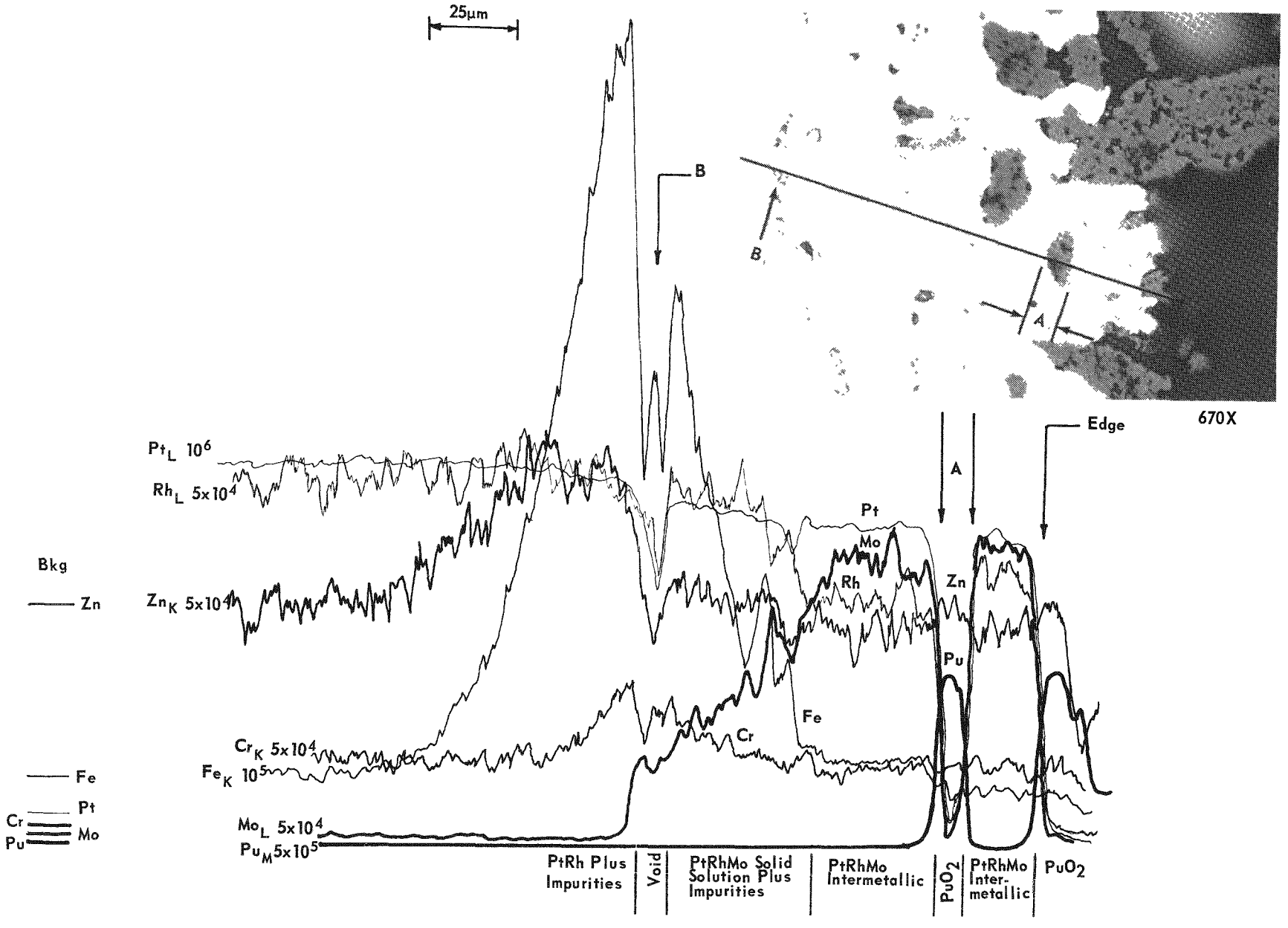

FIGURE 71 - X-ray strip chart analysis of platinum-20 wt % rhodium in contact with $^{238}PuO_2$ for 180 days at 1000°C in a molybdenum container.

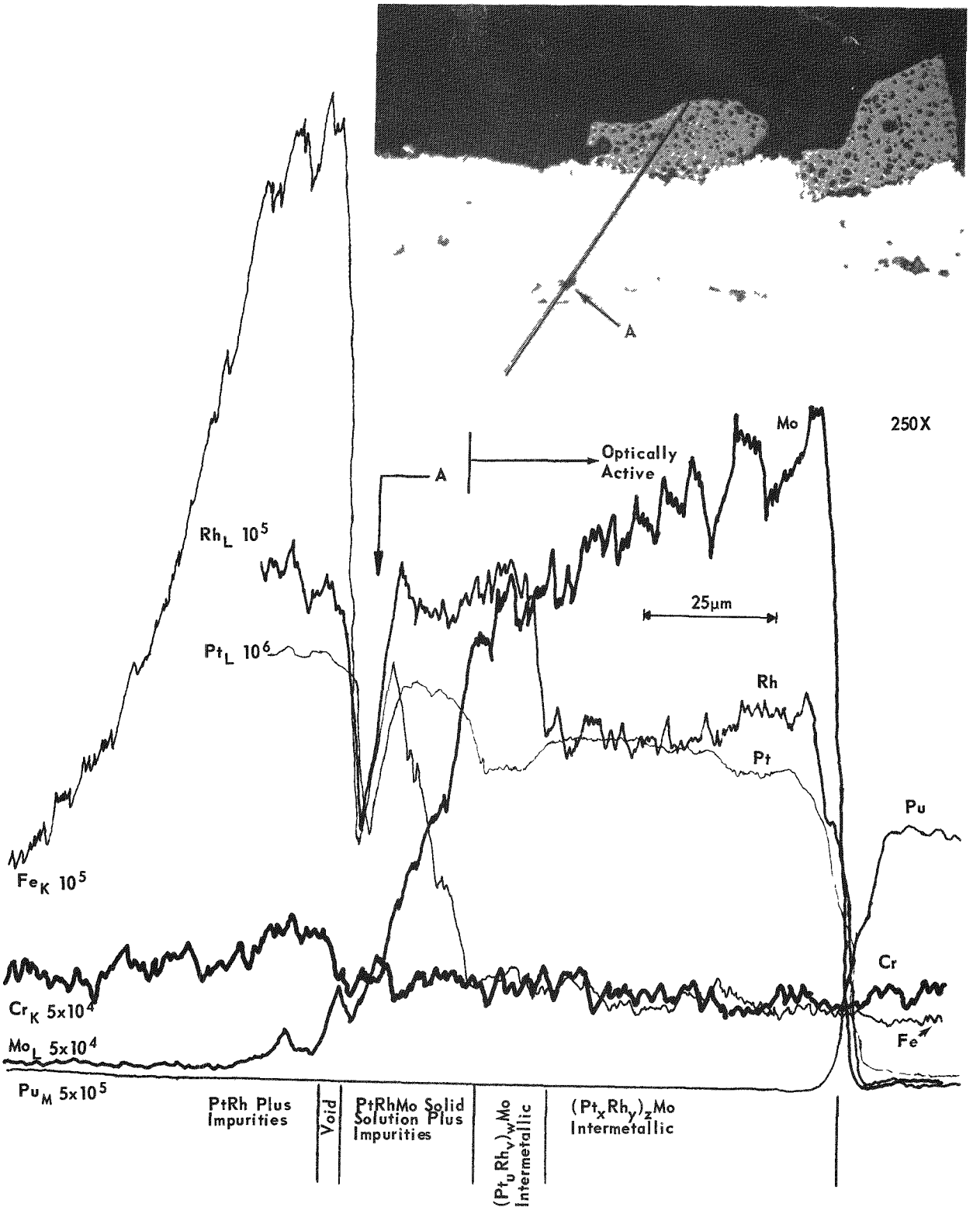

FIGURE 72 - X-ray strip chart analysis of platinum-40 wt % rhodium in contact with $^{238}PuO_2$ for 180 days at 1000°C in a molybdenum container

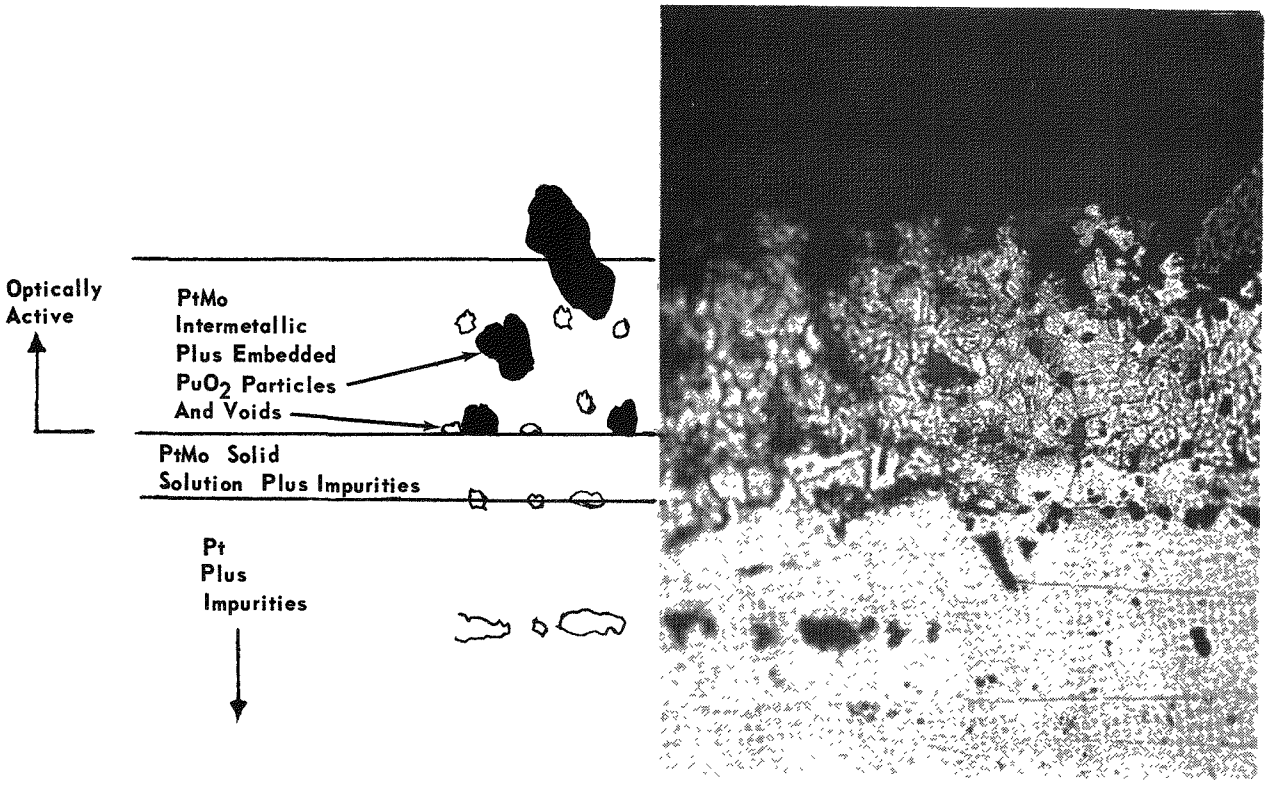

FIGURE 73 - Photomicrograph of platinum in contact with $^{238}PuO_2$ for 180 days at 1000°C in a molybdenum container. Note absence of Pt_3 (Fe,Zn) grains. Electrolytic etch 250X

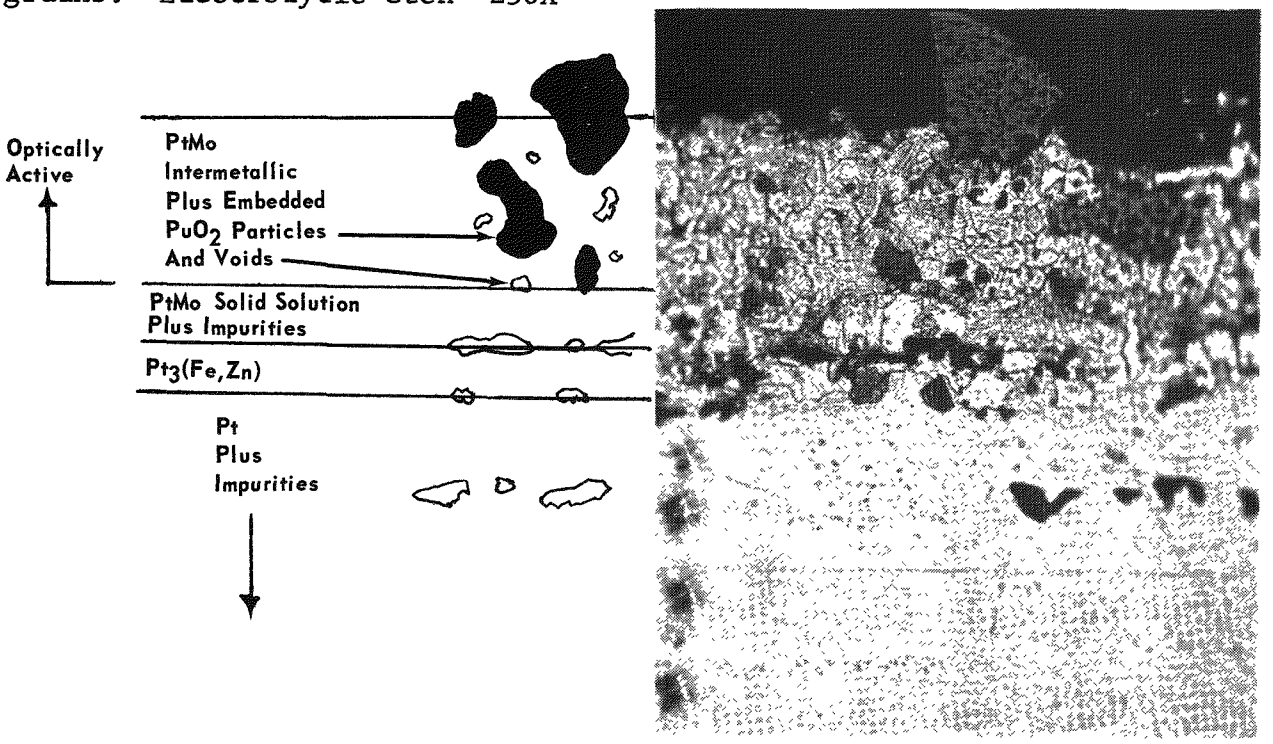

FIGURE 74 - Photomicrograph of platinum in contact with $^{238}PuO_2$ for 180 days at 1000°C in a molybdenum container. Electrolytic etch 250X

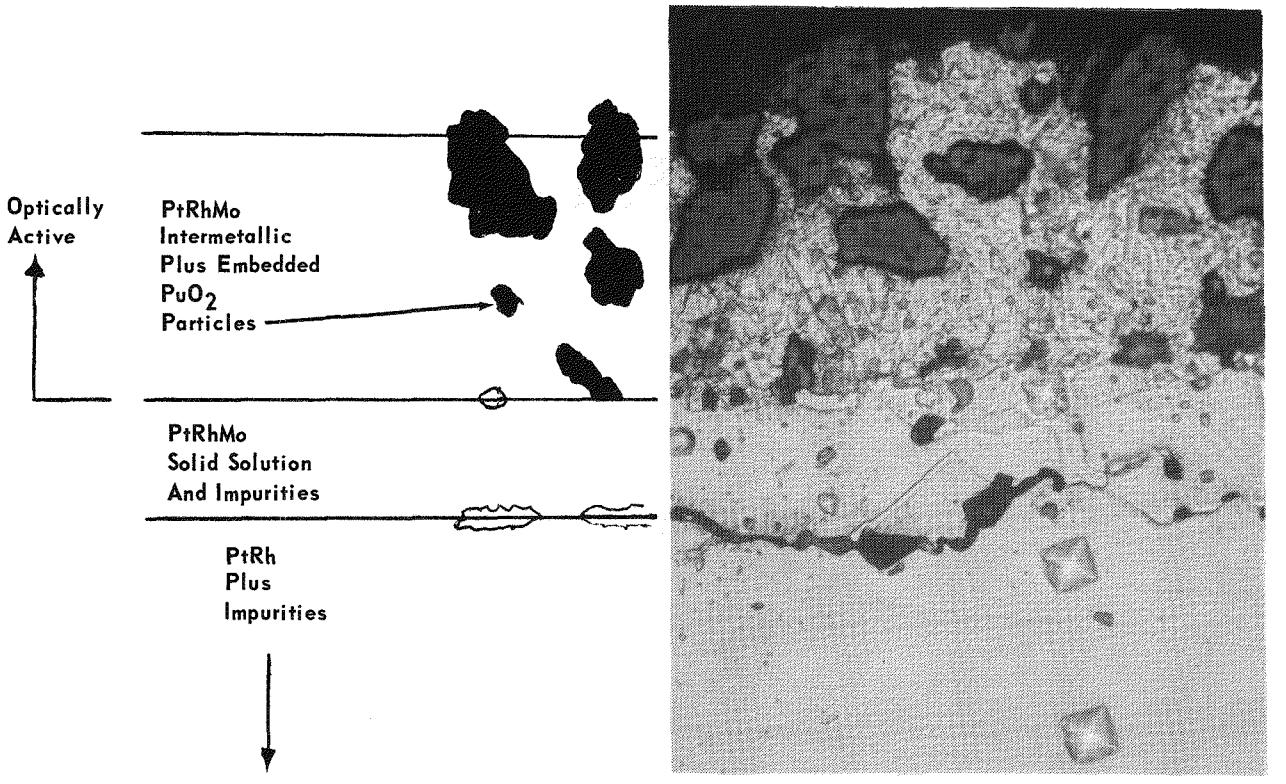

FIGURE 75 - Photomicrograph of platinum-20 wt % rhodium in contact with $^{238}PuO_2$ for 180 days at 1000°C in a molybdenum container.
Electrolytic etch 670X

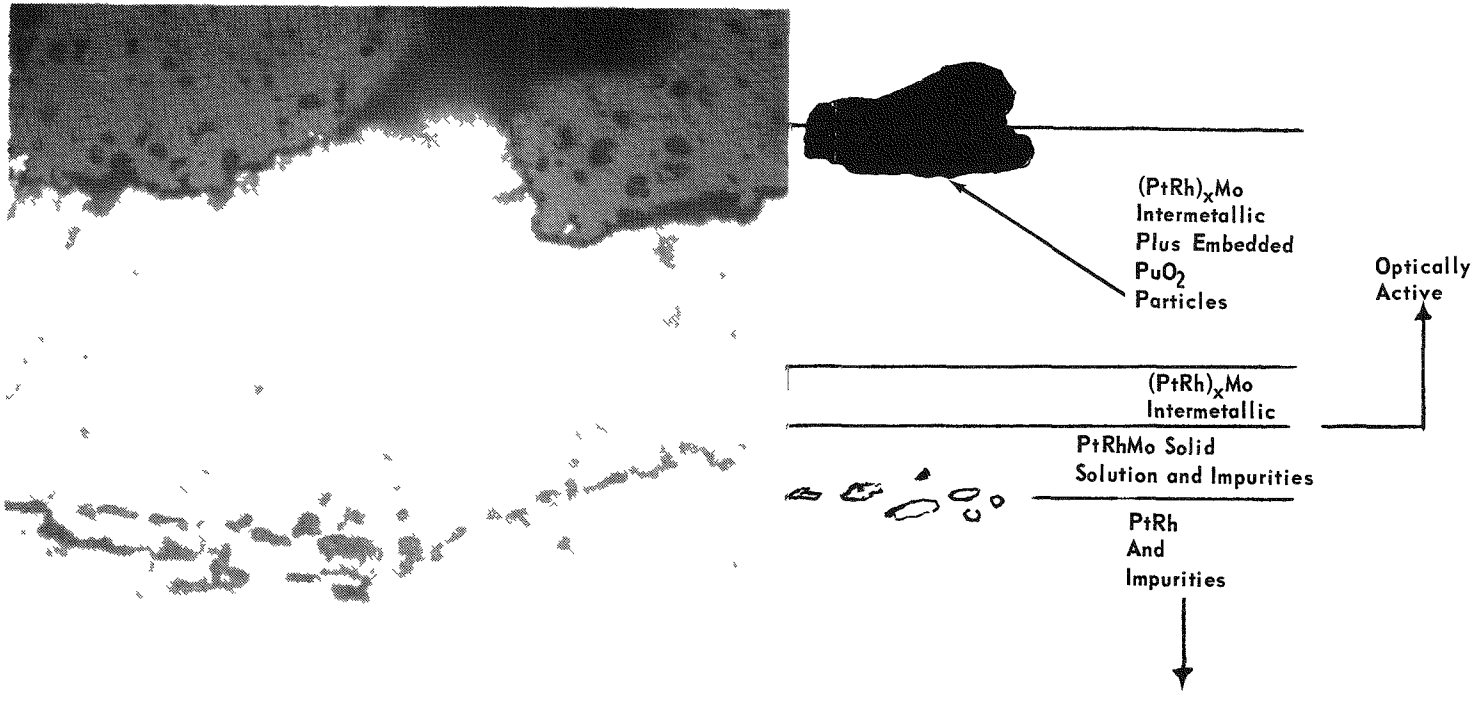

FIGURE 76 - Photomicrograph of platinum-40 wt % rhodium in contact with $^{238}PuO_2$ for 180 days at 1000°C in a molybdenum container. Electrolytic etch 250X

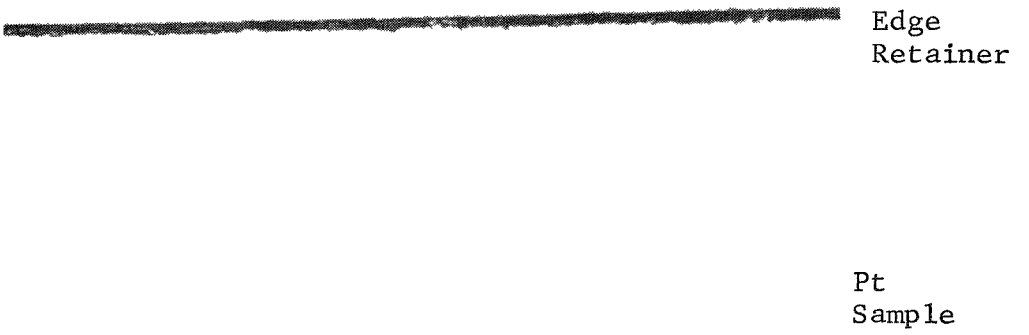

FIGURE 77 - Photomicrograph of platinum in contact with $^{238}PuO_2$ for 30 days at 800°C in a molybdenum container. Unetched 135X

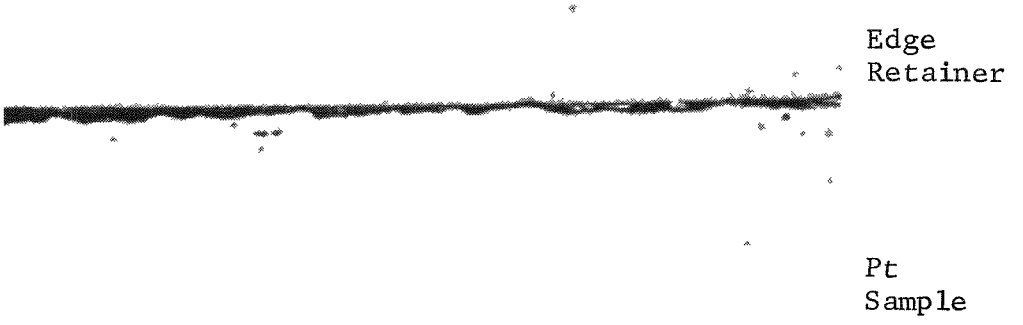

FIGURE 78 - Photomicrograph of platinum in contact with $^{238}PuO_2$ for 60 days at 800°C in a molybdenum container. Unetched 250X

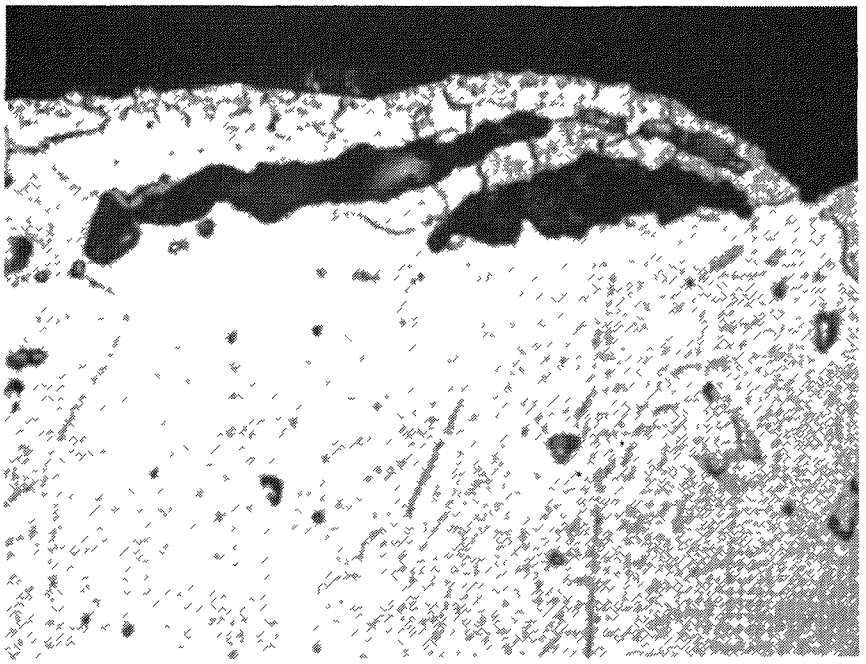

FIGURE 79 - Photomicrograph of platinum in contact with $^{238}PuO_2$ for 90 days at 800°C in a molybdenum container, showing partial separation of the surface layer. Electrolytic etch 1345X

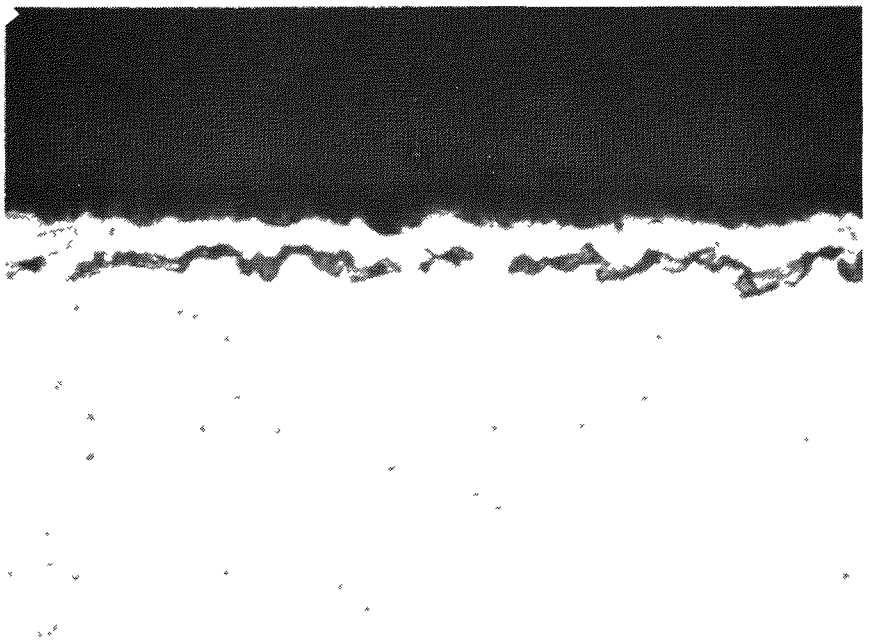

FIGURE 80 - Photomicrograph of platinum in contact with $^{238}PuO_2$ for 180 days at 800°C in a molybdenum container, showing typical line of voids 10 μm below the interface and small grains in reaction layer.
Electrolytic etch 670X

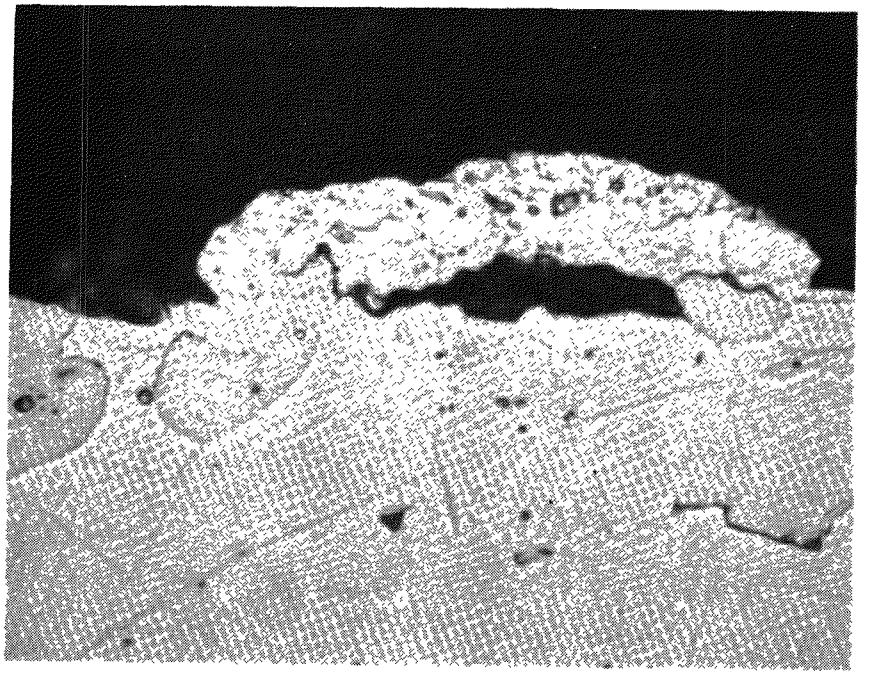

FIGURE 81 - Photomicrograph of platinum in contact with $^{238}PuO_2$ for 180 days at 800°C in a molybdenum container showing partial separation of surface layer at the end of the coupon. Electrolytic etch 1345X

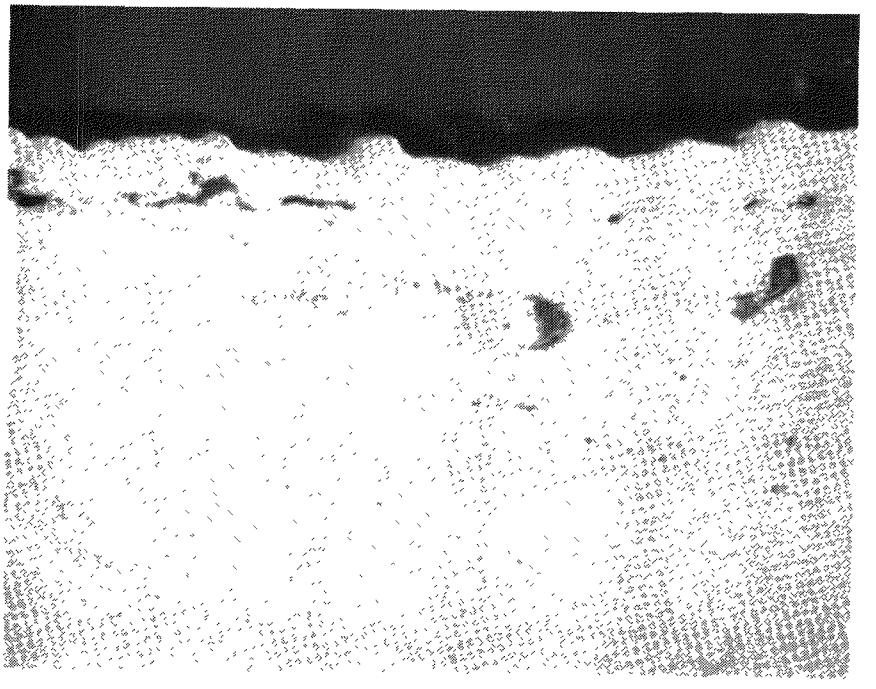

FIGURE 82 - Photomicrograph of platinum in contact with $^{238}PuO_2$ for 180 days at 800°C in a molybdenum container showing formation of voids about 30 μm below the interface. This area was not typical of the overall sample. Unetched 670X

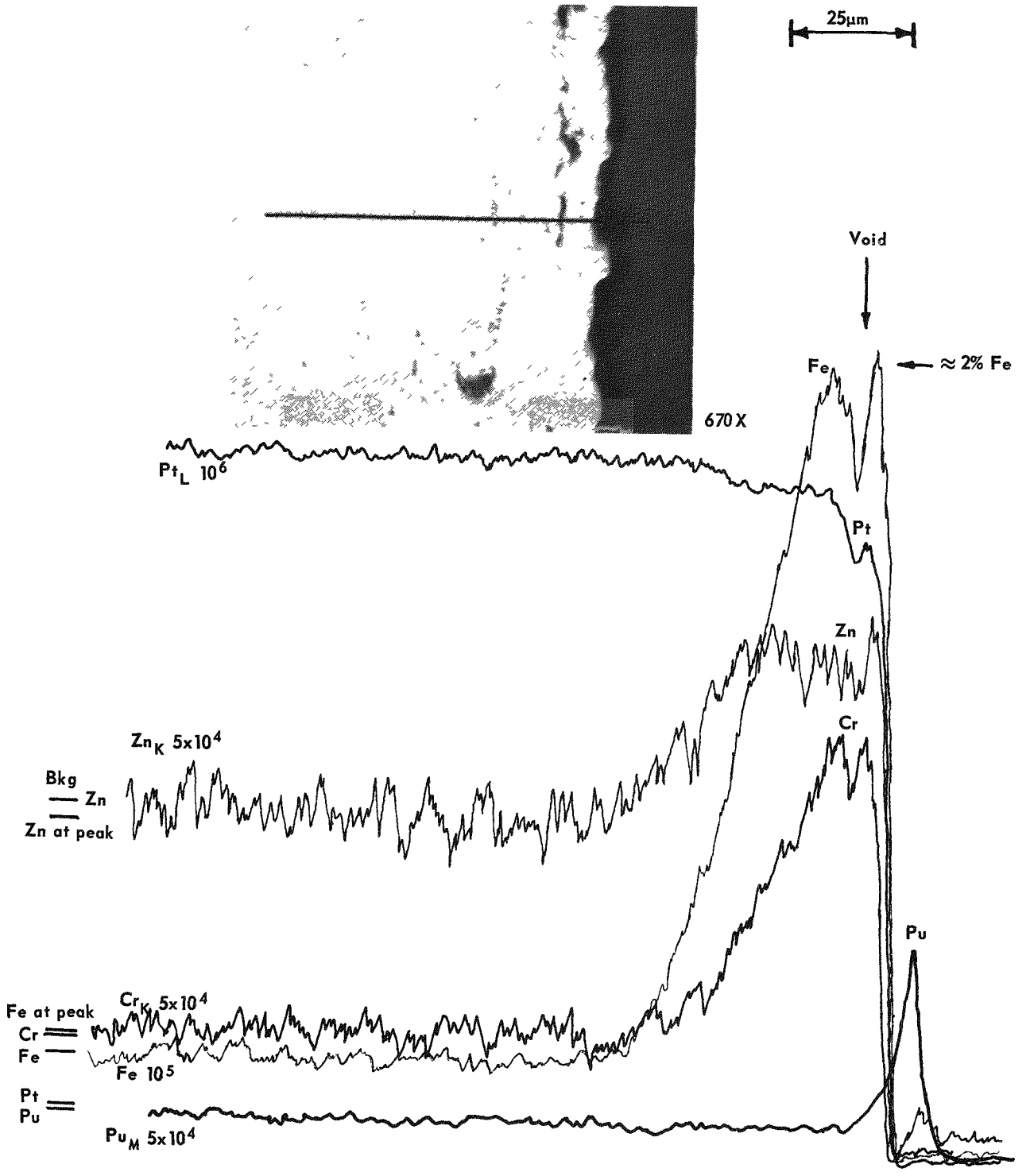

FIGURE 83 - X-ray strip chart analysis of platinum in contact with $^{238}PuO_2$ for 180 days at 800°C in a molybdenum container: same area as Figure 82.

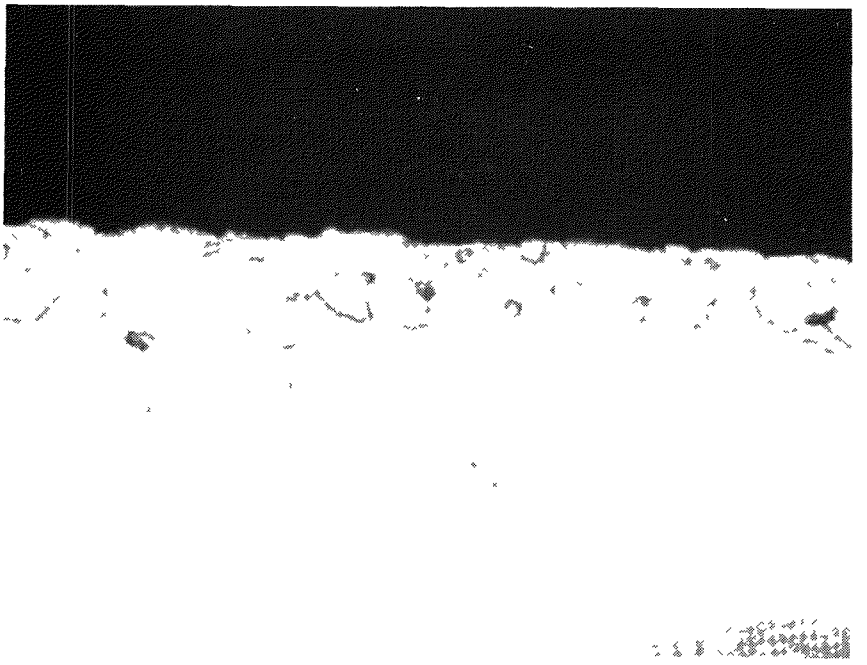

FIGURE 84 - Photomicrograph of platinum-20 wt % rhodium in contact with $^{238}PuO_2$ for 90 days at 800°C in a molybdenum container.
Electrolytic etch 1660X

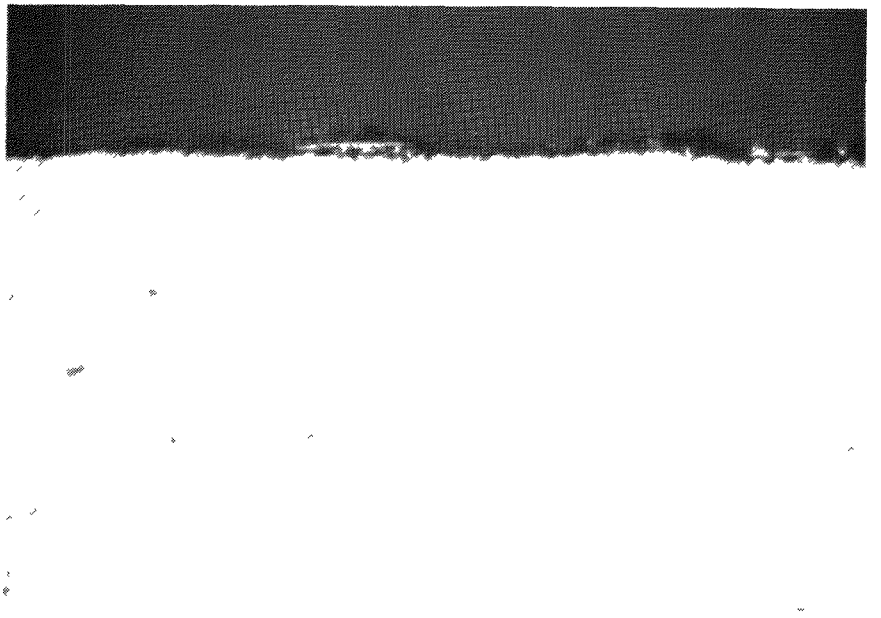

FIGURE 85 - Photomicrograph of platinum-20 wt % rhodium in contact with $^{238}PuO_2$ for 90 days at 800°C in a molybdenum container showing a layer partially separated from the parent material on one end of the sample.
Unetched 670X

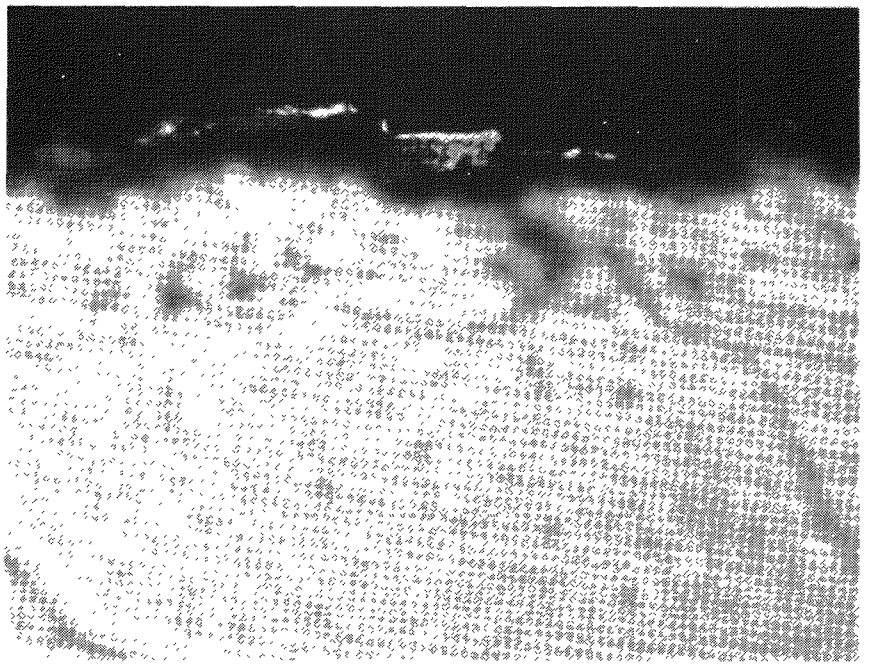

FIGURE 86 - Photomicrograph of platinum-20 wt % rhodium in contact with $^{238}PuO_2$ for 90 days at 800°C in a molybdenum container, showing small grain size in separated layer. Electrolytic etch 1660X

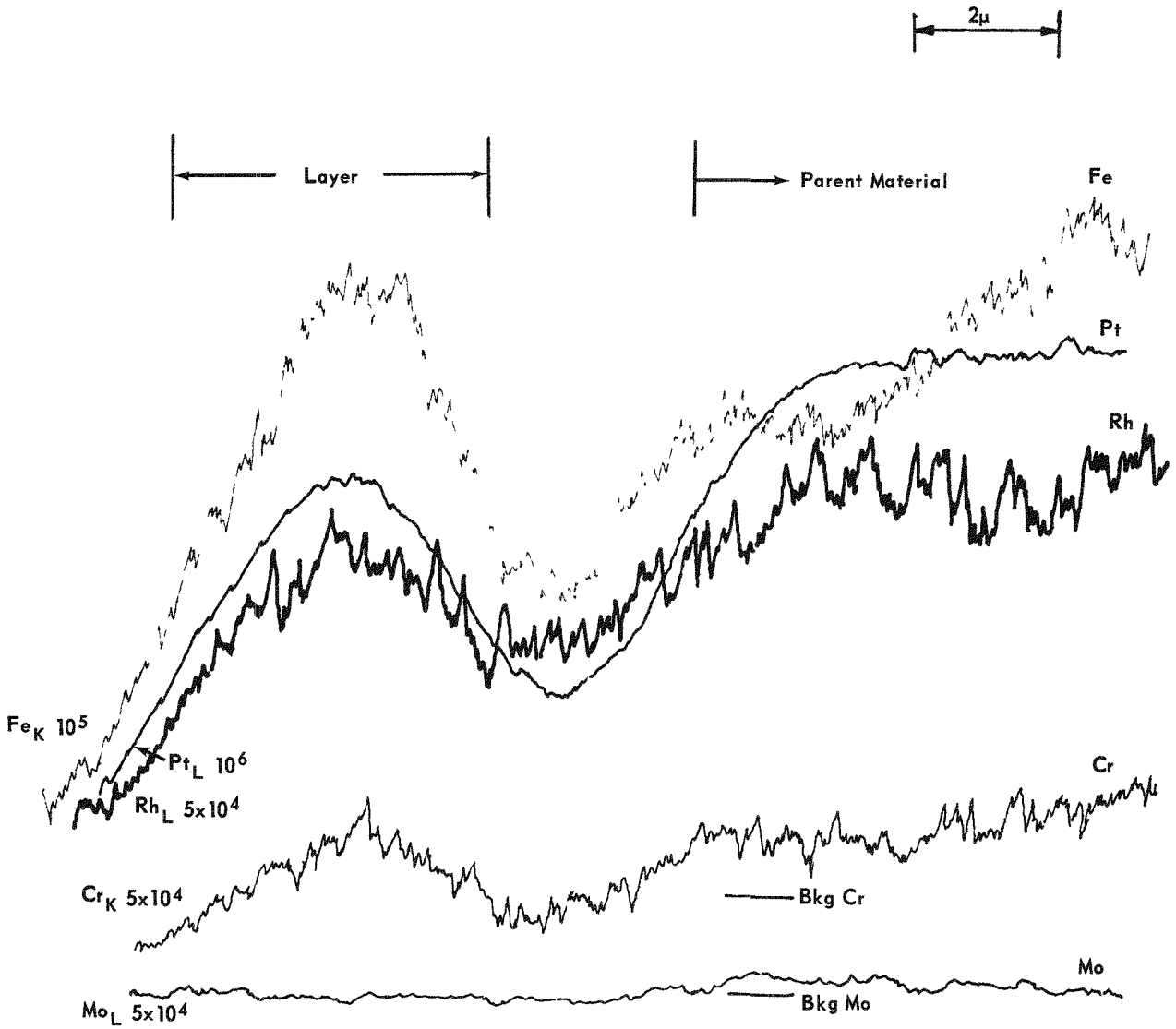

FIGURE 87 - X-ray strip chart analysis of partially separated layer in platinum-20 wt % rhodium in contact with $^{238}PuO_2$ for 90 days at 800°C in a molybdenum container.

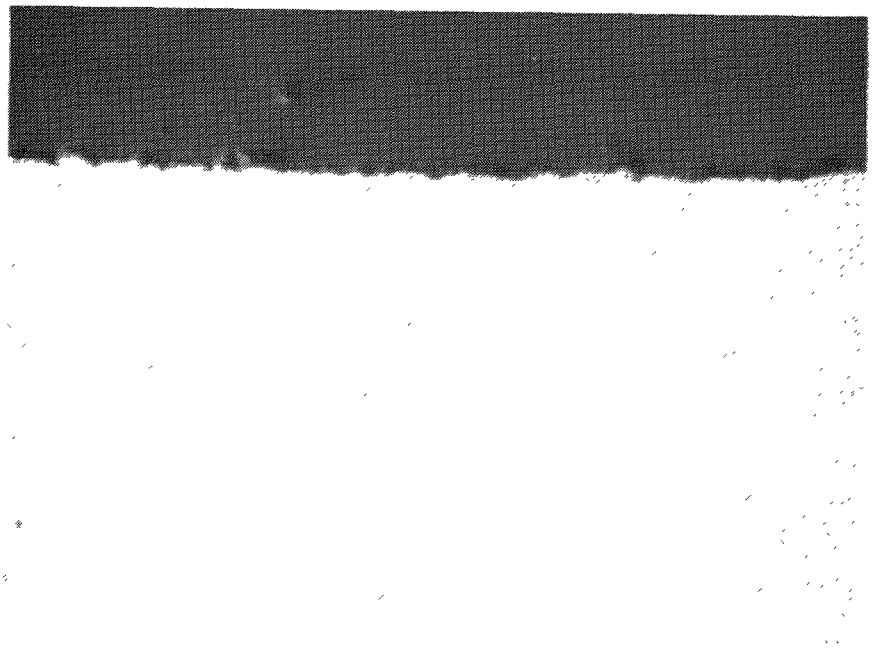

FIGURE 88 - Photomicrograph of platinum-20 wt % rhodium in contact with $^{238}PuO_2$ for 180 days at 800°C in a molybdenum container. Unetched 670X

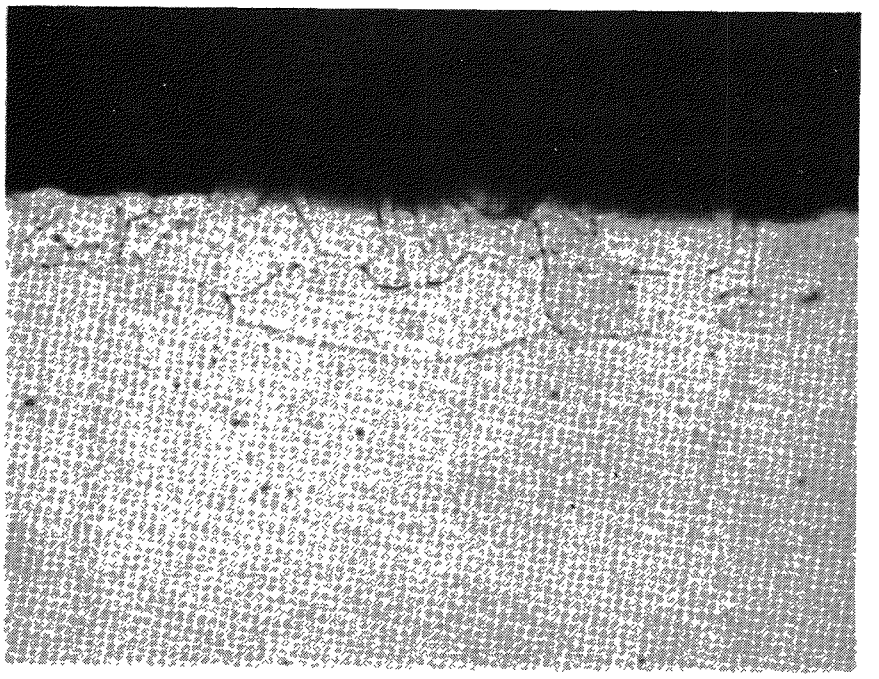

FIGURE 89 - Photomicrograph of platinum-20 wt % rhodium in contact with $^{238}PuO_2$ for 180 days at 800°C in a molybdenum container.
Electrolytic etch 1345X

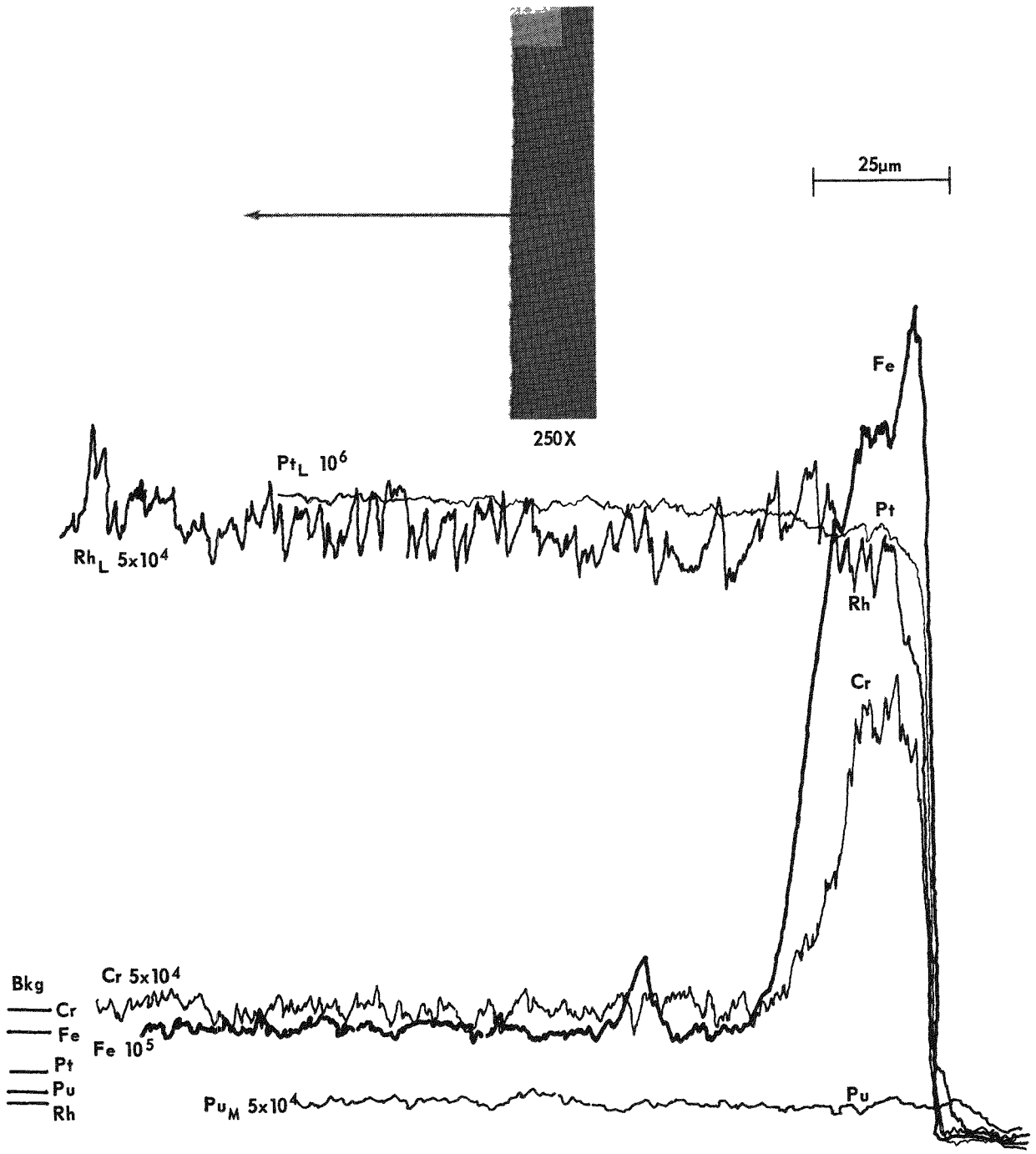

FIGURE 90 - X-ray strip chart analysis of reaction interface of platinum-20 wt % rhodium in contact with $^{238}PuO_2$ for 180 days at 800°C in a molybdenum container.

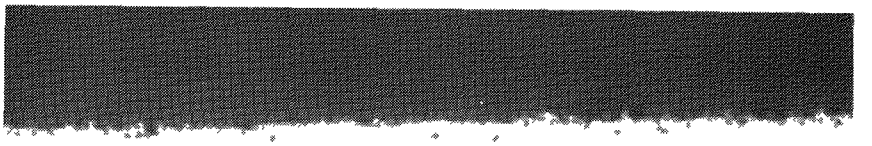

FIGURE 91 - Photomicrograph of platinum-40 wt % rhodium in contact with $^{238}PuO_2$ for 90 days at 800°C in a molybdenum container, showing void formation. Unetched 670X

FIGURE 92 - Photomicrograph of reaction interface of platinum-40 wt % rhodium in contact with $^{238}PuO_2$ for 90 days at 800°C in a molybdenum container. Electrolytic etch 1660X

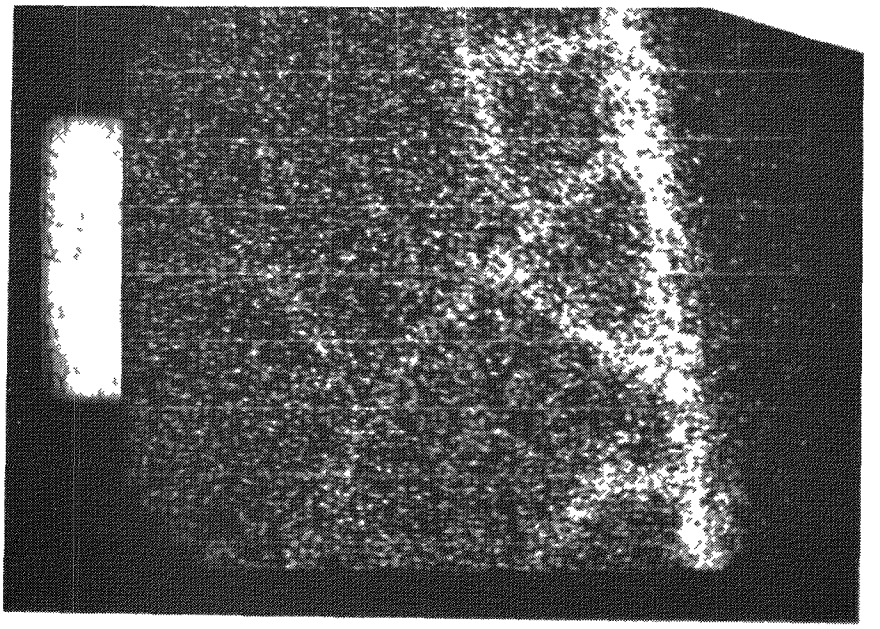

FIGURE 93 - Photomicrograph of the area shown in Figure 92, taken with iron Kα radiation showing grain boundary diffusion of iron. 1660X

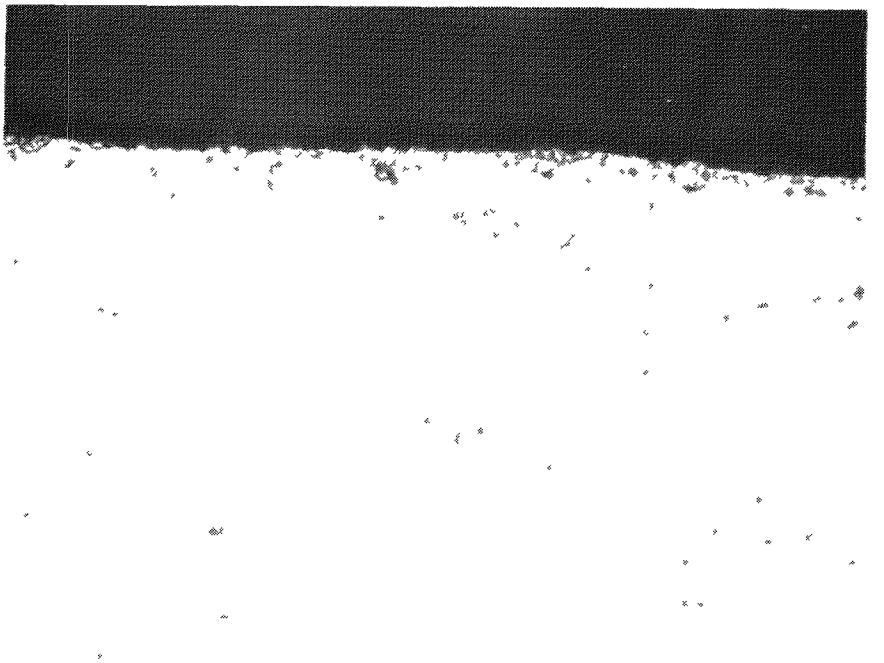

FIGURE 94 - Photomicrograph of platinum-40 wt % rhodium in contact with $^{238}PuO_2$ for 180 days at 800°C in a molybdenum container, showing small grains in reaction layer. Electrolytic etch 670X

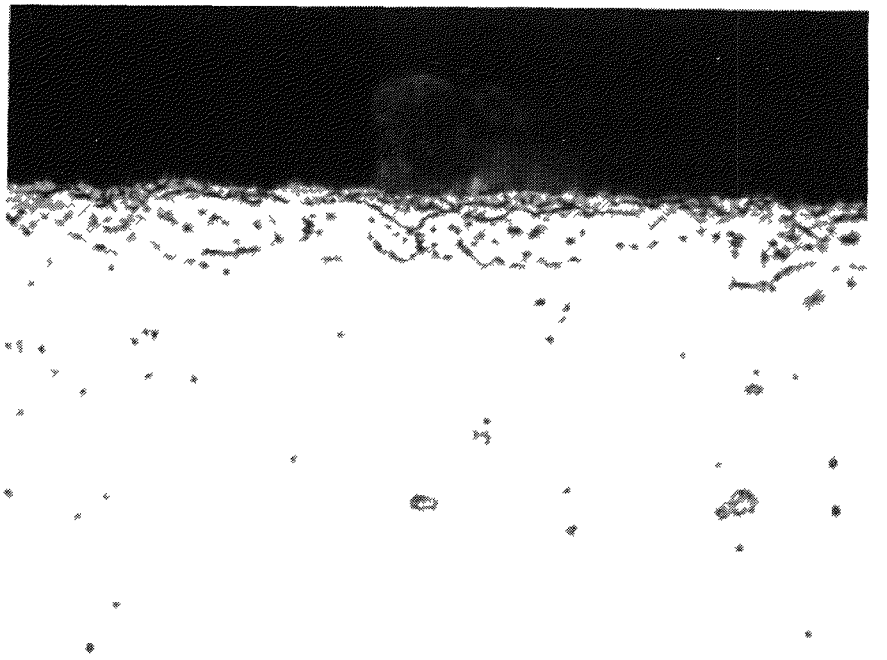

FIGURE 95 - Photomicrograph of platinum-40 wt % rhodium in contact with $^{238}PuO_2$ for 180 days at 800°C in a molybdenum container.
Electrolytic etch 1345X

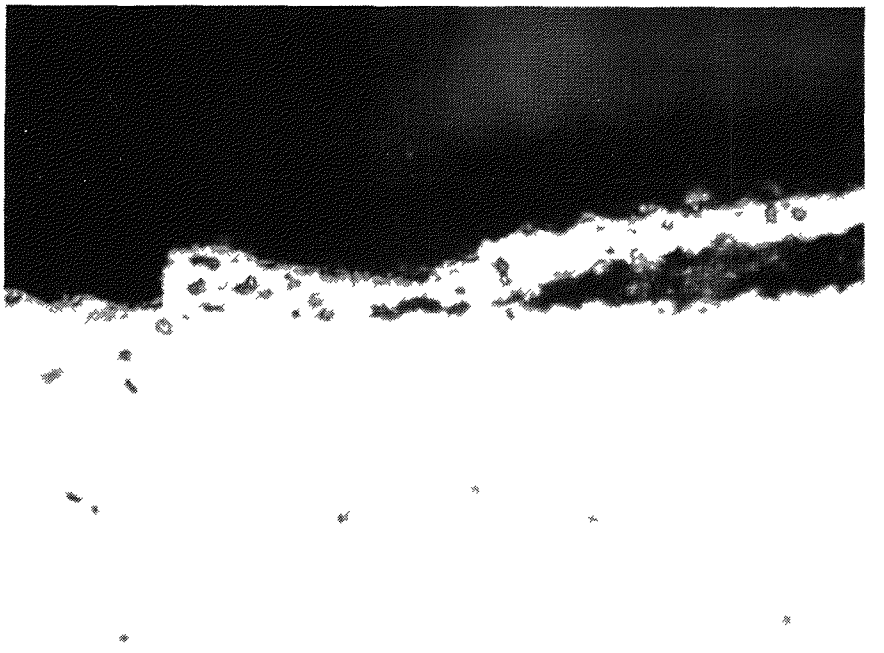

FIGURE 96 - Photomicrograph of platinum-40 wt % rhodium in contact with $^{238}PuO_2$ for 180 days at 800°C in a molybdenum container, showing partial separation of reaction layer. Electrolytic etch 1345X

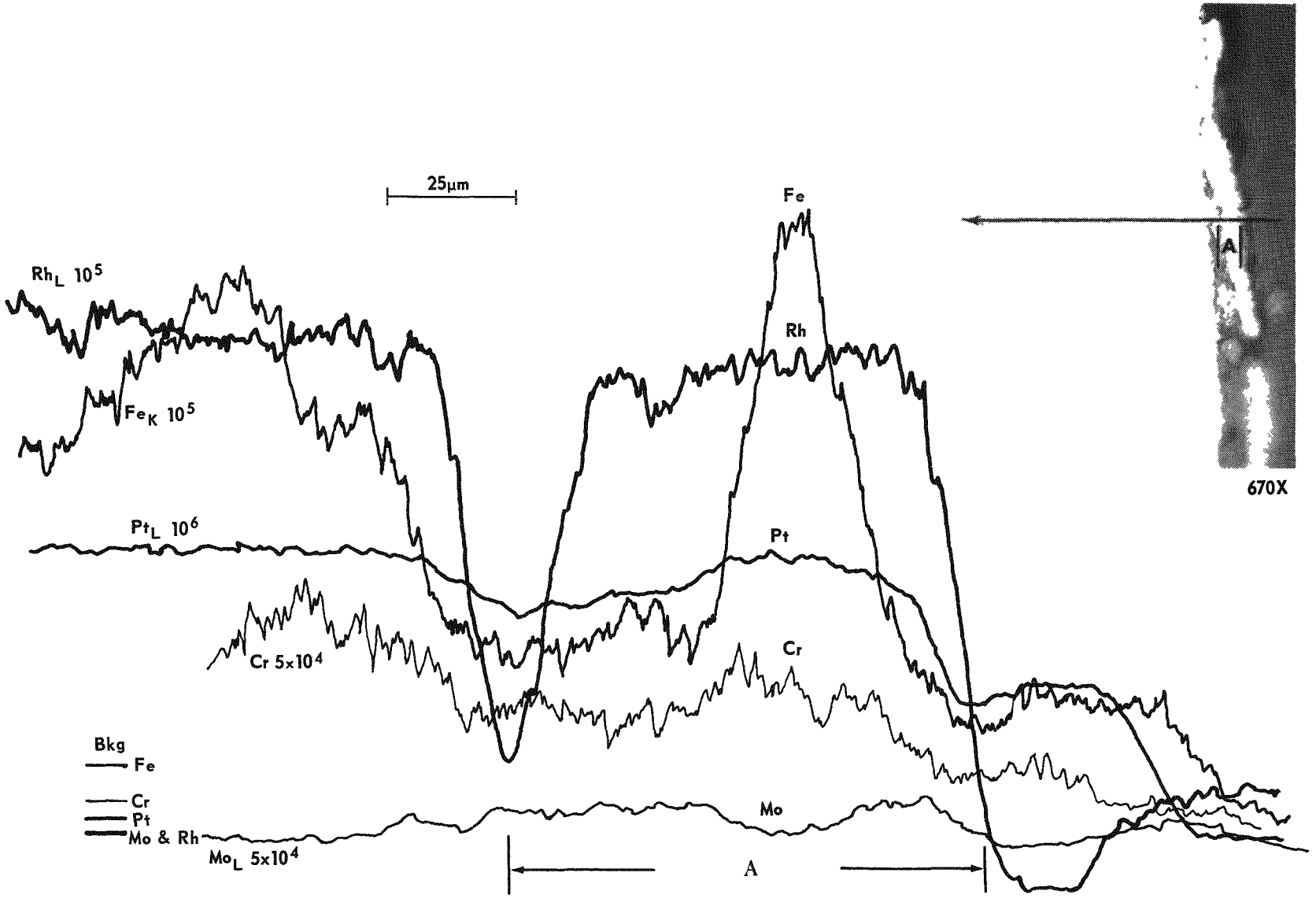

FIGURE 97 - X-ray strip chart analysis of partially separated reaction layer on platinum-40 wt % rhodium in contact with $^{238}PuO_2$ for 180 days at 800°C in a molybdenum container.

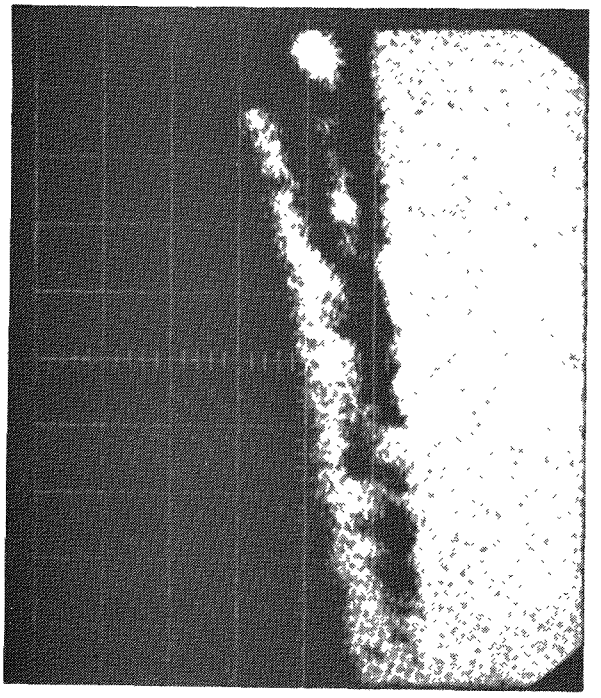

FIGURE 98 - Photomicrograph of platinum-40 wt % rhodium taken with back-scattered electrons: 180 days at 800°C in a molybdenum container. 1760X

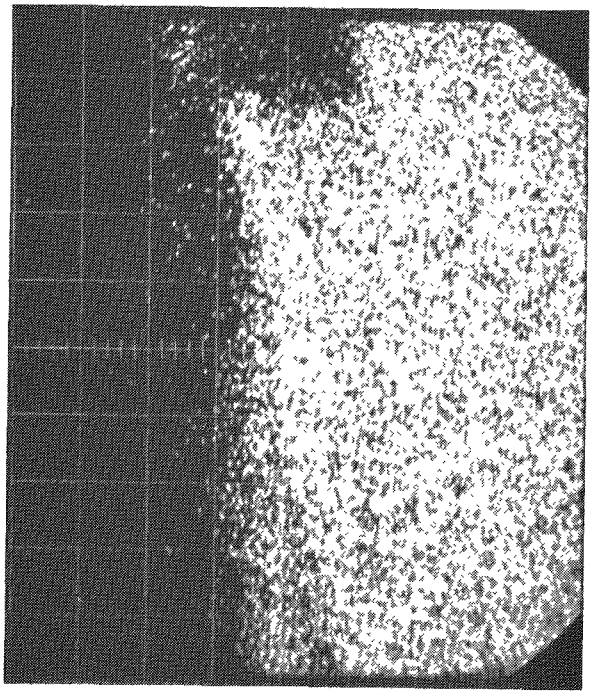

FIGURE 99 - Photomicrograph of platinum-40 wt % rhodium taken with platinum Lα radiation: 180 days at 800°C in a molybdenum container. 1760X

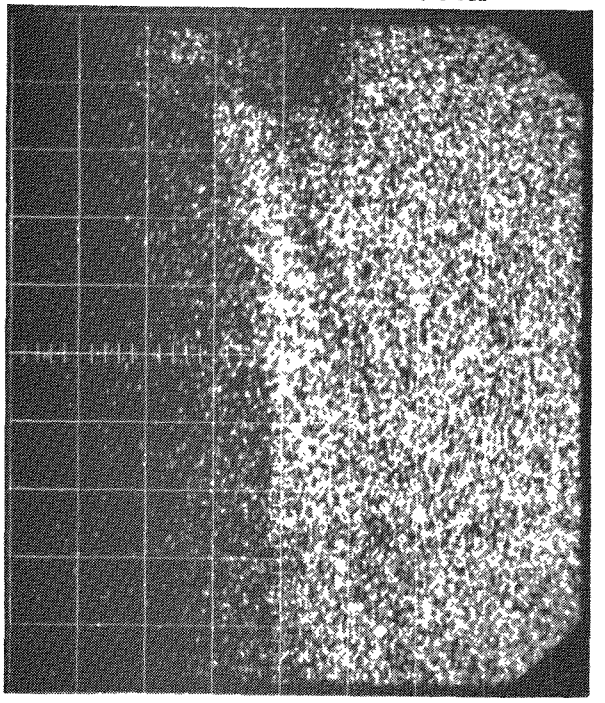

FIGURE 100 - Photomicrograph of platinum-40 wt % rhodium taken with rhodium Lα radiation: 180 days at 800°C in a molybdenum container. 1760X

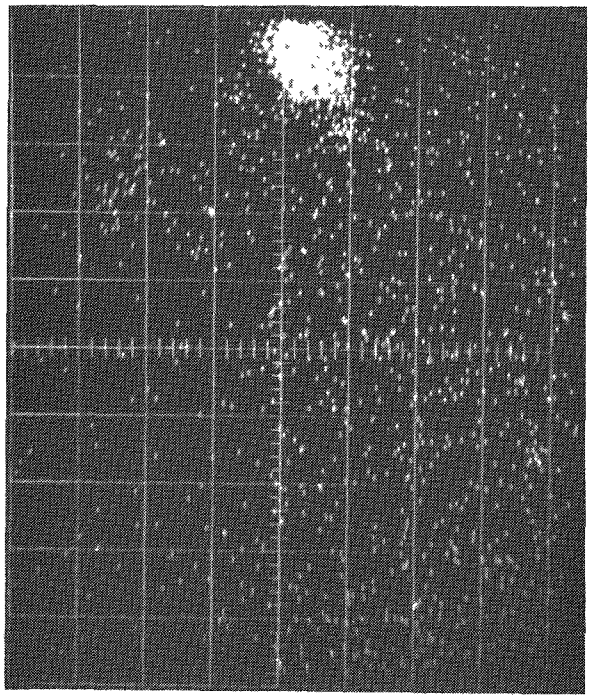

FIGURE 101 - Photomicrograph of platinum-40 wt % rhodium taken with plutonium Mα radiation: 180 days at 800°C in a molybdenum container. 1760X

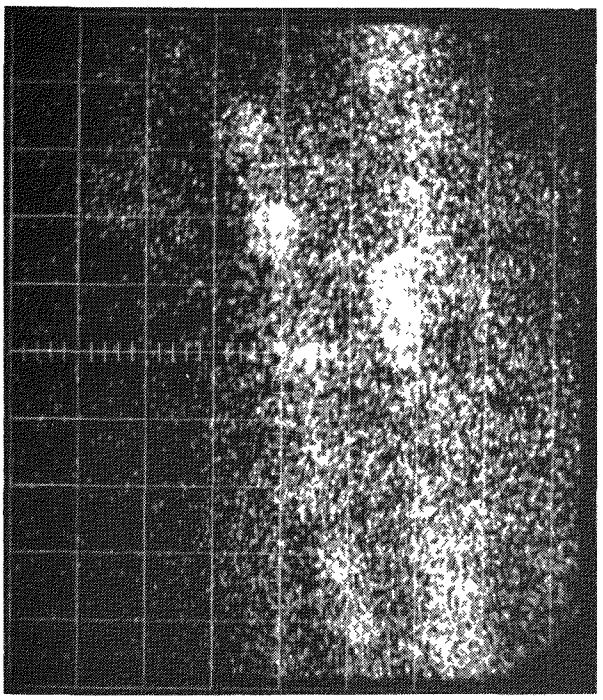

FIGURE 102 - Photomicrograph of platinum-40 wt % rhodium taken with iron Kα radiation: 180 days at 800°C in a molybdenum container. 1760X

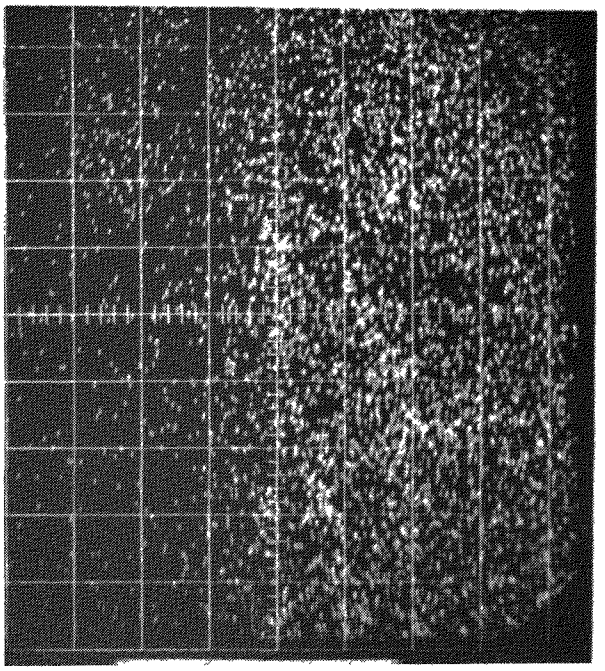

Figure 103 - Photomicrograph of platinum-40 wt % rhodium taken with chromium Kα radiation: 180 days at 800°C in a molybdenum container. 1760X

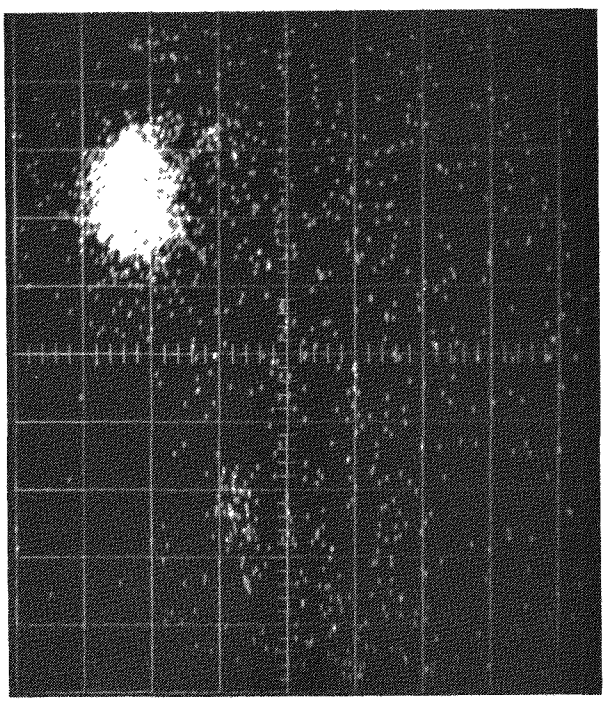

FIGURE 104 - Photomicrograph of platinum-40 wt % rhodium taken with molybdenum Lα radiation: 180 days at 800°C in a molybdenum container. 1760X

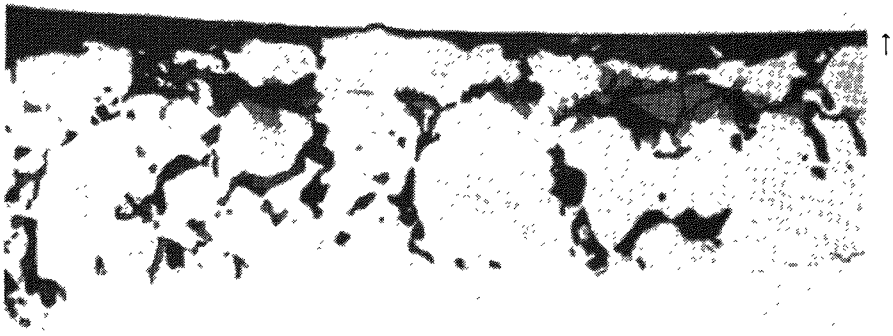

FIGURE 105 - Photomicrograph of typical reaction between $^{238}PuO_2$ and platinum after 30 days at 1000°C in a tantalum container. Unetched 135X

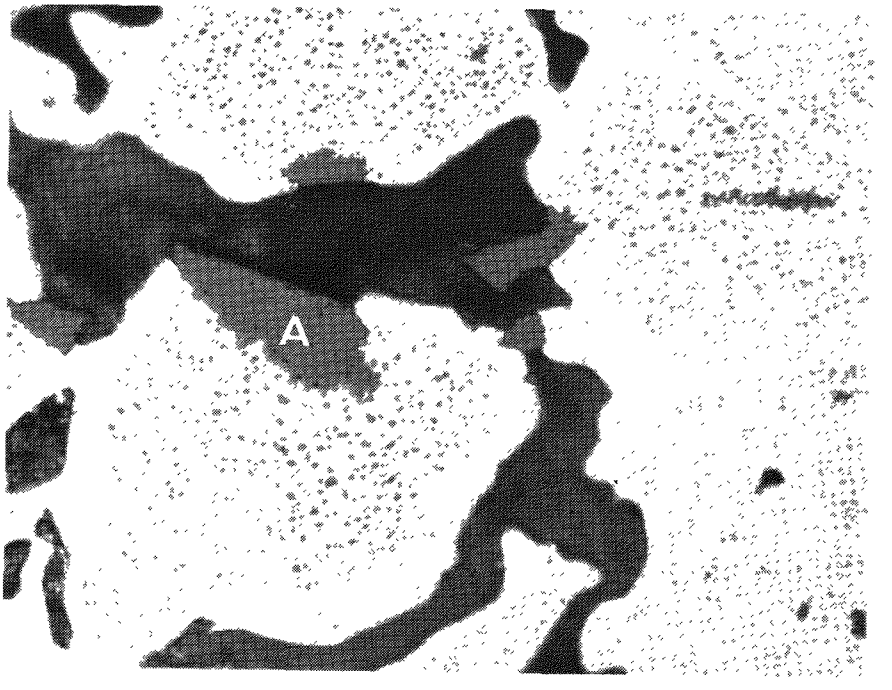

FIGURE 106 - Photomicrograph of two phase reaction product between $^{238}PuO_2$ and platinum after 30 days at 1000°C in a tantalum container. A represents the remainder of a particle of $^{238}PuO_2$ fuel, and B the massive two phase particles. Unetched 640X

Edge retainer

Edge of substrate

FIGURE 107 - Photomicrograph of the reaction interface between $^{238}PuO_2$ and platinum-20 wt % rhodium after 60 days at 1000°C in a tantalum container. Unetched 135X

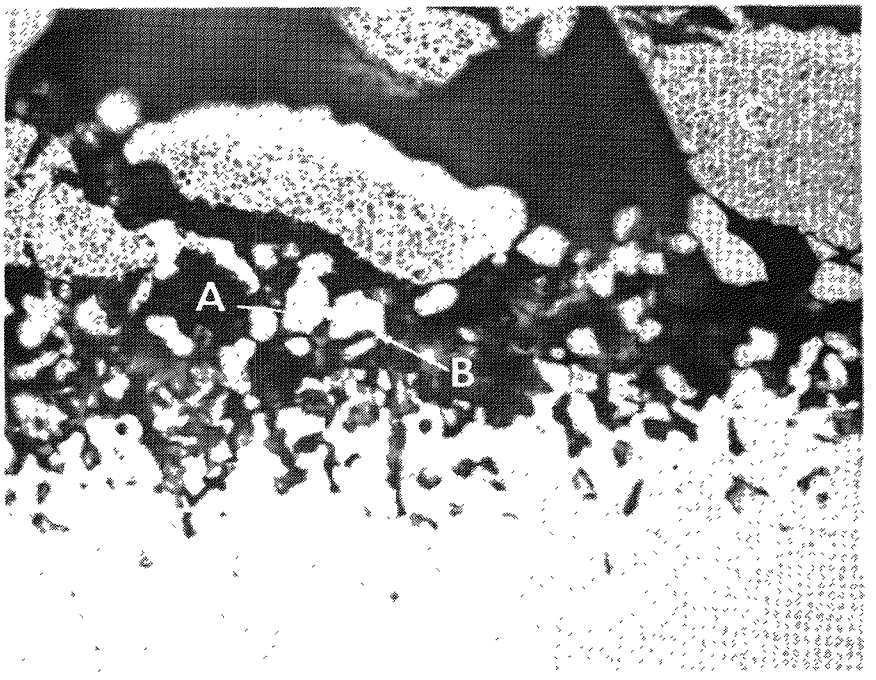

FIGURE 108 - Photomicrograph of the reaction products present at the interface between $^{238}PuO_2$ and platinum-20 wt % rhodium after 60 days at 1000°C in a tantalum container. A contains plutonium, platinum and rhodium and B contains rhodium, iron and chromium. C indicates the massive two phase particles and D indicates the small plutonium bearing precipitate. Unetched 640X

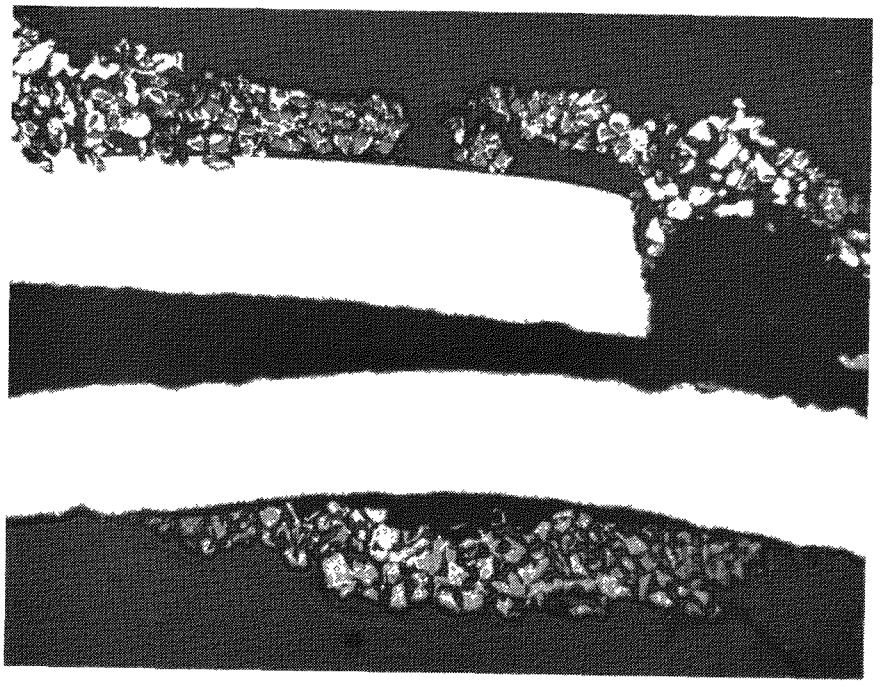

FIGURE 109 - Photomicrograph of platinum-20 wt % rhodium (top sample) and platinum-40 wt % rhodium (bottom sample) in contact with $^{238}PuO_2$ for 90 days at 1000°C in a tantalum container. Unetched 23.2X

FIGURE 110 - Photomicrograph of reaction in platinum-20 wt % rhodium in contact with $^{238}PuO_2$ for 90 days at 1000°C in a tantalum container showing large pits on one side, uniform reaction on the other with part of the reaction product missing. Unetched 100X

FIGURE 111 - Photomicrograph of platinum-20 wt % rhodium in contact with $^{238}PuO_2$ for 90 days at 1000°C in a tantalum container showing reaction product within pits, with unreacted regions. Unetched 135X

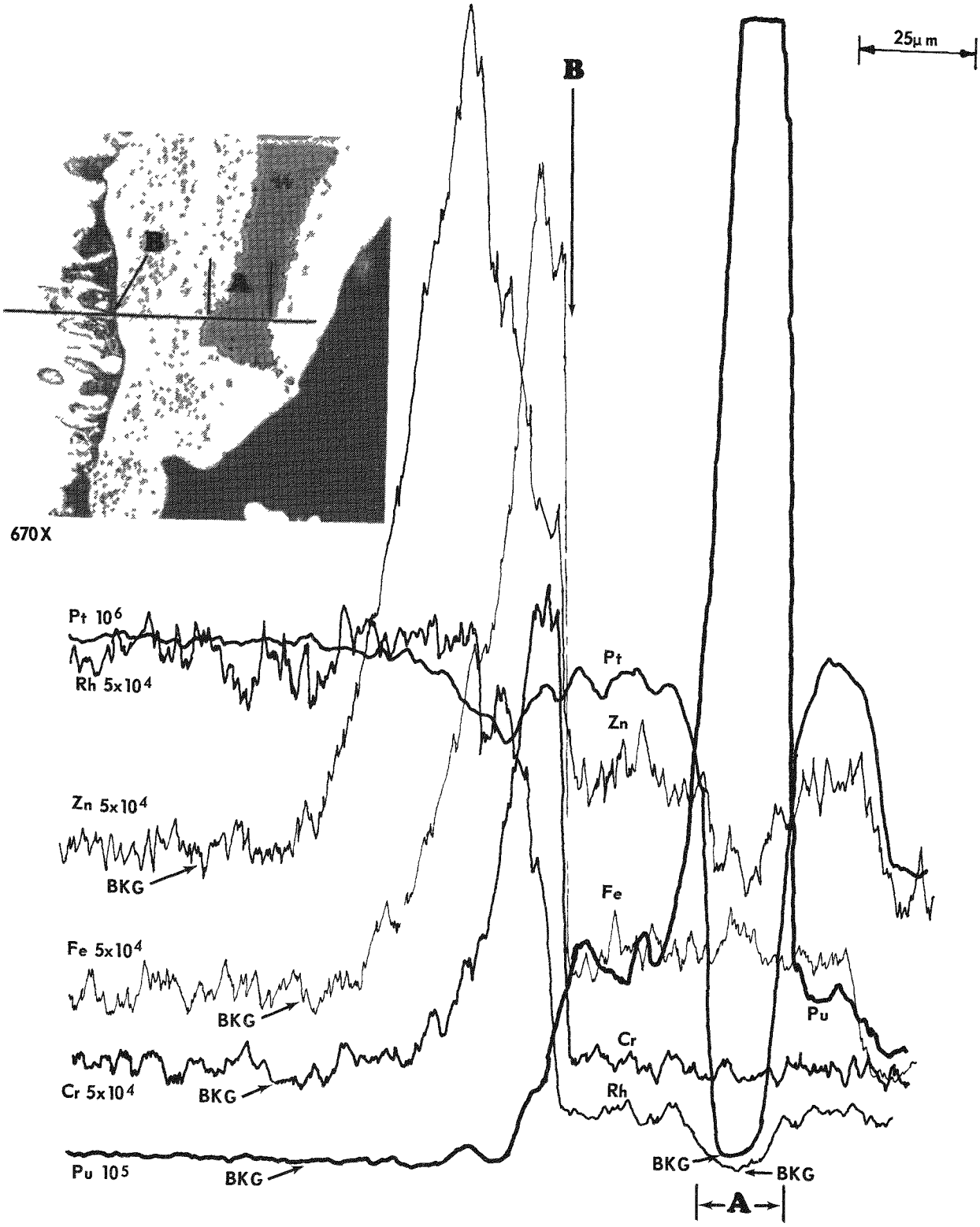

FIGURE 112 - X-ray strip chart analysis of platinum-20 wt % rhodium in contact with $^{238}PuO_2$ for 90 days at 1000°C in a tantalum container.

FIGURE 113 - Photomicrograph of platinum-20 wt % rhodium taken with back-scattered electrons: 90 days at 1000°C in a tantalum container. 440X

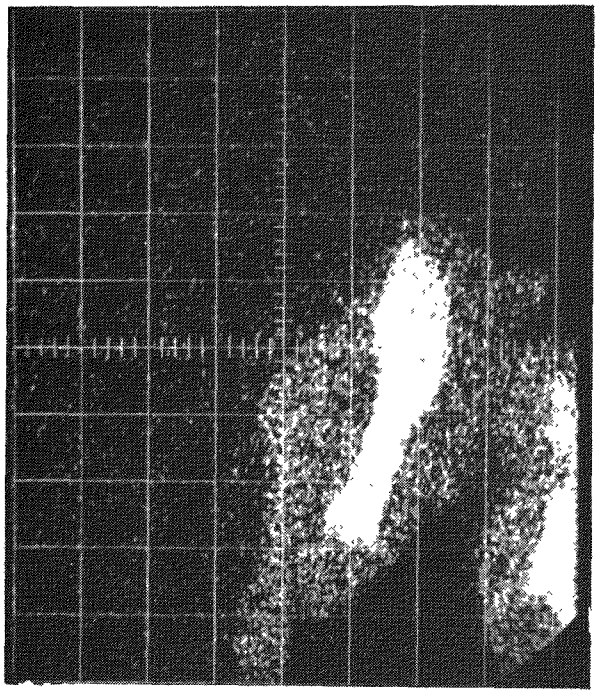

FIGURE 114 - Photomicrograph of platinum-20 wt % rhodium taken with plutonium Mα radiation: 90 days at 1000°C in a tantalum container. 440X

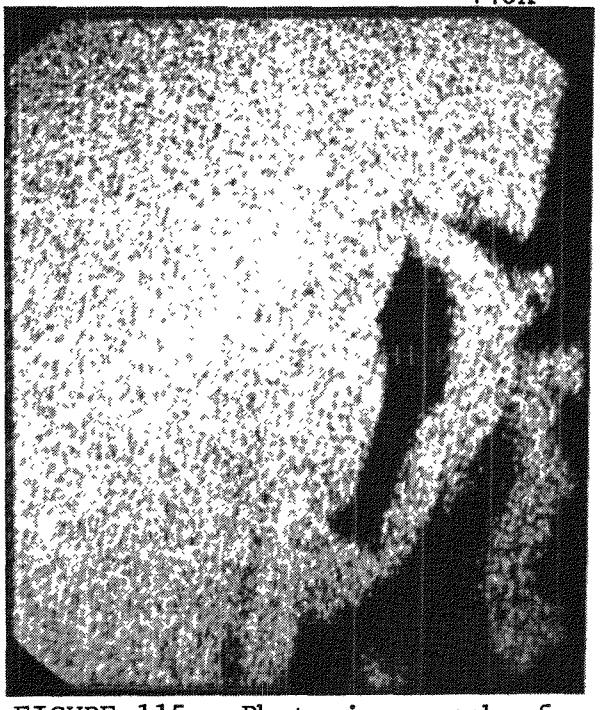

FIGURE 115 - Photomicrograph of platinum-20 wt % rhodium taken with platinum Lα radiation: 90 days at 1000°C in a tantalum container. 440X

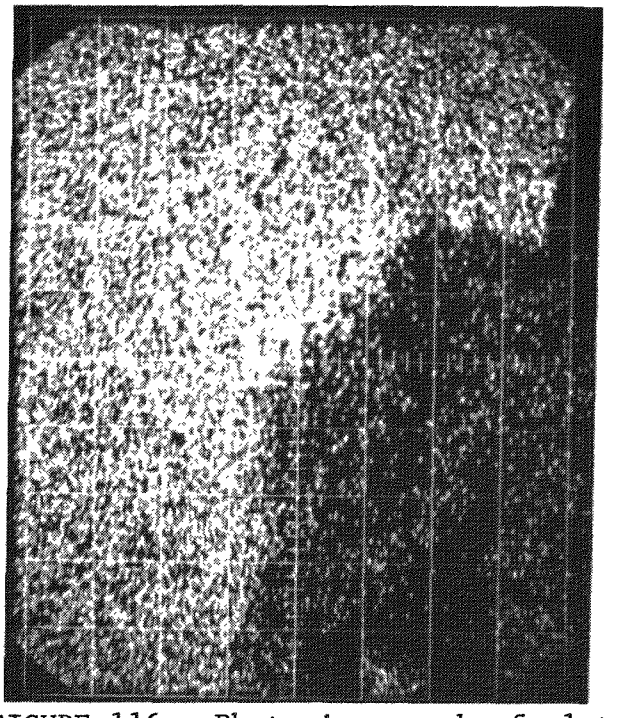

FIGURE 116 - Photomicrograph of platinum-20 wt % rhodium taken with rhodium Lα radiation: 90 days at 1000°C in a tantalum container. 440X

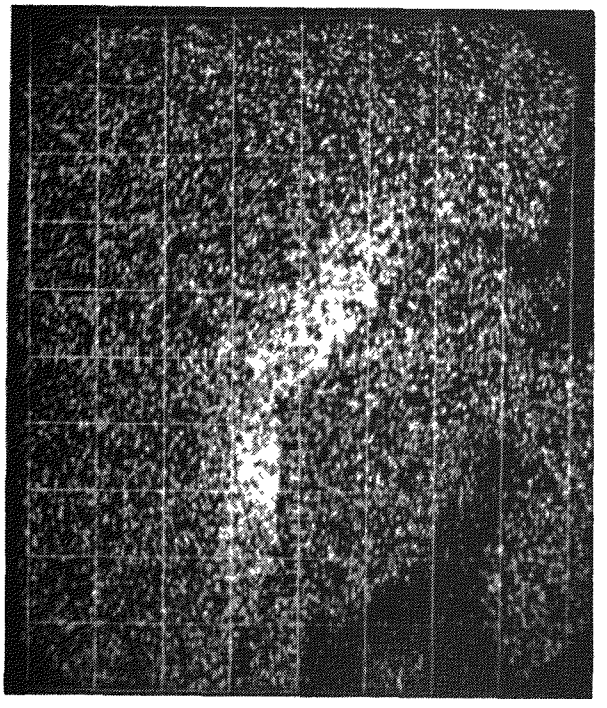

FIGURE 117 - Photomicrograph of platinum-20 wt % rhodium taken with iron Kα radiation: 90 days at 1000°C in a tantalum container. 440X

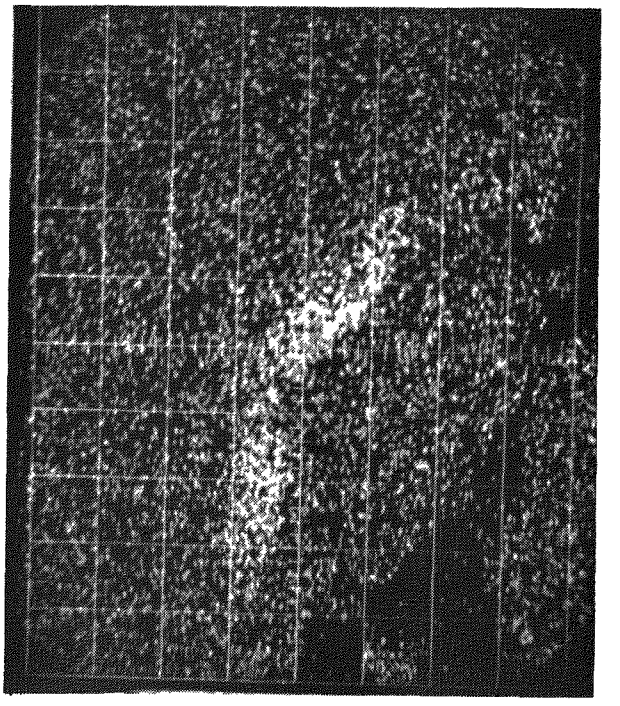

FIGURE 118 - Photomicrograph of platinum-20 wt % rhodium taken with chromium Kα radiation: 90 days at 1000°C in a tantalum container. 440X

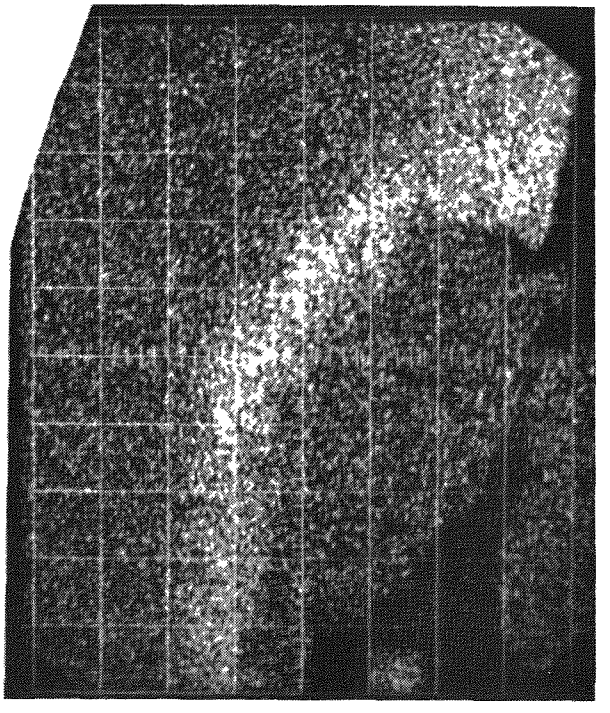

FIGURE 119 - Photomicrograph of platinum-20 wt % rhodium taken with zinc Kα radiation: 90 days at 1000°C in a tantalum container. 440X

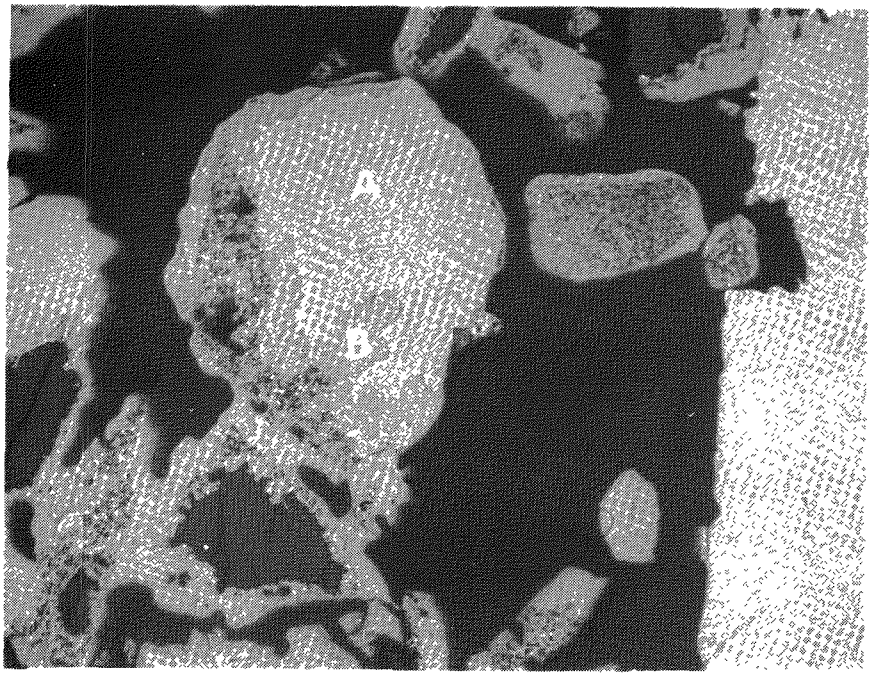

FIGURE 120 - Photomicrograph of massive reaction product formed between $^{238}PuO_2$ and platinum-20 wt % rhodium after 90 days at 1000°C in a tantalum container. Composition of A and B are given in Table X. Unetched 250X

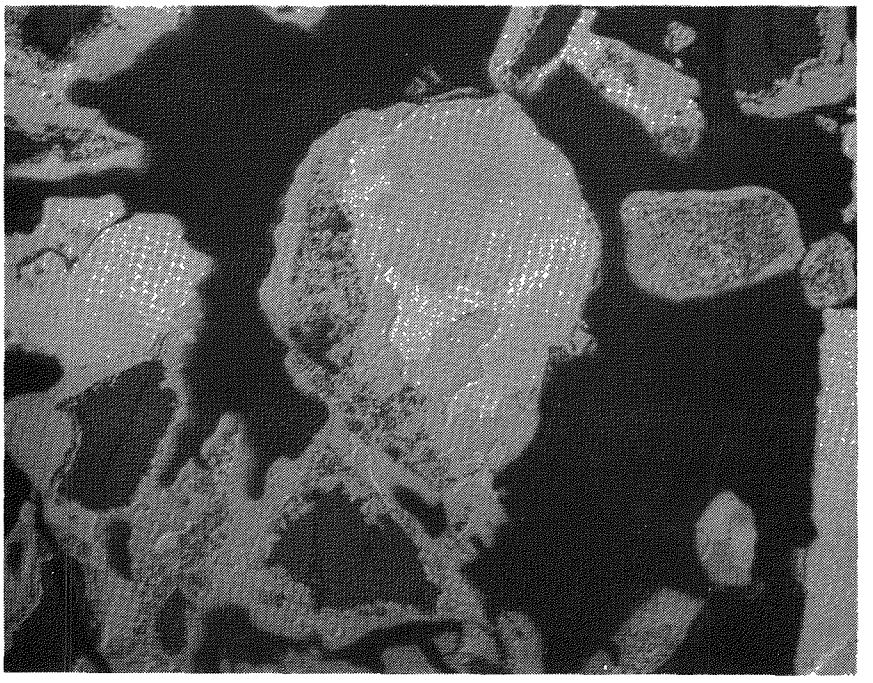

FIGURE 121 - Photomicrograph of region shown in Figure 120 taken in polarized light. Unetched 250X

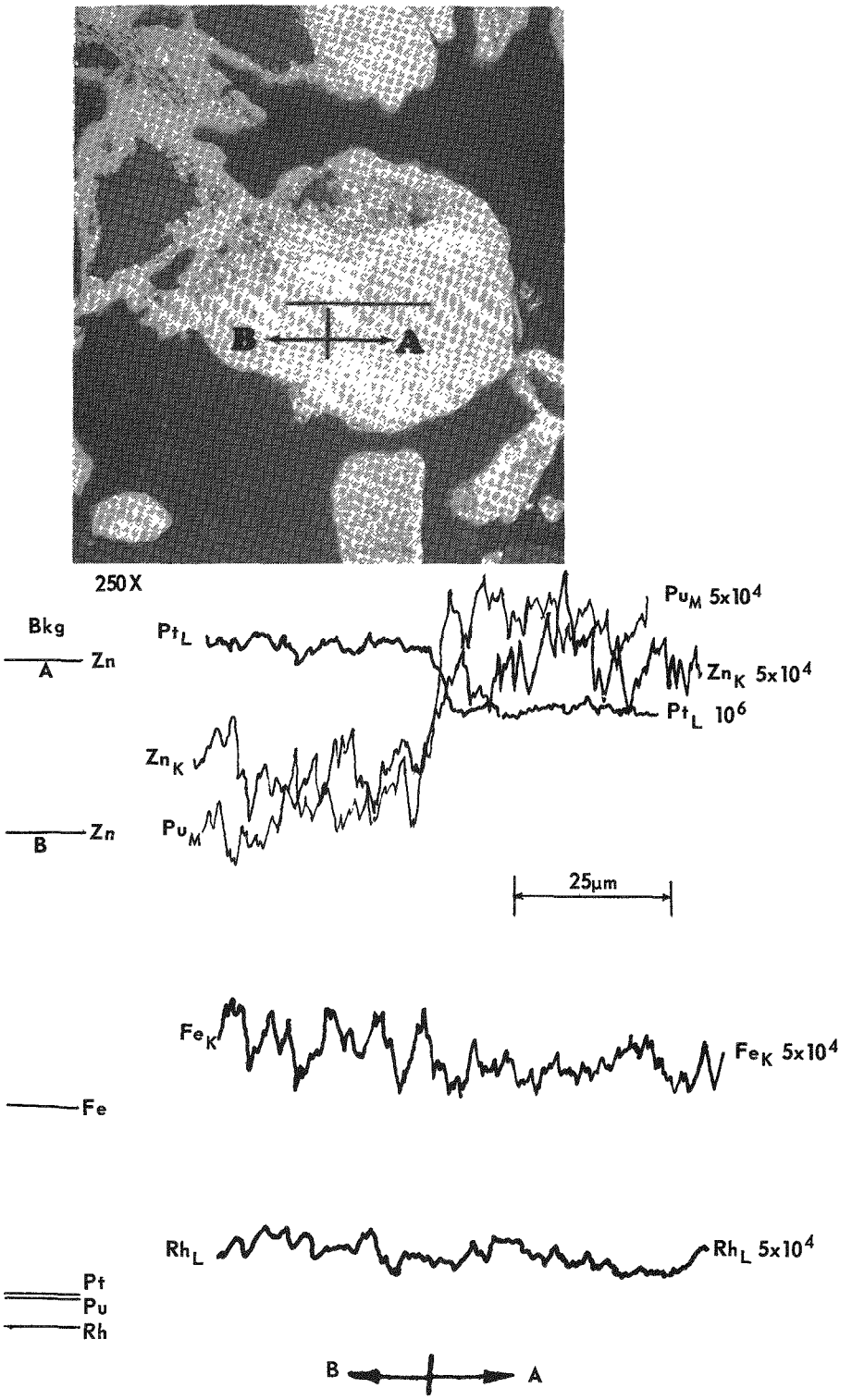

FIGURE 122 - X-ray strip chart analysis of two phase region shown in Figure 120.

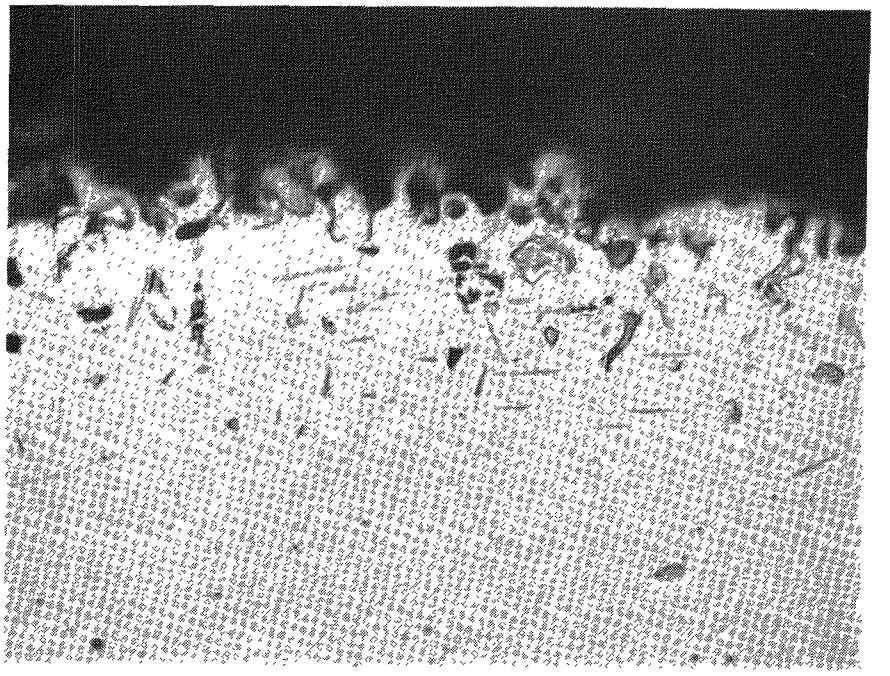

FIGURE 123 - Photomicrograph of porous edge of platinum-20 wt % rhodium in contact with $^{238}PuO_2$ for 90 days at 1000°C in a tantalum container showing dark precipitation in the parent material.

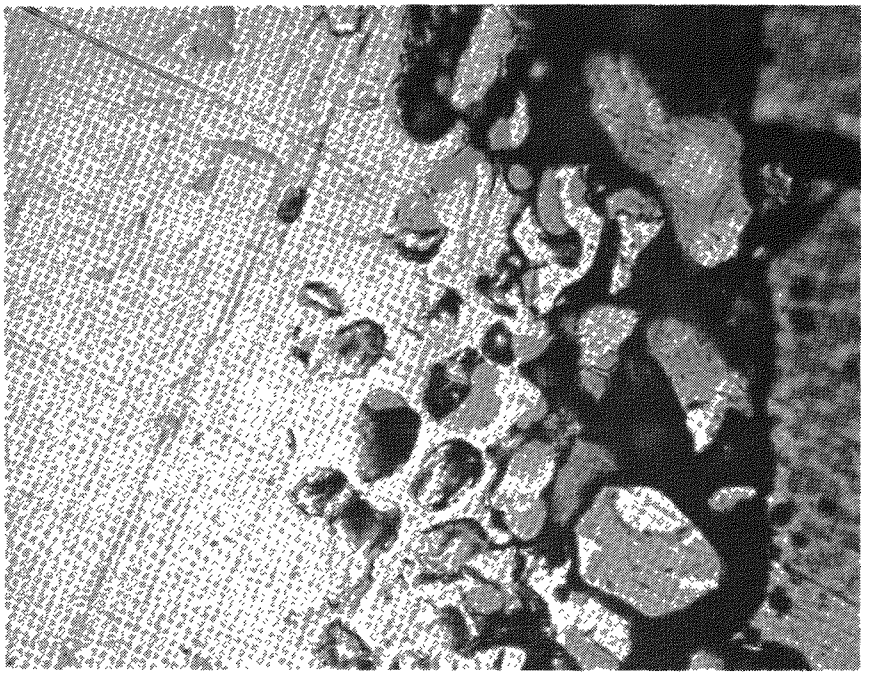

FIGURE 124 - Photomicrograph of porous edge of platinum-20 wt % rhodium in contact with $^{238}PuO_2$ for 90 days at 1000°C in a tantalum container, showing small two phase particles similar to those in Figure 108.
Unetched 1560X

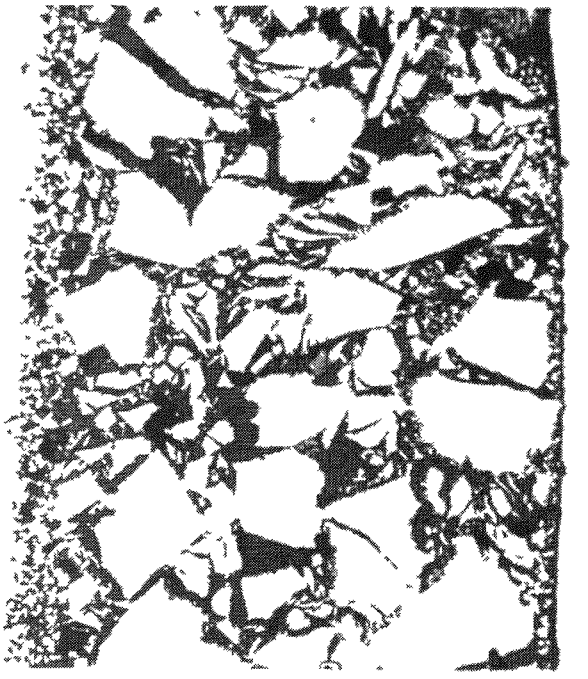

← ~20 mils →

FIGURE 125 - Photomicrograph of typical reaction between $^{238}PuO_2$ and platinum-40 wt % rhodium after 60 days at 1000°C in a tantalum container. Unetched 135X

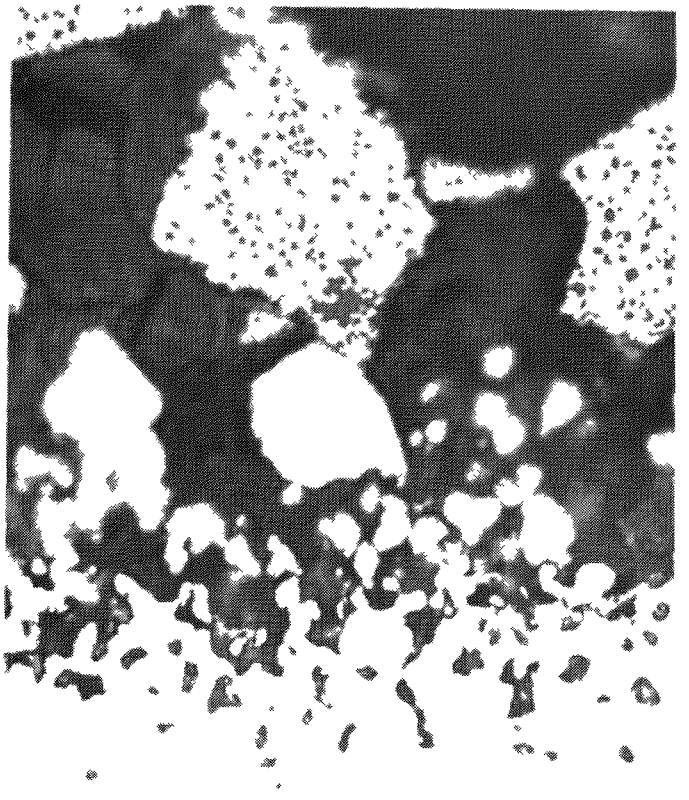

FIGURE 126 - Photomicrograph of the reaction products present at the interface between $^{238}PuO_2$ and platinum-40 wt % rhodium after 60 days at 1000°C in a tantalum container. Phase A contains platinum, rhodium and plutonium, B contains rhodium, chromium and iron, C indicates the massive two phase particles and D contains plutonium, platinum and possibly rhodium. Unetched 670X

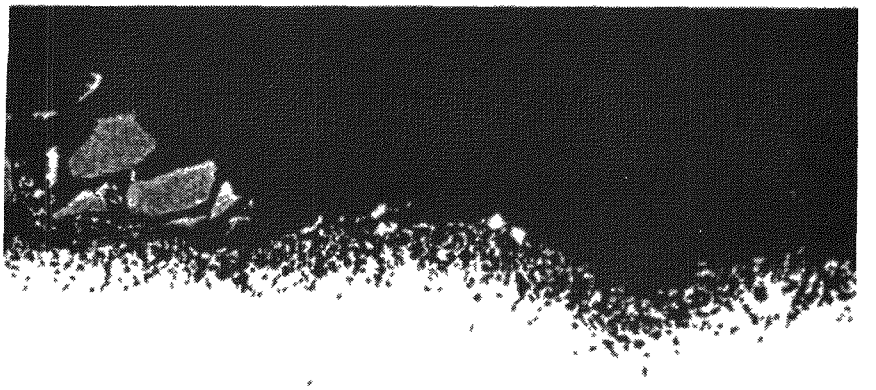

FIGURE 127 - Photomicrograph of the porous edge of platinum-40 wt % rhodium in contact with $^{238}PuO_2$ for 90 days at 1000°C in a tantalum container. Unetched 135X

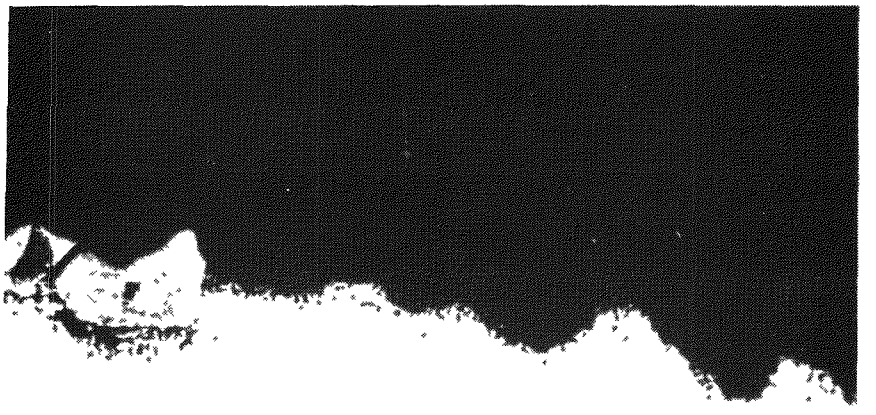

FIGURE 128 - Photomicrograph of the porous edge of platinum-40 wt % rhodium in contact with $^{238}PuO_2$ for 90 days at 1000°C in a tantalum container showing pitting at PuO_{2-x} particle and reaction product. Unetched 135X

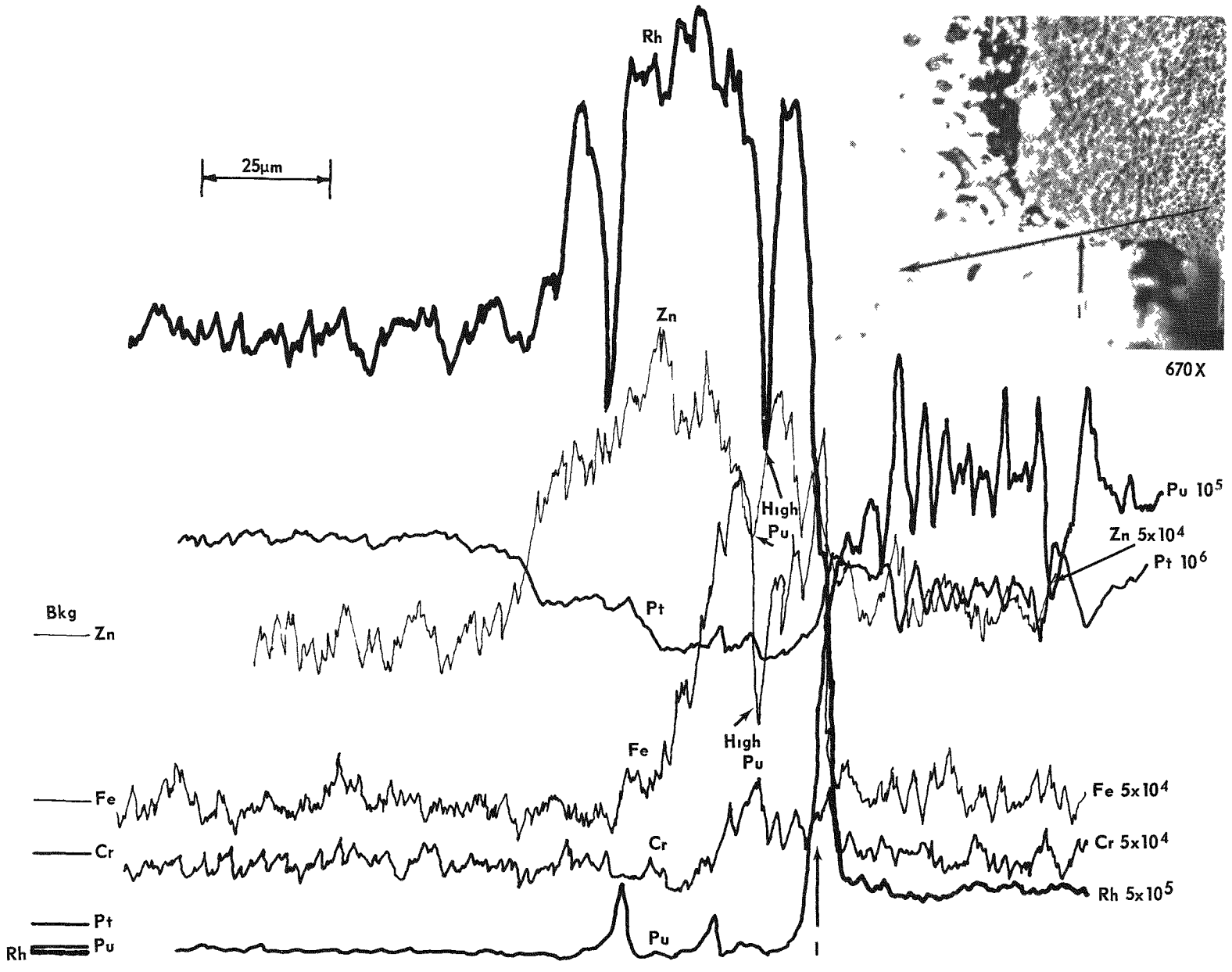

FIGURE 129 - X-ray strip chart analysis of platinum-40 wt % rhodium in contact with $^{238}PuO_2$ for 90 days at 1000°C in a tantalum container.

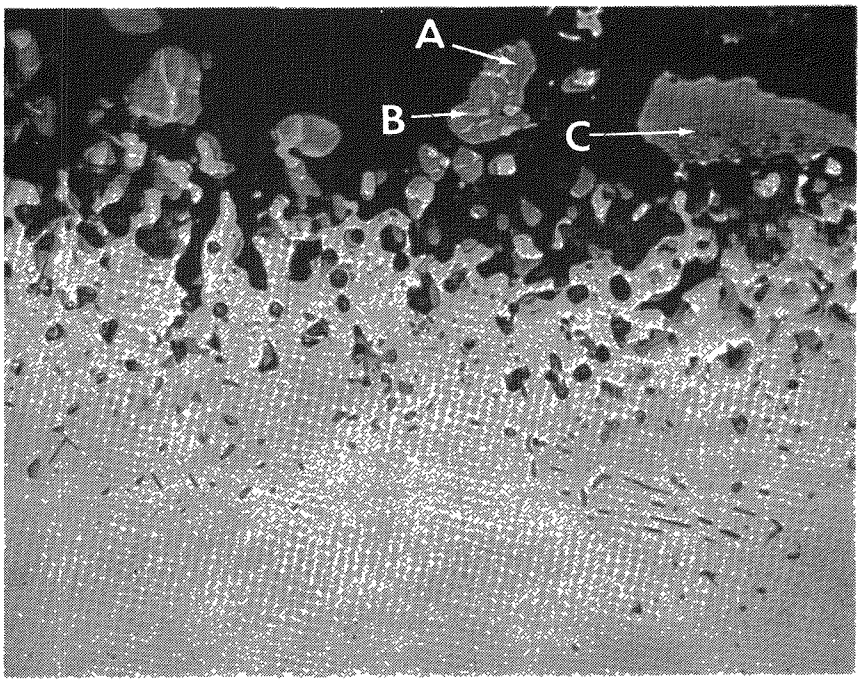

FIGURE 130 - Photomicrograph of porous edge of platinum-40 wt % rhodium in contact with $^{238}PuO_2$ for 90 days at 1000°C in a tantalum container. A and B are phases of the small two phase particles, C is a small portion of the massive two phase reaction product. Unetched 670X

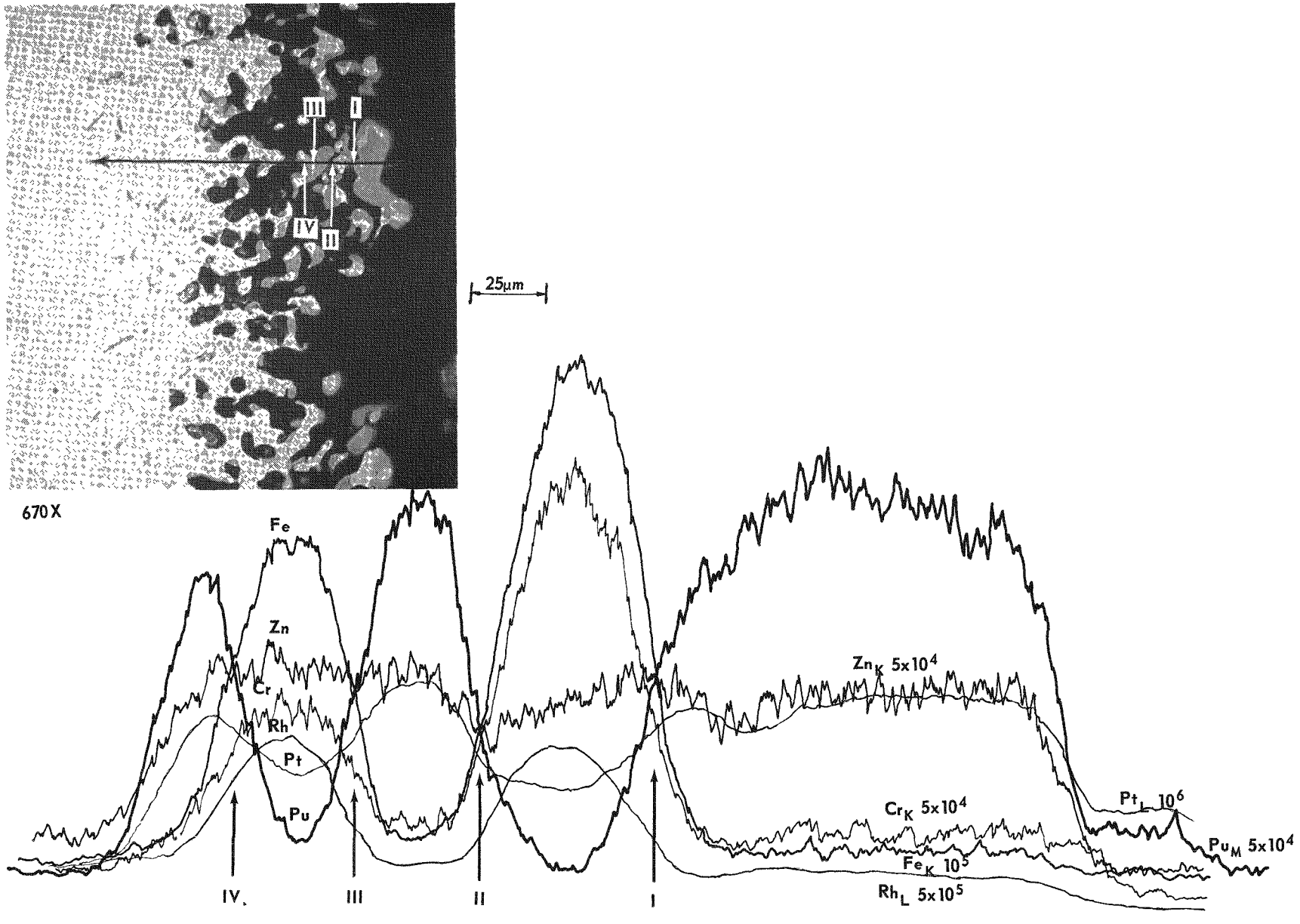

FIGURE 131 - X-ray strip chart analysis of platinum-40 wt % rhodium in contact with $^{238}PuO_2$ for 90 days at 1000°C in a tantalum container.

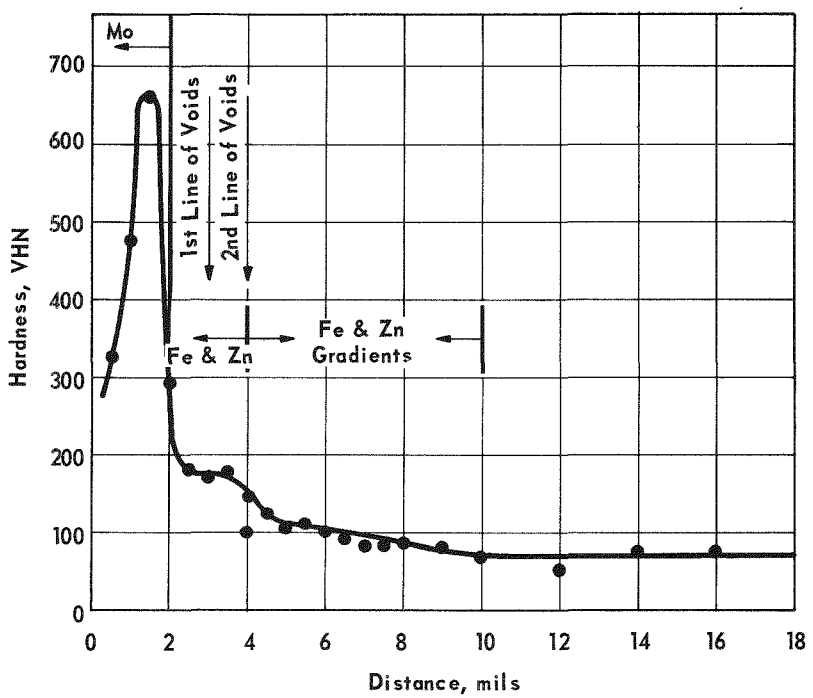

FIGURE 132 - Microhardness traverse across platinum sample in contact with $^{238}PuO_2$ for 60 days at 1000°C. Note good correlation with electron microprobe results of Figure 65.

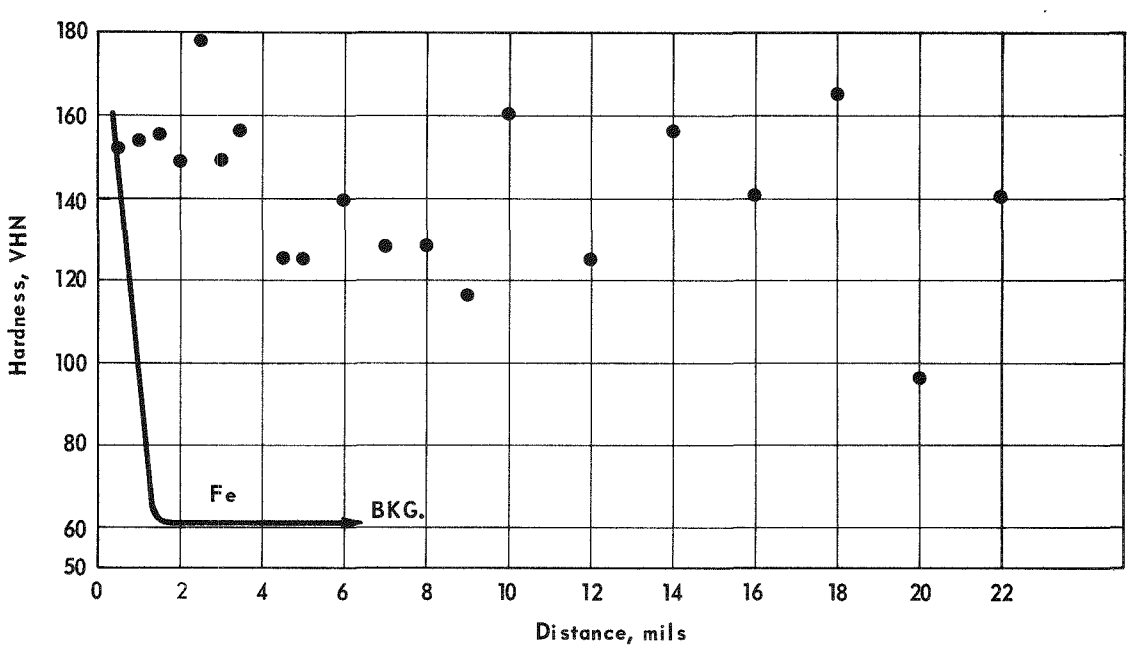

FIGURE 133 - Microhardness traverse across platinum-20 wt % rhodium in contact with $^{238}PuO_2$ for 66 days at 800°C. Correlation with microprobe data (Fe concentration) is poor.

APPENDIX A

IMPURITY ANALYSES OF PLATINUM AND PLATINUM-RHODIUM ALLOYS USED IN COMPATIBILITY TESTS

Element	Analysis Number[a]								
	569 Pt	567 Pt-Rh	568 Pt	360 Pt-Rh	361 Pt-Rh	542 Pt	543 Pt-20 Rh	673 Pt-40 Rh	730 Pt-30 Rh
Ag	--	--	0.0005	--	--	0.005	0.005	<0.0005	0.001
Al	--	<0.0005	0.001	0.002	0.002	--	--	<0.0005	<0.0005
B	--	0.005	0.0005	0.005	0.003	--	0.003	0.0005	0.003
Ca	--	--	--	--	--	<0.05	--	--	--
Cr	--	--	--	0.003	0.002	--	--	--	--
Cu	0.003	0.003	0.005	0.002	0.003	0.0008	0.005	0.003	0.001
Fe	--	0.03	0.002	0.01	0.008	0.003	0.04	0.01	0.006
Mg	--	<0.0005	<0.0005	<0.0005	<0.0005	<0.0005	0.0005	<0.0005	<0.0005
Mo	--	0.005	--	--	--	--	--	--	--
Ni	--	0.005	--	<0.005	0.005	--	0.04	--	--
Pb	--	--	--	--	0.003	--	--	--	--
Pd	0.005	0.01	0.02	0.005	0.02	--	0.05	0.02	0.02
Si	--	0.005	0.001	0.001	0.001	0.0008	0.0008	0.001	0.02
Zr	--	--	--	0.003	0.001	--	--	--	--
C	0.002	0.004	--	0.002	0.001	0.001	0.001	<0.002	0.002
H	<0.0001	<0.0001	--	0.001	0.001	0.0001	0.0001	0.0001	<0.001
O	0.0006	<0.0001	--	0.003	0.007	0.001	0.002	0.005	0.003
N	0.0001	<0.0001	--	0.001	0.001	0.0003	0.0007	0.0002	0.001

[a] See Table 1.

APPENDIX B

CHEMICAL ANALYSES OF FUEL SAMPLES USED IN PLATINUM AND PLATINUM-RHODIUM COMPATIBILITY TESTS[a]

Element	Batch Number						
	MS-45	P-377 & 378	69-S-9	PP-6	PPX-25-IV	69-S-52	PPX-18-1
Al	0.09	--	0.05	<0.02	0.09	0.07	0.08
B	0.03	--	<0.02	<0.01	<0.03	<0.01	<0.06
Ca	0.07	0.03	0.12	0.08	0.08	0.03	0.09
Co	0.42	0.11	--	0.15	--	--	--
Cr	0.32	0.09	--	0.06	0.08	<0.03	0.10
Cu	0.01	--	--	--	<0.03	Trace	<0.03
Fe	0.46	0.28	0.21	0.27	0.47	0.06	0.43
Mg	0.12	0.01	0.02	0.01	0.04	0.01	0.08
Mn	0.11	--	--	<0.02	<0.01	--	<0.03
Na	--	--	Trace	Trace	Trace	Trace	Trace
Ni	0.07	--	<0.007	<0.03	<0.04	<0.02	<0.05
Pb	0.44	--	--	--	--	--	<0.27
Si	--	--	Trace	Trace	Trace	Trace	Trace
Sn	--	--	--	--	--	--	--
Mo	--	--	--	--	--	--	--
Zn	0.11	--	--	--	0.08	<0.03	0.32
Zr	--	--	--	--	--	--	--
Total	2.25	0.52	0.43	0.65	0.95	0.26	1.54

[a]Compositions are in wt %.

APPENDIX C

CAPSULE DESIGNS

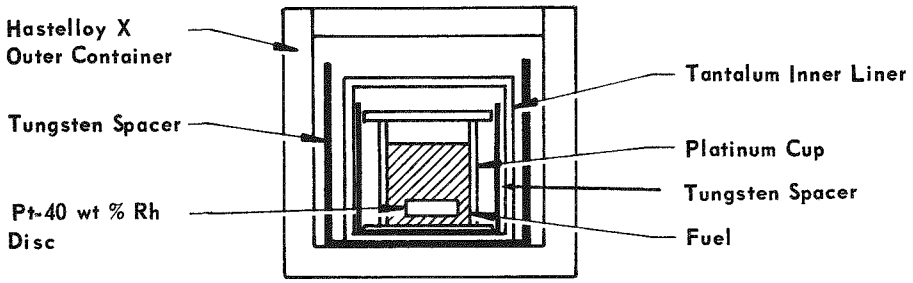

Test Capsule C-1

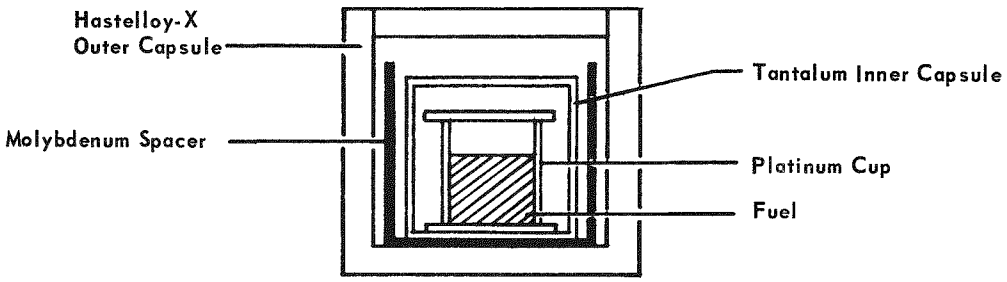

Test Capsule C-2

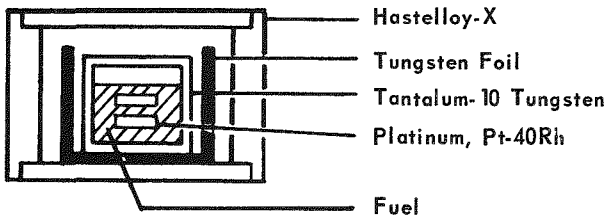

Test Capsule C-3

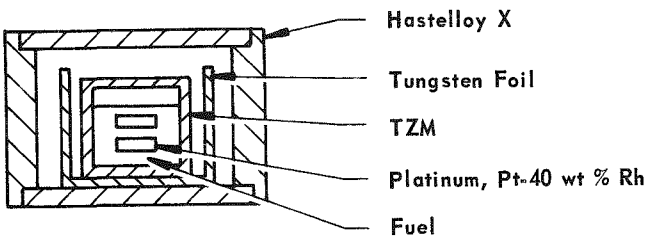

Test Capsule C-4

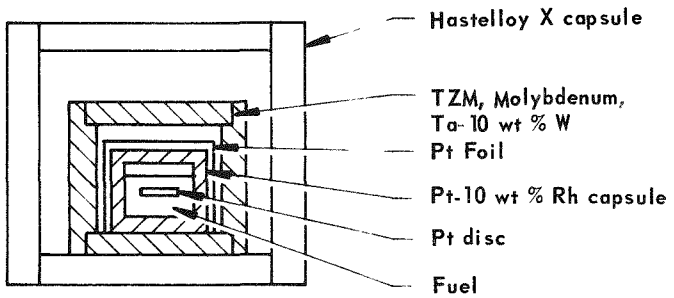

Test Capsule C-5

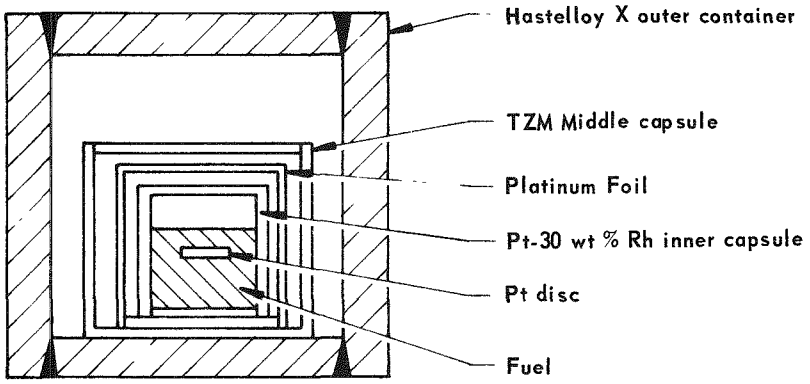

Test Capsule C-6

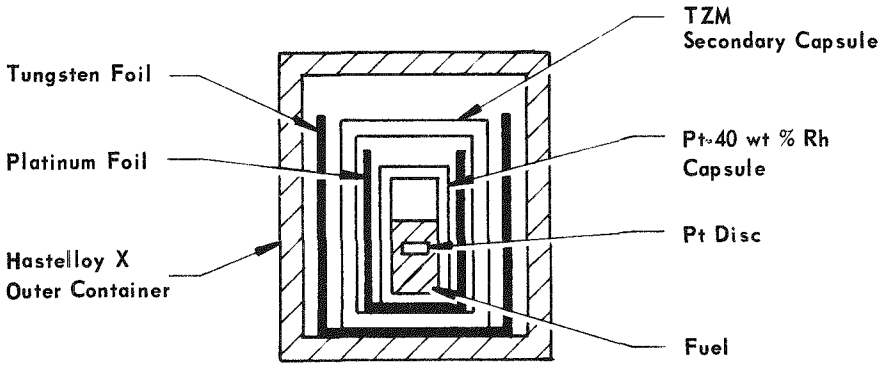

Test Capsule C-7

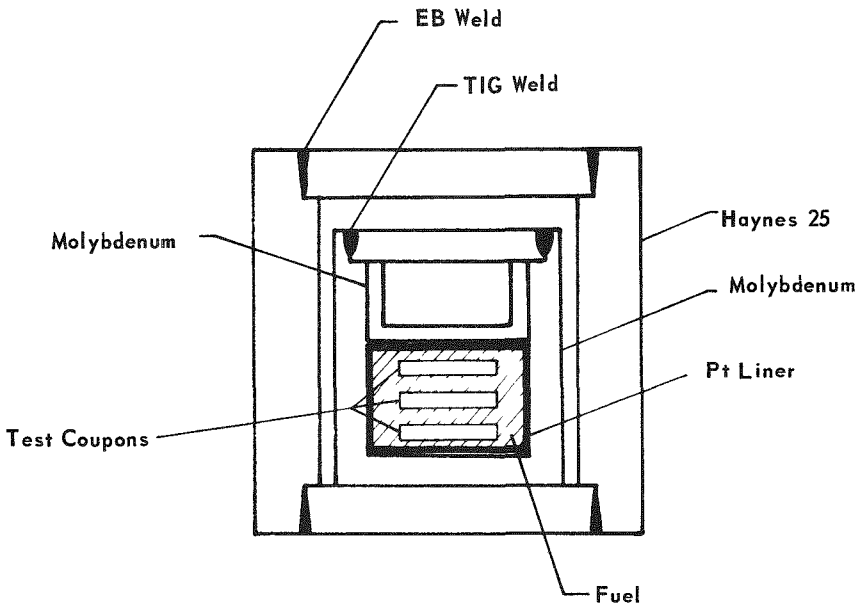

Capsule Design C-8

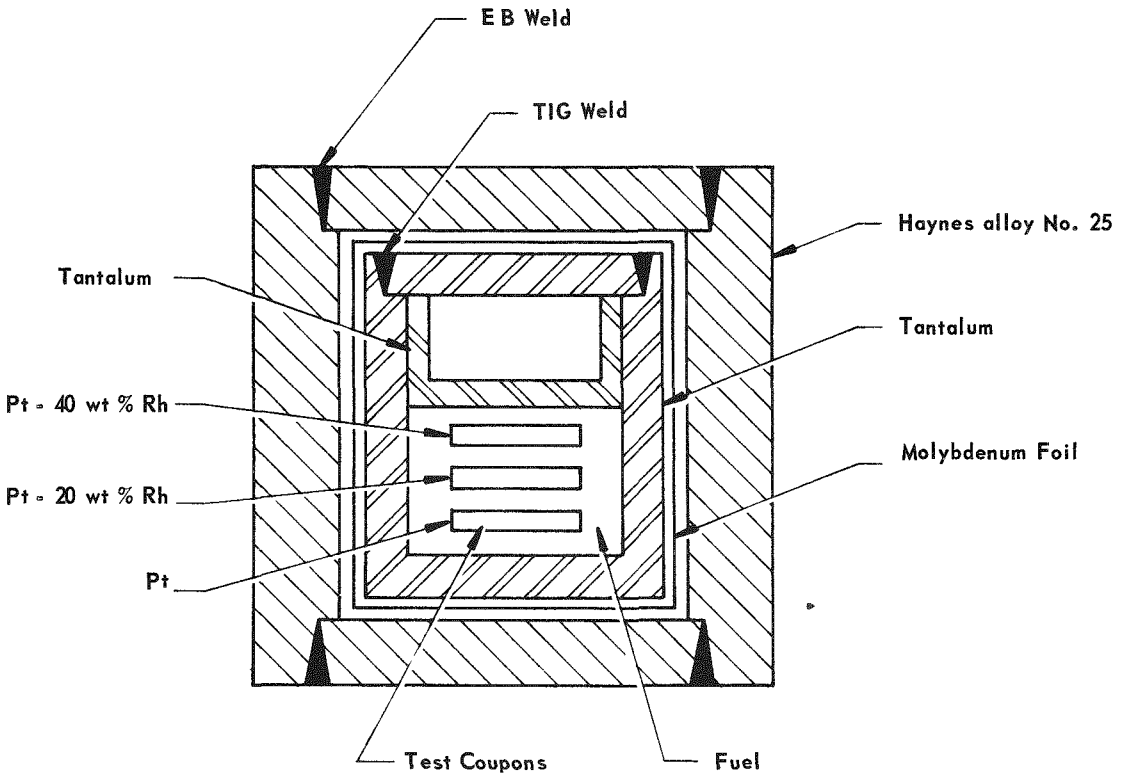

Capsule Design C-9

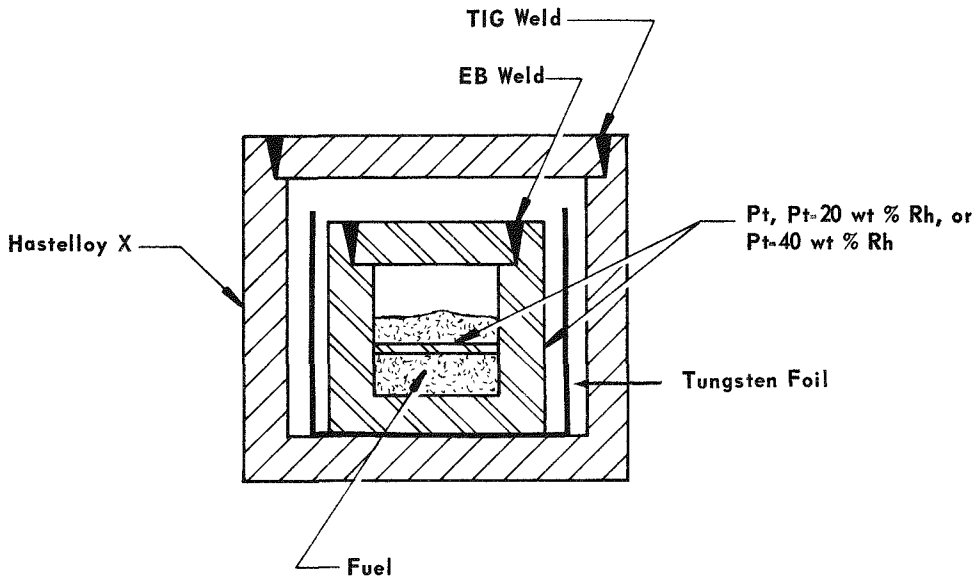

Capsule Design C-10